# UC Santa Barbara

## UC Santa Barbara Electronic Theses and Dissertations

### Title

Targeting DNMT3A Regulatory Interactions for Selective Epigenetic Inhibition

### Permalink

https://escholarship.org/uc/item/16p212h7

### ISBN

9798186384977

### Author

Schmelmer, Ben Manfred Felix

### Publication Date

2026-06-15

Peer reviewed|Thesis/dissertation

eScholarship.org Powered by the California Digital Library
University of California

UNIVERSITY OF CALIFORNIA

Santa Barbara

# Targeting DNMT3A Regulatory Interactions for Selective Epigenetic Inhibition

A Thesis submitted in partial satisfaction of the

requirements for the degree Master of Science

in Chemistry

by

Ben Manfred Felix Schmelmer

Committee in charge:

Professor Norbert Reich, Chair

Professor Yang Hai

Professor Andrea Carlini

June 2026

The thesis of Ben Manfred Felix Schmelmer is approved.

_____

Yang Hai

_____

Andrea Carlini

_____

Norbert Reich, Committee Chair

June 2026

Targeting DNMT3A Regulatory Interactions for Selective Epigenetic Inhibition

Copyright © 2026

by

Ben Manfred Felix Schmelmer

ACKNOWLEDGEMENTS

I would like to thank my family and friends whose unwavering support has carried me through my graduate studies. I am also incredibly grateful to my PI, Dr. Norbert Reich, for providing the space and opportunities to explore meaningful science. I would also like to especially thank Chi-Ping Lin, Nathan Michellys, Ellie Lindenfeld, and Mikayla Gardias for their time and support across my various projects.

ABSTRACT

Targeting DNMT3A Regulatory Interactions for Selective Epigenetic Inhibition

by

Ben Manfred Felix Schmelmer

DNA Methyltransferase 3A (DNMT3A) is an epigenetic enzyme known to drive gene silencing, genomic imprinting, and X-chromosome inactivation in a variety of organisms, including humans. By catalyzing the *de novo* methylation of DNA at CpG sites, DNMT3A establishes the methylation pattern imperative for transcriptional regulation and cellular differentiation during embryonic development. DNMT3A achieves this through interactions with other cellular partners (ncRNA, nucleosomes, p53, and EZH2) to precisely methylate the human genome. Dysregulation of DNMT3A, whether through overexpression, mutation, or loss of regulatory control, leads to aberrant hypermethylation and contributes to various forms of cancer development. For instance, DNMT3A mutations are found in 20-30% of all acute myeloid leukemia (AML) cases, making DNMT3A the most mutated gene in AML patients. Current FDA-approved mechanism-based inhibitors targeting DNMT3A (Azacitidine and Decitabine) are nucleoside analogs that are highly toxic due to their non-discriminant incorporation into the DNA. Considering that AML typically affects older patients, there is a crucial need for more selective, non-cytotoxic DNMT3A inhibitors to control overexpression and aberrant hypermethylation.

In this work, we develop fluorescence anisotropy and AlphaLISA assays for high-throughput screening of small-molecules capable of selectively disrupting DNMT3A interactions with histone-tails, central to chromatin recruitment and enzyme activation. Furthermore, we investigate biologically relevant allosteric inhibition of DNMT3A through RNA-mediated epigenetic regulation.

TABLE OF CONTENTS

I. INTRODUCTION ..... 1

A. HUMAN DNA METHYLTRANSFERASES ..... 1

B. HISTONE REGULATION OF DNMT3A ..... 5

C. RNA EPIGENETIC REGULATION ..... 9

D. DNMT3A DYSREGULATION IN AML AND CURRENT THERAPEUTIC STRATEGIES ..... 12

II. OPTIMIZING RECOMBINANT EXPRESSION AND PURIFICATION OF DNMT3A ..... 16

A. ABSTRACT ..... 16

B. INTRODUCTION ..... 16

C. RESULTS & DISCUSSION ..... 19

D. METHODS ..... 34

E. SUPPLEMENTARY INFORMATION ..... 38

III. DEVELOPING HIGH-THROUGHPUT SCREENING ASSAYS FOR SMALL-MOLECULE INHIBITORS OF DNMT3A REGULATORY INTERACTIONS ..... 41

A. ABSTRACT ..... 41

B. INTRODUCTION ..... 41

C. RESULTS & DISCUSSION ..... 46

D. METHODS ..... 58

E. SUPPLEMENTARY INFORMATION ..... 61

IV. RNA-MEDIATED REGULATION OF DNMT3A BY *FOS-1* ECRNA ..... 64

A. ABSTRACT ..... 64

B. INTRODUCTION ..... 64

C. RESULTS & DISCUSSION ..... 67

D. METHODS ..... 72

E. SUPPLEMENTARY INFORMATION ..... 74

REFERENCES ..... 76

# I. Introduction

## A. Human DNA Methyltransferases

DNA methylation is one of the most studied epigenetic modifications in mammalian cells and plays a central role in regulating gene expression, genomic imprinting, X-chromosome inactivation, and cellular differentiation[1–3]. The epigenetic modification adds of a methyl group at the C5 position of cytosine, generating 5-methylcytosine (5mC), which serves as an epigenetic mark that influences chromatin structure and transcriptional activity [4,5]. Proper establishment and maintenance of DNA methylation patterns are essential for cellular development, whereas aberrant methylation is associated with various diseases including neuronal development disorders and cancer[6–9]. In mammals, DNA methylation patterns are established and maintained by a family of DNA methyltransferases (DNMTs) consisting of DNMT1, DNMT3A, DNMT3B, and the catalytically inactive DNMT3A-like (DNMT3L) (Figure 1). DNMT1 functions as a maintenance methyltransferase, restoring methylation patterns following DNA replication by preferentially recognizing hemimethylated DNA substrates[10,11]. In contrast, DNMT3A and DNMT3B are *de novo* DNA methyltransferases that establish methylation patterns during embryonic development and cellular differentiation[12]. Although DNMT3A and DNMT3B share sequence homology and catalytic mechanisms, they exhibit distinct genomic localization patterns and biological functions[13] DNMT3L lacks catalytic activity but functions as an important regulatory partner that stimulates DNMT3A and DNMT3B activity through formation of higher-order oligomeric complexes[14].

The DNMT family possess multidomain architectures composed of N-terminal regulatory domains and a C-terminal catalytic methyltransferase domain (MTase). While DNMT1

primarily functions in maintenance methylation, DNMT3A and DNMT3B establish *de novo* DNA methylation patterns during development and cellular differentiation and therefore share conserved N-terminal regulatory domains[12] (Figure 1). DNMT3A and DNMT3B's N-terminal regulatory region consisting of the ubiquitin-dependent recruitment (UDR) domain, the Pro-Trp-Trp-Pro (PWWP) domain, and the ATRX-DNMT3-DNMT3L (ADD) domain[15,16]. These regulatory domains dictate recruitment mechanisms by coordinating the localization and activity of DNMT3A in response to the surrounding chromatin environment. DNMT3A exists as two major isoforms, DNMT3A1 and DNMT3A2. The longer DNMT3A1 differs by an extended N-terminal region (NTR), which is involved in nonspecific DNA binding and H2A histone interactions[17,18]. Although the methyltransferase domain performs the methyl transfer reaction, the N-terminal regulatory domains largely determine where and when DNA methylation occurs within the genome. Consequently, disruption of these regulatory interactions can profoundly alter DNA methylation patterns and has been implicated in developmental disorders, cancer, and other diseases associated with epigenetic dysregulation[7,8].

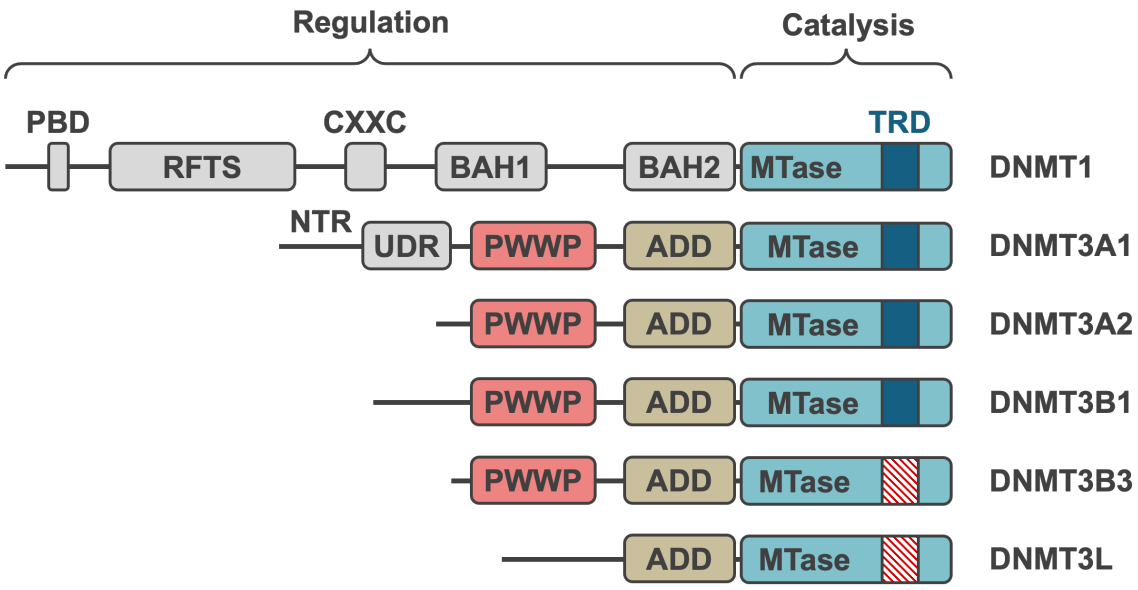
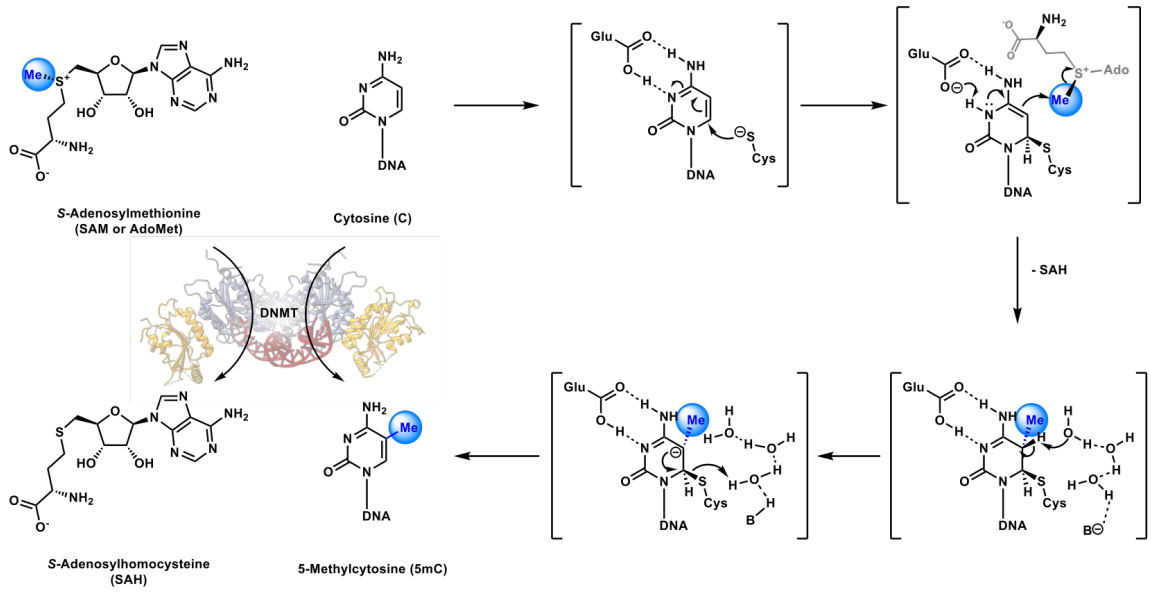



**Figure 1.** Gene map homology of various human DNMTs. N-terminal regions are primarily associated with enzyme regulation, whereas the C-terminal methyltransferase domain is responsible for catalysis.

The C-terminal methyltransferase (MTase) domain contains the catalytic machinery responsible for DNA methylation. This domain is highly conserved among cytosine methyltransferases and contains motifs required for DNA binding, target cytosine recognition, S-adenosyl-L-methionine (SAM) cofactor binding, and catalysis[19] (Figure 1). Within the MTase domain resides the target recognition domain (TRD), a flexible loop that inserts into the major groove of DNA and mediates sequence-specific recognition of CpG dinucleotides[20]. Together with catalytic-loop residues that facilitate target base flipping, the TRD positions the target cytosine for methyl transfer. Because the TRD is essential for DNA recognition and catalysis, proteins lacking this region are unable to perform their own catalysis. Among the DNMTs family members, DNMT3B3 and DNMT3L are catalytically inactive because they lack critical portions of the target recognition domain[21,22]. Although these proteins retain the ability to interact with histones and partner proteins through their PWWP and ADD domains, they cannot independently methylate DNA. Instead, DNMT3L

acts as an auxiliary partner-protein that stimulates DNMT3A and DNMT3B activity through formation of heterotetrameric complexes, whereas DNMT3B3 is thought to contribute to chromatin recruitment and regulatory functions independent of catalytic activity. DNMT3 enzymes function as oligomeric complexes *in vivo*, with DNMT3A and DNMT3B forming homotetramers through interactions within their MTase domains[22]. Although homodimeric DNMT3 complexes retain catalytic activity, tetramerization enhances processivity, cooperativity, and overall methylation activity[23]. Notably, formation of DNMT3A/3L and DNMT3A/3B3 heterotetramers further stimulates catalytic activity beyond that observed for DNMT3A homotetramers alone, highlighting the important regulatory role of DNMT3L and DNMT3B3 in *de novo* DNA methylation[23,24].

DNA methyltransferases catalyze the transfer of a methyl group from the SAM cofactor to the C5 position of cytosine, generating 5-methylcytosine (5mC) and S-adenosyl-L-homocysteine (SAH). The reaction proceeds through a conserved base-flipping mechanism in which the target cytosine is rotated out of the DNA helix and inserted into the enzyme active site[5]. A cysteine residue inside the methyltransferase domain nucleophilically attacks the C6 position of cytosine, generating a covalent enzyme-DNA intermediate that activates the C5 carbon for methyl transfer. Following transfer of the methyl group from SAM, elimination restores aromaticity of the pyrimidine ring and releases 5mC (Scheme 1). The resulting 5mC marker is responsible for transcriptional silencing. Through the coordination of DNMT3A, DNMT3B, DNMT1, and their other regulatory partners, mammalian cells establish and maintain DNA methylation landscapes that govern cellular identity and genome stability.




**Scheme 1.** Reaction scheme for 5mC DNA methylation.

### B. Histone regulation of DNMT3A

DNA methylation and histone modifications are intertwined epigenetic mechanisms that collectively establish gene regulation. Rather than functioning independently, DNA methylation and histone modifications engage in extensive molecular crosstalk that guides cellular differentiation, gene silencing, genomic imprinting, and maintenance of genome stability[25,26]. This coordinated regulation is dictated by "writers," "readers," and "erasers" that deposit, recognize, and remove chromatin modifications. DNA Methyltransferase 3A (DNMT3A) is strongly influenced by its recruitment and activation through various histone post-translational modifications (PTMs) (Figure 2).

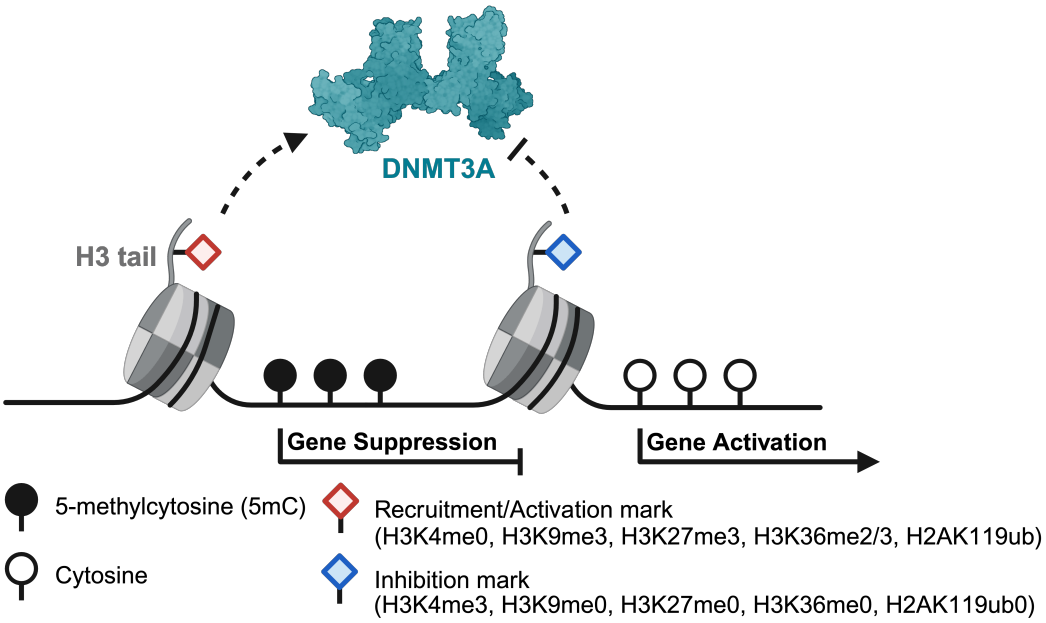



**Figure 2.** Histone modifications regulate DNMT3A activity and recruitment. Histone methylation and ubiquitination markers either promote or inhibit DNMT3A recruitment directly through interactions with chromatin reader domains or indirectly through associated partner proteins. Figure created with BioRender.

Histone H3 lysine 4 methylation (H3K4me) serves as one of the best-characterized regulators of DNMT3A. H3K4 can exist in unmethylated, mono-, di-, or trimethylated states, each associated with distinct chromatin environments[27]. H3K4 trimethylation (H3K4me3) is highly enriched at active promoters and transcription start sites, whereas unmethylated H3K4 (H3K4me0) is commonly found in inactive chromatin regions. The ADD domain of DNMT3A specifically recognizes H3K4me0 through hydrogen-bonding interactions with residues D529 and D531[28]. ADD domain-binding of H3K4me0 induces a conformational rearrangement that relieves autoinhibition of the methyltransferase domain and stimulates DNA methylation activity. Conversely, H3K4 methylation disrupts ADD-domain recognition and prevents DNMT3A activation. Through this mechanism, H3K4 methylation protects

active promoters from aberrant DNA methylation while directing DNMT3A activity toward transcriptionally silent genomic regions[29].

Histone H3 lysine 36 methylation functions as a major recruitment signal for DNMT3A. Di- and trimethylated H3 lysine 36 residues (H3K36me2/3) are deposited by nuclear SET domain-containing (NSD) family methyltransferases and SET domain-containing 2 (SETD2), respectively[30–32]. Recognition of H3K36me2/3 occurs through the PWWP domain of DNMT3A, which binds methylated H3K36 using an aromatic cage that accommodates the modified di/trimethylated lysine residue[33]. Recent genomic and biochemical studies have demonstrated that H3K36me2 serves as a dominant recruitment signal for DNMT3A throughout intergenic regions, whereas H3K36me3 can recruit DNMT3A to actively transcribed gene bodies[34]. These interactions position DNMT3A adjacent to chromatin regions requiring *de novo* DNA methylation and help establish cell-type-specific methylation landscapes.

In contrast to H3K36 methylation, histone H3 lysine 9 trimethylation (H3K9me3) promotes DNA methylation indirectly through recruitment of chromatin-associated regulatory proteins[35]. Histone methyltransferases such as suppressor of variegation 3-9 homologs 1 and 2 (SUV39H1 and SUV39H2) deposit H3K9me3, which subsequently recruits heterochromatin protein 1 (HP1) and additional silencing factors[36,37]. These proteins facilitate the localization of DNMT3A and DNMT3B to heterochromatic regions, resulting in coordinated deposition of DNA methylation and stabilization of long-term transcriptional repression.

Histone H3 lysine 27 trimethylation (H3K27me3) represents another important chromatin mark involved in DNMT3A regulation. H3K27me3 is deposited by Polycomb Repressive

Complex 2 (PRC2) whose catalytic subunit, enhancer of zeste homolog 2 (EZH2), functions as the primary H3K27 methyltransferase[38–40]. Polycomb-mediated repression is essential for silencing developmental genes during differentiation and lineage commitment. Although DNMT3A does not directly recognize H3K27me3 through a dedicated reader domain, increasing evidence suggests substantial functional crosstalk between Polycomb complexes and DNA methylation machinery. EZH2 can physically interact with DNMT proteins and promote recruitment of DNA methyltransferases to target loci, resulting in cooperative gene silencing[41].

Histone H2A lysine 119 monoubiquitination (H2AK119ub) is an additional chromatin signal capable of recruiting DNMT3A. H2AK119ub is deposited by Polycomb Repressive Complex 1 (PRC1) and functions downstream of Polycomb-mediated gene silencing[42,43]. Unlike H3K27me3, which serves primarily as a transcriptional repression mark, H2AK119ub directly participates in chromatin recruitment of DNMT3A through the ubiquitin-dependent recruitment (UDR) domain located within the N-terminal region of DNMT3A[44,45]. Recognition of H2AK119ub enables DNMT3A localization to Polycomb-regulated chromatin and facilitates *de novo* methylation of CpG-rich regions.

The complex interactions between histone PTMs and DNA methylation are coordinated by a diverse network of chromatin-modifying enzymes. Histone methyltransferases such as EZH2, NSD1, NSD2, SETD2, and SUV39H1 function as epigenetic writers that establish histone methylation landscapes[30,36,38,40]. The epigenetic eraser histone deacetylases (HDACs) remove acetyl groups from histone tails, promoting chromatin compaction and facilitating recruitment of repressive complexes[46]. These histone modifications later recruit DNMT3A to

specific genomic locations or activate DNA methylation, ultimately leading to gene silencing.

### C. RNA Epigenetic Regulation

In addition to DNA methylation and histone modifications, RNAs have emerged as regulators of chromatin structure and epigenetic inheritance[47,48]. Once considered passive intermediates between DNA and protein synthesis, non-coding RNAs (ncRNAs) are now recognized as active participants in epigenetic signaling[49–51]. These RNAs operate through multiple distinct mechanisms, including recruitment of chromatin-modifying enzymes, regulation of transcription factors, modulation of chromatin architecture, and direct interactions with epigenetic proteins. Overall, RNA-mediated pathways provide another layer of epigenetic regulation that works complementary and in parallel to DNA methylation and histone modifications.

Non-coding RNAs are generally classified according to their size and biological function. Small non-coding RNAs include microRNAs (miRNAs), small interfering RNAs (siRNAs), and PIWI-interacting RNAs (piRNAs). Long non-coding RNAs (lncRNAs), typically defined as transcripts longer than 200 nucleotides that lack protein-coding potential, yet represent a diverse class of epigenetic regulators[52,53]. Small interfering RNAs (siRNAs) are double-stranded RNAs approximately 21-23 nucleotides in length that function through the RNA interference (RNAi) pathway[54,55]. Following processing by the RNase III enzyme Dicer, siRNAs are loaded into the RNA-induced silencing complex (RISC) where they guide sequence-specific recognition and degradation of their messenger RNAs counterparts. Through this mechanism, siRNAs mediate post-transcriptional gene silencing and play important roles in antiviral defense, transposon suppression, and experimental gene

knockdown strategies[56]. MicroRNAs (miRNAs) are endogenous small RNAs that similarly function through RISC-mediated targeting of mRNAs[57]. Unlike siRNAs, miRNAs exhibit partial complementarity to their targets and often regulate multiple transcripts simultaneously[58]. By repressing translation or promoting mRNA degradation, miRNAs influence multiple cellular pathways. Dysregulation of miRNA expression has been implicated in numerous diseases, especially cancer, where improper miRNA content contributes to aberrant gene expression. PIWI-interacting RNAs (piRNAs) are a distinct class of small RNAs that associate with PIWI proteins to silence transposable elements within germ cells. Unlike siRNAs and miRNAs, piRNAs are generated independently of the Dicer enzyme and are generally 24-32 nucleotides in length[59,60]. The piRNA pathway is essential for maintaining genome stability during gametogenesis by suppressing transposon activity through both post-transcriptional and epigenetic mechanisms. In many organisms, piRNAs can recruit DNA methyltransferases and histone-modifying enzymes to transposable elements, thereby establishing heritable transcriptional silencing[61,62].

Among non-coding RNAs, long non-coding RNAs have emerged as particularly important regulators of epigenetic processes. LncRNAs function through diverse molecular mechanisms including scaffolding of protein complexes, recruitment of chromatin-modifying enzymes, and inhibiting transcription factors[63]. Many lncRNAs act locally at their sites of transcription, while others operate in *trans* to regulate distant genomic loci[64]. Through these mechanisms, lncRNAs establish cell-type-specific gene expression programs and contribute to developmental transitions. One of the most extensively studied lncRNAs is X-inactive specific transcript (Xist), which orchestrates X-chromosome inactivation (XCI) in female mammals[65,66]. XCI is a dosage-compensation mechanism that equalizes X-linked gene

expression between XX females and XY males by transcriptionally silencing one X chromosome during early embryonic development. Xist is transcribed exclusively from the future inactive X chromosome and accumulates across the chromosome from which it is produced, functioning *in cis* to establish chromosome-wide gene repression[66]. Xist mediates X-chromosome inactivation through multiple mechanisms in paralell[67]. Following transcription, Xist spreads along the inactive X chromosome and recruits numerous chromatin-modifying proteins through distinct structural domains[67]. The A-repeat region of Xist interacts with the transcriptional repressor SPEN, which subsequently recruits histone deacetylase complexes to initiate gene silencing. Additional regions of Xist recruit hnRNPK, which facilitates localization of PRC1 and deposition of H2AK119ub. PRC1 activity then promotes recruitment of PRC2, resulting in accumulation of H3K27me3 across the inactive chromosome[67,68]. Rather than relying on a single regulatory pathway, Xist exhibits how lncRNAs can integrate multiple chromatin-modifying mechanisms simultaneously.

Recent evidence further suggests that non-coding RNAs can directly regulate DNA methyltransferases[49,69,70]. Several extra-coding RNAs (ecRNAs) have been shown to interfere with DNA methylation, some of which bind directly with DNMTs, impacting their catalytic activity[70,71]. EcRNAs are sense-strand, non-polyadenylated transcripts that overlap the boundaries of their protein-coding genes[69]. Unlike many repressive lncRNAs, ecRNAs frequently correlate with low DNA methylation and elevated gene expression[70]. Studies have demonstrated that ecRNAs can inhibit DNA methylation by binding to the DNMT3A tetramer interface, providing a mechanism through which actively transcribed genes may protect themselves from *de novo* methylation[71].

Together, small and long non-coding RNAs form a diverse regulatory network that influences gene expression through both post-transcriptional and chromatin-based mechanisms. Through interactions with chromatin-modifying enzymes, transcription factors, and DNA methyltransferases, RNA molecules establish and maintain epigenetic states during development and cellular differentiation. Understanding these RNA-mediated pathways is therefore essential for elucidating the mechanisms by which chromatin structure and DNA methylation are coordinated in normal physiology and disease.

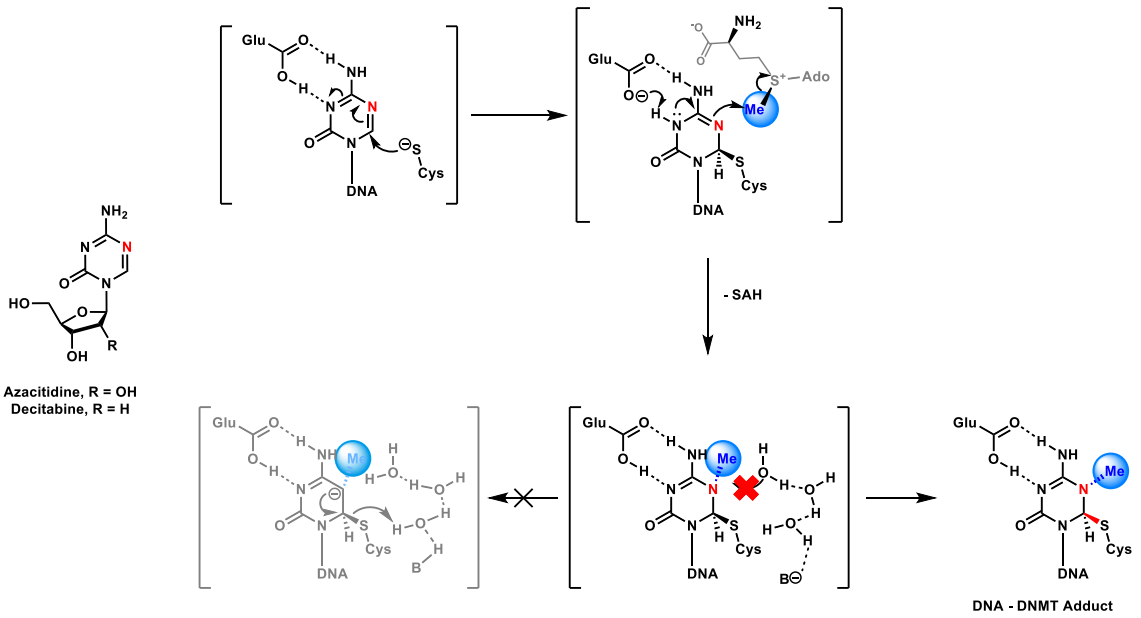
**D. DNMT3A Dysregulation in AML and Current Therapeutic Strategies**

DNA methylation patterns are tightly regulated during hematopoietic development to ensure proper lineage commitment, self-renewal, and cellular differentiation[72]. Among the proteins responsible for establishing these methylation patterns, DNMT3A plays a prominent role in hematopoietic stem and progenitor cells[73,74]. Consequently, mutations in DNMT3A are among the most frequently observed epigenetic alterations in hematological malignancies such as acute myeloid leukemia (AML)[75]. These mutations disrupt normal DNA methylation programs, resulting in aberrant gene expression and impaired cellular differentiation that contribute to malignant transformation.

DNMT3A mutations are detected in approximately 20-30% of AML patients, making DNMT3A the most frequently mutated gene in the disease[76–78]. Although mutations have been identified throughout the DNMT3A coding sequence, a large proportion occur within the catalytic methyltransferase domain. The most common mutation is the loss-of-function substitution of arginine 882, which accounts for approximately 60-70% of all DNMT3A mutations identified in AML patients[79]. Structural studies have shown that R882 resides within the dimer interface of DNMT3A, where it participates in intermolecular interactions

required for formation of catalytically active oligomeric complexes[80]. Mutation of this residue, most common being with histidine (R882H), disrupts tetramerization, effectively disabling DNMT3A's methylation capability by 80%[81]. The R882H mutation alters flanking sequence preferences surrounding CpG sites and generates a methylation pattern that resembles DNMT3B more closely than wild-type DNMT3A. As a result, R882H produces aberrant methylation patterns rather than simple reductions in overall DNA methylation[82]. This explain why AML-associated DNMT3A mutations generate highly specific changes in the methylation landscape despite retaining partial catalytic activity.

Consequently, pharmacological inhibition of DNA methyltransferases has emerged as an effective strategy for treating hematological cancers characterized by dysregulated epigenetic landscapes[83]. Currently, two FDA-approved therapies target DNA methylation in patients with acute myeloid leukemia (AML): azacitidine[84] and decitabine[85]. Both compounds are cytidine analogs that function as hypomethylating agents by inhibiting DNA methyltransferases. Following cell uptake, azacitidine and decitabine are incorporated into newly synthesized nucleic acids during DNA replication. Decitabine is incorporated into DNA, whereas azacitidine is incorporated into both DNA and RNA. Once incorporated into DNA, these analogs exploit the conserved catalytic mechanism of cytosine methyltransferases to induce suicide inhibition (Scheme 2).




**Scheme 2.** Mechanism of azacitidine and decitabine inhibition of DNA methyltransferases. Nucleoside analogs become incorporated into DNA during replication and form irreversible covalent complexes with DNA methyltransferases, resulting in enzyme depletion and loss of DNA methylation.

Although azacitidine and decitabine have demonstrated adequate clinical benefit in AML patients, these therapies suffer from several important limitations[86]. Because they act by incorporating into replicating DNA, their activity is restricted primarily to rapidly dividing cells[87]. This lack of specificity for DNMT3A results in substantial cytotoxicity due to off-target effects from nonspecific incorporation into DNA and RNA[88]. The pharmacokinetic properties of these drugs also present significant challenges. Both compounds exhibit poor chemical stability and are rapidly degraded by cytidine deaminase, resulting in short plasma half-lives and limited bioavailability. Azacitidine and decitabine have a terminal half-life of less than one hour, requiring repeated dosing to maintain therapeutic efficacy[89]. Additionally, because these drugs induce global DNA hypomethylation rather than selectively targeting pathogenic methylation events, treatment can disrupt normal epigenetic regulation

throughout the genome. The resulting loss of specificity may contribute to adverse effects and variable therapeutic responses among patients.

The limitations of nucleoside analogs have stimulated considerable interest in the development of non-nucleoside inhibitors that selectively target individual DNA methyltransferases. However, designing selective active-site inhibitors has proven challenging because the methyltransferase domains of mammalian DNMTs are highly conserved, increasing the likelihood of off-target effects and cytotoxicity. Recent efforts have demonstrated the feasibility of this approach[90,91]. Small-molecule screens have identified non-nucleoside compounds capable of selectively inhibiting DNMT3A while exhibiting minimal activity toward DNMT1 and unrelated methyltransferases[90,91]. In particular, phthalazinone-derived compounds were shown to inhibit DNMT3A through a noncompetitive mechanism consistent with allosteric regulation[91]. Because these compounds do not rely on incorporation into DNA, they avoid many of the liabilities associated with nucleoside analogs and represent promising leads for the development of next-generation epigenetic therapeutics.

## II. Optimizing Recombinant Expression and Purification of DNMT3A

### A. Abstract

DNMT3A is an epigenetic *de novo* DNA methyltransferase that plays a crucial role in establishing the methylation patterns for transcriptional regulation and cellular differentiation during embryonic development. Biochemical and structural investigations of DNMT3A require the recombinant production of soluble, full-length protein; however, expression of DNMT3A1 in *E. coli* is complicated by truncation or proteolytic degradation products that co-elute with standard $Ni^{2+}$ IMAC purification. In this work, western immunoblot assays were optimized to evaluate the expression and stability of the DNMT3A1 enzyme and associated truncation products under varying induction temperatures and duration. Western blot analysis revealed that induction at 16˚C for 15 hours produced the highest yield of DNMT3A1 and highest ratio of the intact enzyme relative to its truncation products, suggesting that low-temperature expression improves dynamic protein folding and stability. Additionally, protease inhibitor treatments and a codon-optimized expression vector were explored to assess the contribution of proteolytic degradation or rare codon usage to DNMT3A1 truncations; neither treatment reduced nor impacted the truncation pattern observed for DNMT3A1. All together, these findings establish an optimized expression workflow for the recombinant expression of DNMT3A1 in *E. coli* required for future biochemical and structural studies of DNMT3A's methylation and regulatory mechanisms.

### B. Introduction

Epigenetic regulation plays an intrinsic role in governing gene expression, cellular differentiation, genomic imprinting, and X-chromosome inactivation[1–3]. Among the major epigenetic modifications, DNA methylation is a critical mechanism for establishing stable

transcriptional states during embryonic development and cellular specialization[4]. In mammals, *de novo* DNA methylation is primarily carried out by DNA methyltransferase 3A (DNMT3A) and DNA methyltransferase 3B (DNMT3B), which catalyze the transfer of a methyl group from *S*-adenosyl methionine (SAM) to cytosine to form 5-methylcytosine (5mC)[4,5]. This DNMT3A-mediated methylation contributes to gene silencing and maintenance of genomic integrity. Aberrant DNA methylation patterns resulting from DNMT3A dysfunction have been implicated in numerous diseases and cancers, particularly hematological malignancies such as acute myeloid leukemia (AML), where DNMT3A is the most frequently mutated gene[6–9].

DNMT3A contains multiple conserved domains that contribute to chromatin recognition, allosteric regulation via partner proteins, and catalytic activity. These include the N-terminal regulatory domains which include the Pro-Trp-Trp-Pro (PWWP) domain, the ATRX-DNMT3-DNMT3L (ADD) domain, and the ubiquitin-dependent recruitment (UDR) domain; as well as the C-terminal methyltransferase (MTase) domain responsible for cytosine methylation[10–14]. DNMT3A forms higher-order oligomeric complexes with itself or partner proteins and, with the N-terminal regulatory domains, interacts with histone modifications and nucleosome substrates that modulate enzymatic activity and genomic targeting[15–19]. The coordinated folding of these domains during protein expression in *E. coli* are essential for biochemical investigation of DNMT3A's function and regulation.

Although the full-length DNMT3A (DNMT3A1) is required to investigate chromatin recruitment, allosteric regulation, and interactions with regulatory proteins or histone modifications, many biochemical studies[20–22] utilize the isolated methyltransferase domain of DNMT3A ($DNMT3A^{MTase}$) due to its improved recombinant expression and stability.

Previous studies have demonstrated that DNMT3A$^{MTase}$ retains catalytic activity and exhibits kinetic properties comparable to DNMT3A1 on naked DNA substrates[23,24], making it a useful model for mechanistic enzymology and inhibitor characterization. Because DNMT3A regulation depends heavily on the N-terminal regulatory domains such as the PWWP, ADD, and UDR domains, investigations into epigenetic crosstalk and nucleosome-mediated regulation ultimately require reliable recombinant production of the full-length enzyme (DNMT3A1). However, expression of large multidomain human proteins in *E. coli* is often challenging due to limitations in protein folding[25,26]. Recombinant DNMT3A expression in *E. coli* frequently results in the formation of truncated protein products[12], likely arising from misfolding, translational instability, or proteolytic degradation by endogenous bacterial proteases. These truncation products complicate downstream purification and biochemical analyses, limiting the ability to obtain homogeneous preparations of DNMT3A1.

Previous efforts from our group[12] and others[13] to express and purify DNMT3A1 in *E. coli* resulted in substantial truncation following $Ni^{2+}$ immobilized metal affinity chromatography (IMAC) purification. This work aims to establish a western blotting workflow capable of distinguishing DNMT3A and associated truncation species to ultimately optimize recombinant expression conditions for improved recovery of the DNMT3A1 enzyme. Expression parameters – including induction temperature and induction duration – were systematically evaluated to identify conditions that minimize truncation while preserving protein expression. Additionally, protease inhibitors were investigated to assess the contribution of proteolytic degradation to DNMT3A instability during expression and sample preparation. These studies provide a foundation for improving the recombinant production of DNMT3A1 for future mechanistic and structural investigations.

## C. Results & Discussion

*Optimization of DNMT3A Methyltransferase Domain Purification and Storage Conditions*

Purification storage conditions for the isolated DNMT3A methyltransferase domain ($DNMT3A^{MTase}$) were investigated to establish improved workflows for recombinant DNMT3A protein preparation. Although $DNMT3A^{MTase}$ lacks the N-terminal regulatory domains required for chromatin recruitment and allosteric regulation, the methyltransferase domain retains robust methyltransferase activity and serves as a valuable biochemical model for mechanistic and inhibitor studies[20,24]. Compared to DNMT3A1, $DNMT3A^{MTase}$ is substantially more tractable for recombinant expression and purification in *E. coli* due to its smaller size and reduced flexibility[21].

Recombinant His-tagged $DNMT3A^{MTase}$ was expressed in 8 L of NiCo21(DE3) *E. coli* culture. Following induction and harvest, collected cell paste (17.5 g) was and lysed in buffer conditions containing Triton X-100, PMSF, and DTT to improve protein solubility and minimize aggregation. Soluble lysate was clarified by centrifugation and purified using $Ni^{2+}$ immobilized metal affinity chromatography (IMAC) with a 1 mL HisTrap Excel column. To reduce contaminating proteins, sequential wash conditions with increasing imidazole concentrations (50 mM and 75 mM) were executed prior to gradient elution (75 mM - 500 mM). Following elution, fractions corresponding to the primary $DNMT3A^{MTase}$ peak were pooled then buffer-exchanged and ultrafiltered into storage buffers of varying pH (pH 7.2, 7.5, 8.0, and 8.5). These storage conditions were motivated by the predicted isoelectric point (pKa ≈ 8.73, determined with Expasy) of $DNMT3A^{Mtase}$ and the possibility that pH influences protein-protein interactions that govern solubility. Proteins are generally least

soluble near their isoelectric point since the reduction in net surface charge minimizes electrostatic repulsion, allowing attractive hydrophobic and van der Waals interactions to dominate; this leads to protein aggregation, precipitation, and a reduced protein recovery during ultrafiltration[27]. pH values below 7.2 were not examined since the objective was to evaluate storage conditions near physiological pH and approaching the predicted isoelectric point.

Comparison of the final purified protein preparations demonstrated that storage pH had minimal impact on overall purity, with all preparations exhibiting purities between approximately 91-94% following IMAC purification and ultrafiltration (Table 1, Figure S1). However, differences in final protein yield and concentration were observed across storage conditions. Storage at pH 7.2 produced the highest adjusted final yield (14.92 µg) and highest final protein concentration (9.44 µM), while pH conditions closer to the DNMT3A$^{MTase}$ isoelectric point (pKa ≈ 8.73) resulted in reduced recovery.

**Table 1.** Purity, yield, and final monomer concentration of DNMT3A$^{MTase}$ at different storage pH conditions.

| Storage Buffer pH | Purity (%) | Yield (µg) | Monomer Concentration (µM) |
|---|---|---|---|
| 7.2 | 93.1 | 14.92 | 9.44 |
| 7.5 | 92.5 | 12.22 | 8.84 |
| 8.0 | 90.8 | 10.48 | 7.08 |
| 8.5 | 93.6 | 9.65 | 7.52 |

As anticipated, conditions closer to the predicted isoelectric point of DNMT3A$^{MTase}$ did not improve protein recovery. Instead, slightly acidic storage conditions relative to the protein pKa appeared to better preserve soluble protein. The likely explanation is that storing DNMT3A$^{MTase}$ at pH values increasingly removed from its isoelectric point, the protein is expected to carry a greater net charge, thereby enhancing intermolecular repulsion and

potentially improving long-term colloidal stability and solubility[27]. Notably, final protein concentration generally followed the same trend observed in total protein yield, further highlighting the ability of pH to solubilize the enzyme into the storage buffer (Table 1). Although all samples subjected to the same ultrafiltration cycles, a modest difference in final concentration was observed between the pH 8.0 (7.08 μM) and pH 8.5 (7.52 μM) storage conditions. This discrepancy may be attributed to subtle differences in the protein's non-specific adsorption to the ultrafiltration membranes. Regardless, the total protein yield remains the ultimate indicator of recovery since it reflects the total amount of soluble protein retained throughout purification and storage.

To determine whether storage pH could influence the catalytic activity of DNMT3A$^{MTase}$, methylation assays were performed on protein samples buffer-exchanged into pH 7.2, 7.5, 8.0, and 8.5 storage buffers. Assays were conducted using 50 nM DNMT3A$^{MTase}$ and 5 μM substrate DNA, a concentration previously established to reside within the $V_{max}$ region of the enzyme's Michaelis-Menten kinetics[21], thereby enabling direct comparison of maximal catalytic rate between storage pH conditions (Figure S2). No statistically significant differences in DNMT3A$^{MTase}$ activity were observed across the storage pH conditions tested. Storage pH within this range does not measurably affect the catalytic competence of DNMT3A$^{MTase}$, suggesting that the recovered and stored protein at all storage pH conditions remains predominantly in its active native conformation. Furthermore, the comparable activities observed across all conditions imply that protein recovered at each storage pH consists largely of properly folded DNMT3A$^{MTase}$ rather than inactive or misfolded species. While the presence of minor amounts of aggregated protein cannot be excluded, the retention

of catalytic activity indicates that aggregation is not a substantial contributor to the recovered protein population.

In sum, storage buffer pH significantly impacts recovery of soluble DNMT3A$^{MTase}$ following purification, even when purity remains largely unchanged. Importantly, the optimized pH 7.2 storage condition improved overall recovery of DNMT3A$^{MTase}$, enabling quality high-yield recovery of DNMT3A$^{MTase}$ for downstream biochemical characterization.

*Optimization of Western Blot Detection for DNMT3A1*

Reliable detection of DNMT3A1 and associated truncation products from whole-cell lysates was necessary to evaluate recombinant expression conditions in *E. coli*. For this western blot method, 0.45 µm polyvinylidene difluoride (PVDF) membranes were selected due to their increased protein-binding capacity and transfer efficiency relative to cellulose membranes[28].

DNMT3A1 has a molecular weight of approximately 130 kDa[29], a 0.45 µm membrane is well suited for the transfer and retention of this relatively large protein, as larger-pore PVDF membranes are generally preferred for proteins >100 kDa[30]. Compared to smaller-pore membranes (i.e. 0.2 µm), 0.45 µm PVDF membranes provide efficient retention and transfer of higher-molecular-weight proteins while minimizing transfer losses, making them well-suited for the detection of DNMT3A1 and its truncation products. Since PVDF membranes exhibit autofluorescence, detection of DNMT3A1 and truncation species were performed with an anti-His primary antibody followed by a horseradish peroxidase (HRP)-conjugated secondary antibody for chemiluminescent detection.

Initial western blot optimization experiments were performed using our lab's standard DNMT3A expression conditions[12,21] consisting of 1 L cultures induced with 1 mM IPTG at

28˚C for 5 hours followed by centrifuging cell culture at 8,000 x g and storing resulting cell pellet at -80˚C. The frozen cell pellet was then lysed by sonication and varying amounts of total lysate protein (0.1-5 µg) were resolved on 8% SDS-PAGE gels and transferred onto a PVDF membrane for chemiluminescent detection. Under these conditions, bands corresponding to DNMT3A1 (~130 kDa) as well as several lower molecular weight truncation products were observed (Figure 1). Notably, this result demonstrates that the optimized immunoblotting workflow can selectively detect DNMT3A and several truncations from all proteins in the lysate without the need for large-scale expressions and labor-intensive protein purifications.

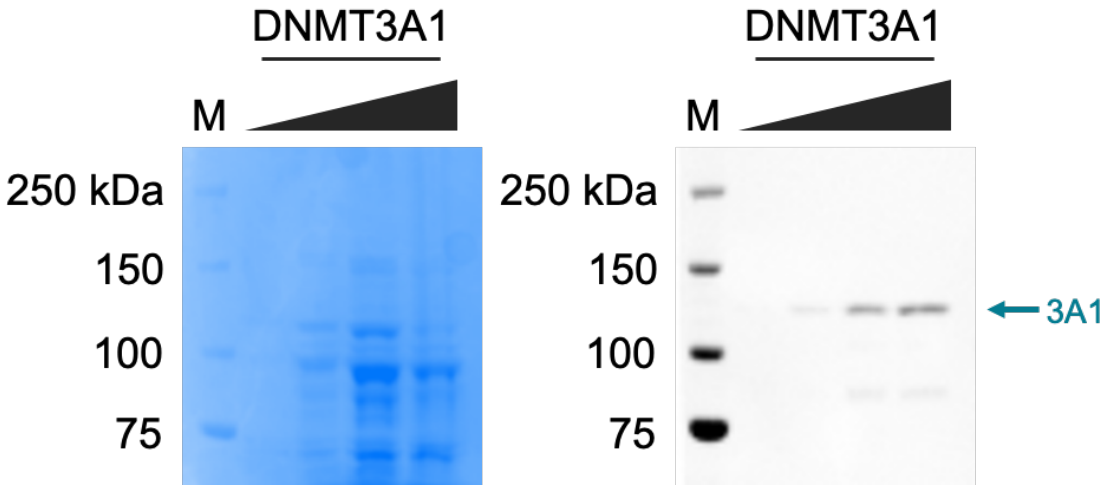



**Figure 1.** Whole-cell lysates from 1 L cultures expressing DNMT3A1 were induced with 1 mM IPTG at 28˚C for 5 h and analyzed by SDS-PAGE (left) and anti-His western blotting (right). Increasing amounts of total lysate protein (0.1-5 µg) were loaded to each well. Bands corresponding to DNMT3A1 (~130 kDa) and lower-molecular-weight truncation products were detected from the crude lysate.

To further investigate the viability of the immunoblot workflow, the same western blot analysis was performed on a previously purified DNMT3A sample. The resulting Western blot banding pattern closely resembled that observed in SDS-PAGE gel, with several truncation products consistently detected alongside DNMT3A1. Because detection was

performed using an anti-His antibody and the His-tag is located at the N-terminus of the DNMT3A expression construct, all observed truncation products must retain the N-terminal region of the protein (Figure 2). Protein degradation post-purification from improper storage conditions would be expected to generate fragments lacking the N-terminal His-tag and therefore escape western blot detection while still detectable with the SDS-PAGE gel. Because DNMT3A was purified using $Ni^{2+}$ IMAC, all detected truncation species must retain the N-terminal His-tag required for affinity capture. Observed fragments are therefore consistent with either premature translational termination or ribosomal stalling that produces truncation products or proteolytic cleavage events rather than protein degradation from storage conditions.

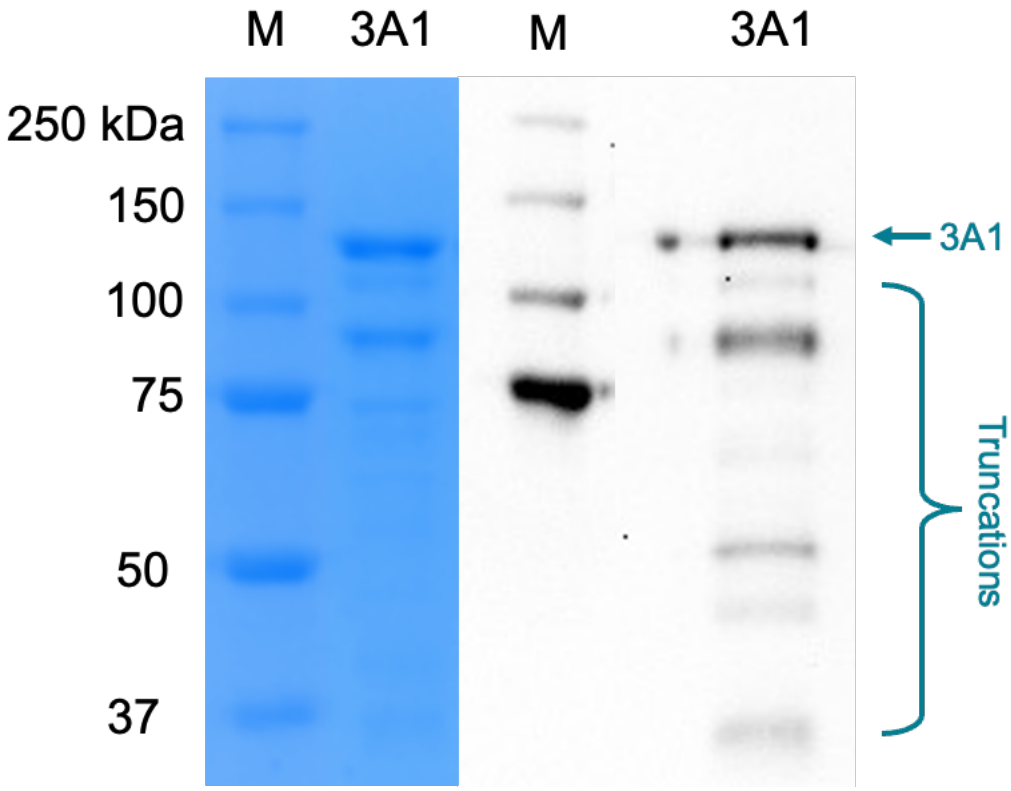



**Figure 2.** Purified DNMT3A1 was analyzed by SDS-PAGE (left) and anti-His western blotting (right). Multiple truncation products were detected alongside DNMT3A1.

To assess of DNMT3A expression and truncation patterns during cell harvest, the expression workflow was adapted from 1 L cultures to 25 mL cultures with 1 mL aliquots collected for analysis. Rather than subjecting samples to cell lysis via sonification, frozen cell pellets were directly resuspended in 2x Laemmli buffer and incubated at 95˚C for 10 min prior to electrophoresis (Figure 3). This approach rapidly denatures cellular proteins and irreversibly inactivates endogenous proteases, thereby preserving the protein population present at the time of cell harvest. As a result, any observed truncation products are more likely to reflect events occurring during protein expression rather than proteolytic degradation during cell lysis or sample preparation. The western blot analysis of these directly denatured samples yielded reproducible detection of DNMT3A1 and its associated truncation products, allowing for future evaluation of expression conditions.

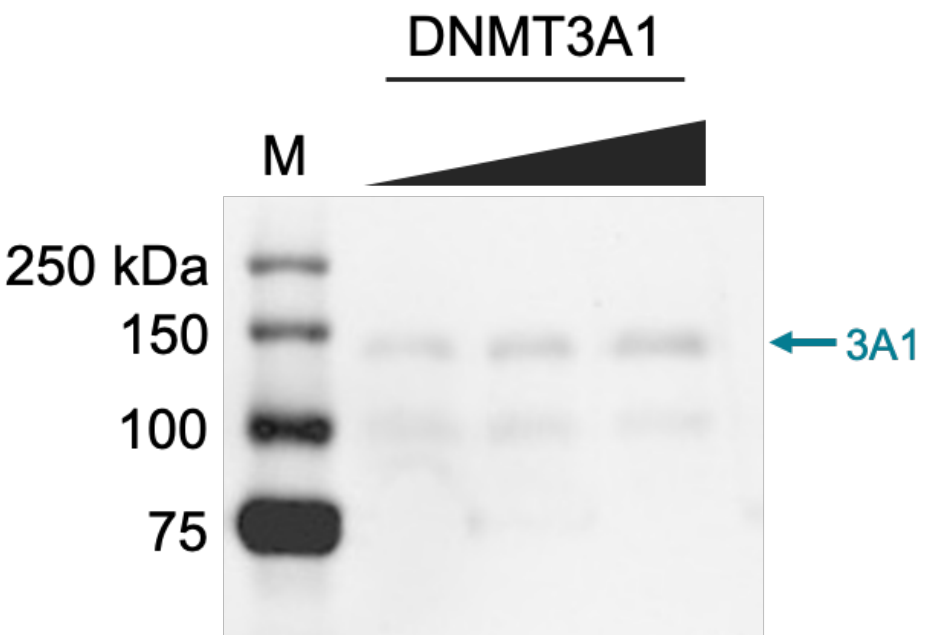



**Figure 3.** Whole-cell pellets obtained from 1 mL aliquots of recombinant DNMT3A1 from E. coli cultures were directly resuspended in 2x Laemmli buffer and heated at 95˚C for 10 min prior to SDS-PAGE and western blot analysis. Sample loading volumes (5-15 µL) were increased from left to right as indicated above each lane.

*Optimization of Induction Temperature and Expression Duration*

Expression of large multidomain eukaryotic proteins in *E. coli* is frequently complicated by misfolding and proteolytic instability. Because reduced growth temperatures can reduce misfolding and aggregation of recombinant proteins[27], induction temperature and duration were systematically evaluated to identify conditions that favor recovery of DNMT3A1. Cultures expressing DNMT3A1 were induced at 16˚C, 28˚C, or 37˚C, and samples were collected at 1, 5, 10, and 15 hours post-induction. Western blot analysis revealed differences in the levels of DNMT3A1 and truncated species across all conditions (Figure 4).

If truncation were driven exclusively by proteolytic degradation occurring after expression of full-length protein, longer induction times would be expected to produce progressively greater accumulation of truncated species relative to DNMT3A1. However, this trend was not observed across all temperatures and time points. Instead, the relative abundance of truncation products varied in a more complex manner, suggesting that truncation likely arises from multiple contributing factors including translational stalling or protein misfolding which both can lead to premature termination[26]. Quantification of western blot band intensities demonstrated that low-temperature expression conditions generally favored accumulation of the intact DNMT3A1 relative to its truncation products (Figure 4). Among all conditions tested, induction at 16 ˚C for 15 hours produced the highest amount of DNMT3A1 (Figure 4b) as well as the highest ratio of DNMT3A1 to truncated species (Figure 4c). Reduced temperature expression likely improves DNMT3A1 stability by slowing translational rates and cellular metabolism, thereby allowing additional time for proper folding of the multidomain protein. This interpretation is consistent with previous reports[27] demonstrating that low-temperature induction can improve solubility and stability

of sensitive eukaryotic proteins expressed in *E. coli*. The PWWP, ADD, and MTase domains of DNMT3A likely require coordinated folding interactions that may not occur efficiently under rapid expression conditions at elevated temperatures. Similar low-temperature, overnight induction strategies have been reported by other groups expressing DNMT3A in *E. coli*[31]. Although these conditions are generally considered favorable for promoting proper protein folding and reducing aggregation, substantial levels of DNMT3A truncation products were still observed. Furthermore, purification by size-exclusion chromatography using a Superdex 200 pg resin was insufficient to fully resolve the DNMT3A1 from its associated truncation species (Figure S3). The persistence of these species throughout both expression and purification which prevent the isolation of pure DNMT3A1 hinder biochemical investigation of DNMT3A; yet, additional strategies to improve the production of DNMT3A1 in *E. coli* are still needed.

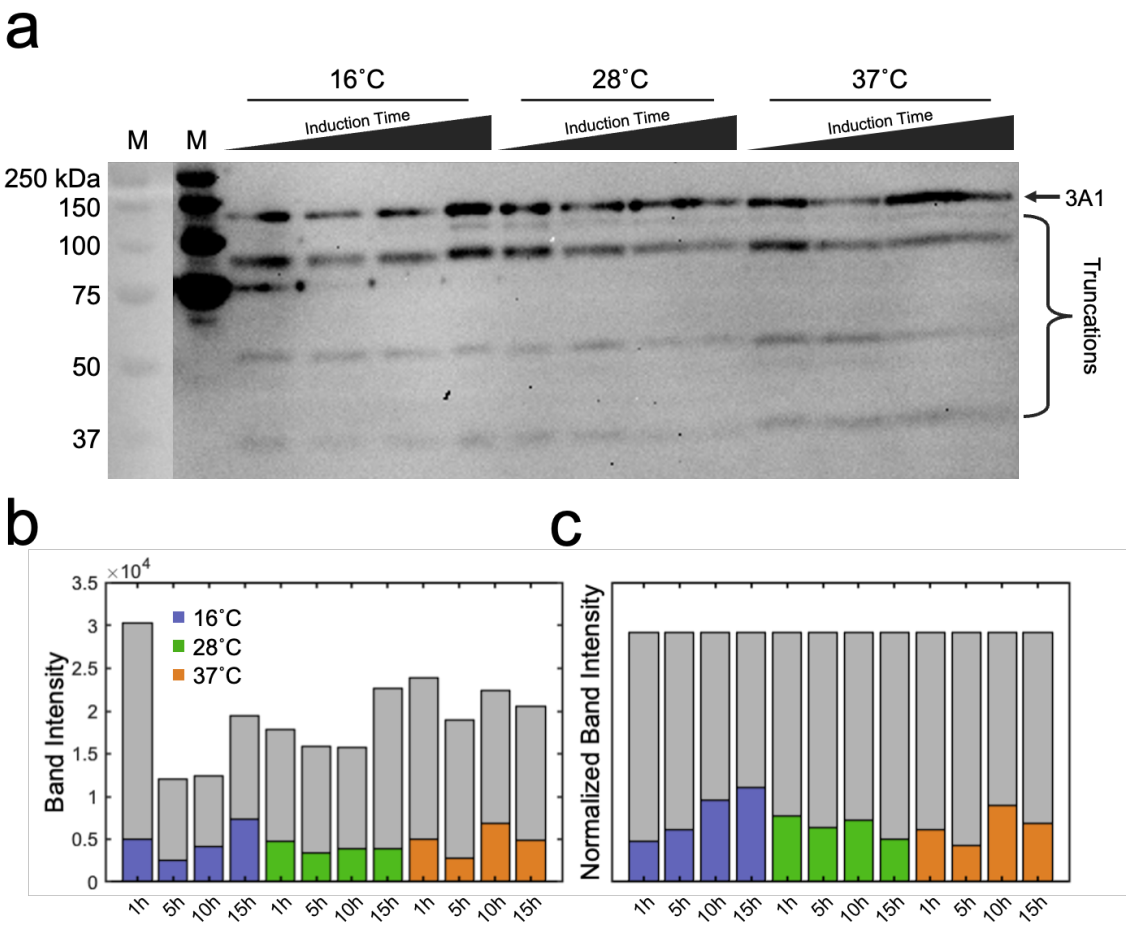



**Figure 4.** a) Western blot analysis of DNMT3A expression following induction at 16˚C, 28˚C, or 37˚C. Samples were collected after 1, 5, 10, and 15 h of expression. b-c) Quantification of b) total and c) relative band intensity of intact and truncated DNMT3A1 species normalized to total DNMT3A signal. Colored segments (purple, green, and orange) correspond to DNMT3A1 expressed at 16˚C, 28˚C, and 37˚C, respectively, while gray segments represent the combined contribution of all truncation products. Low-temperature expression at 16˚C for 15 h produced the highest accumulation of DNMT3A1 and the greatest ratio of full-length protein to truncation products.

*Evaluation of Protease Inhibitors During DNMT3A Expression*

Initially, we hypothesized that the DNMT3A1 truncation products arose primarily through proteolytic cleavage at structurally flexible regions of the protein. Proteases preferentially cleave disordered or solvent-accessible regions due to their increased

conformational mobility and accessibility[32]. To investigate this possibility, truncation product positions identified from western blot analysis were mapped onto the DNMT3A amino acid sequence and compared against predicted disorder regions using predictor of natural disordered regions (PONDR) analysis[33] as well as experimentally derived crystallographic B-factors from available DNMT3A1 protein crystal structures (PDB: 4U7T, 3LLR)[34,35] (Figure 5, Figure S4). Comparison of the truncation positions with predicted disorder regions revealed no clear relationship between truncation position and protein flexibility. While several truncation sites occurred near regions of elevated disorder or solvent accessible regions, multiple truncation products also mapped to relatively ordered regions of the protein. Notably, no consistent enrichment of truncation sites within disordered domains was observed. These findings suggested that proteolytic cleavage at structurally disordered regions alone does not fully account for the truncation pattern.

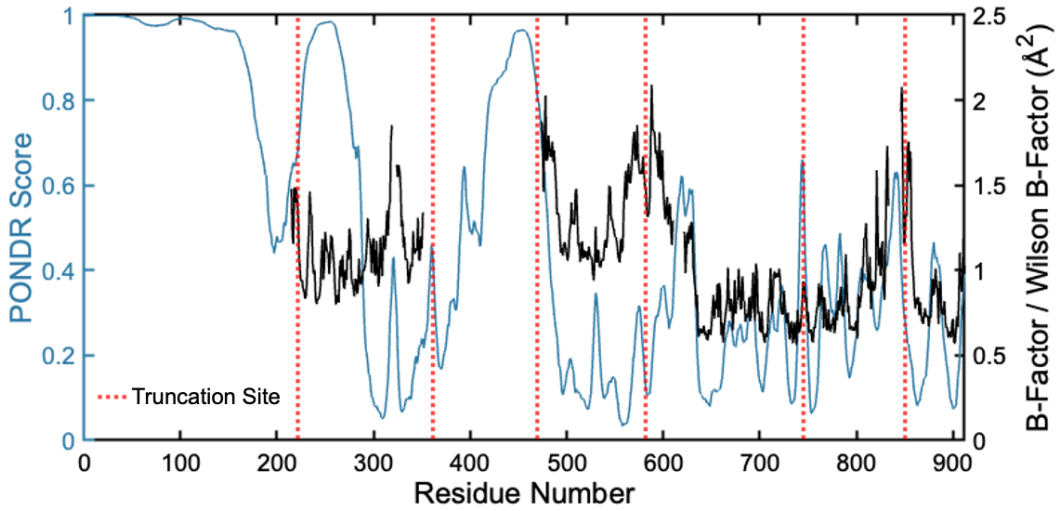



**Figure 5.** Truncation positions (red dashed) estimated from western blot molecular weights were mapped onto the DNMT3A1 amino acid sequence and compared with PONDR (blue) and crystallographic B-factor values (black) (PDB: 4U7T, 3LLR).

Proteolytic cleavage is unlikely to be a major contributor to DNMT3A's truncation products since the observed truncation sites do not consistently correspond to structurally

flexible regions of the protein (Figure 5). However, because DNMT3A truncation products were observed across all expression conditions tested and some truncation sites are associated with flexible or solvent accessible regions of the protein (Figure 5, Figure S4), the contribution of proteolytic degradation was investigated using serine protease inhibitors during cell lysis. PMSF has been previously used in our lab's standard expression and purification protocol[12,21]. To test the capability of other serine protease inhibitors, AEBSF and an EDTA-free protease inhibitor cocktail were selected. Whole-cell pellets were resuspended directly into 2x Laemmli buffer containing the respective protease inhibitors prior to denaturation and western blotting. Western blot analysis revealed no noticeable difference in the band pattern of truncation products across conditions (Figure 6). These findings further suggest that the truncation pattern arises before cell lysis, likely during protein expression.

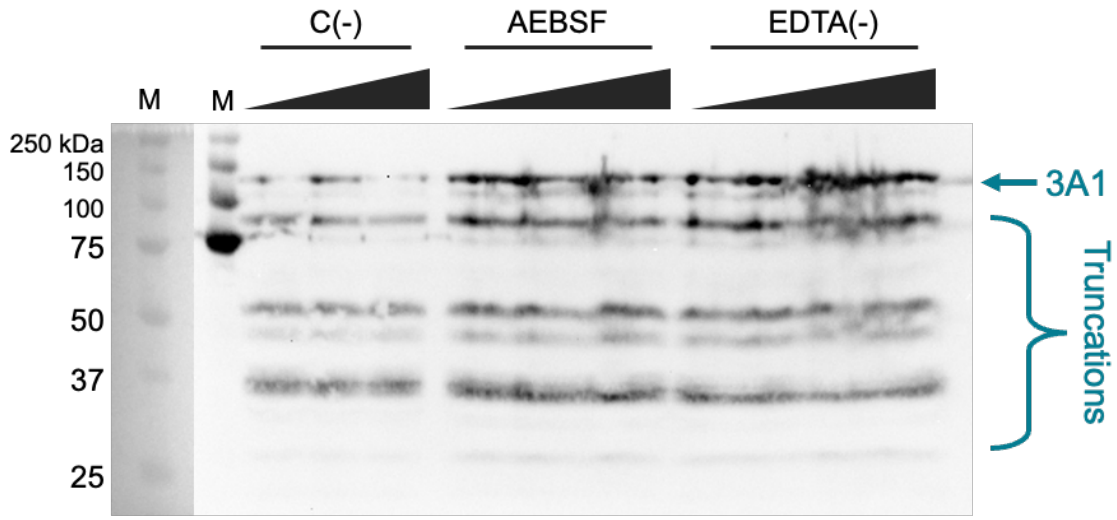



**Figure 6.** Western blot analysis of DNMT3A1 expression in the absence of protease inhibitors, in the presence of AEBSF, or in the presence an EDTA-free protease inhibitor cocktail. No substantial changes in the truncation pattern were observed following protease inhibition.

*Investigation of Codon Usage in Recombinant DNMT3A1 Expression*

One potential explanation for the truncations of recombinant DNMT3A1 in *E. coli* is the incompatibility between human codon usage and bacterial translational machinery. Human proteins frequently contain codons that are considered rare in *E. coli*, where the corresponding tRNAs are present at substantially lower abundance[36]. Translation through these rare codons can promote translational stalling or premature termination[36]. Because DNMT3A1 is a large, multidomain human enzyme containing 912 amino acids, codon bias represents a plausible mechanism contributing to the observed truncation products.

Because the truncation products did not strongly correlate with predicted structural flexibility (Figure 5), rare codon usage contributing to truncation products were investigated. Approximate truncation positions were estimated from the molecular weights of the western blot bands observed in Figure 4 and mapped onto the DNMT3A1 amino acid sequence. Analysis of codon usage surrounding these truncation sites revealed the presence of multiple codons considered rare in *E. coli*. Specifically, codons with frequencies below either 10% or 16% relative abundance in *E. coli* were identified in close proximity to several truncation positions (Table 2). These rare codons were located near residues corresponding to truncation products at approximately amino acids 221, 362, 469, 581, 745, and 851.

**Table 2.** Rare *E. coli* codons located near estimated DNMT3A truncation positions.

| | *E. Coli* Codon Frequency | |
|---|---|---|
| Truncation Position | <10% Frequency | <16% Frequency |
| 221 | R212 | G223 |
| 362 | R320 | P363 |
| 469 | R476 | P465 |
| 581 | R556 | P580 |
| 745 | R736 | R742 |
| 851 | n/a | L859 |

The apparent association between truncation positions and nearby rare codons supported the hypothesis that ribosomal pausing may contribute to premature truncation during recombinant DNMT3A1 expression. Prolonged ribosomal pausing at rare codons can destabilize translation complexes and increase susceptibility to incomplete protein synthesis or co-translational misfolding[26,36]. Additionally, translational stalling within large multidomain proteins may impair proper folding coordination between domains, increasing the likelihood of degraded or partially translated intermediates.

To test whether codon usage was a major determinant of DNMT3A1 truncation products, a codon-optimized DNMT3A1 construct was purchased in which rare human codons were replaced with codons most frequently utilized in *E. coli* while preserving the amino acid sequence. Western blot analysis comparing expression of the original DNMT3A1 construct and the codon-optimized construct revealed no substantial reduction in truncation products (Figure 7). The codon-optimized construct exhibited a truncation pattern highly similar to that observed with the original DNMT3A1 plasmid, indicating that codon optimization alone does not rescue expression of the intact DNMT3A1. These findings suggest that although translational pausing at rare codons may contribute to expression instability, codon bias is unlikely to represent the sole mechanism driving DNMT3A truncation. Instead, DNMT3A1 instability during recombinant expression likely arises from a combination of factors such as translational stalling, multidomain folding complexity, co-translational misfolding, or intrinsic instability of large eukaryotic proteins in bacteria. The inability of codon optimization to substantially improve DNMT3A1 recovery further highlights the difficulty of expressing large chromatin-associated human proteins in prokaryotic systems.

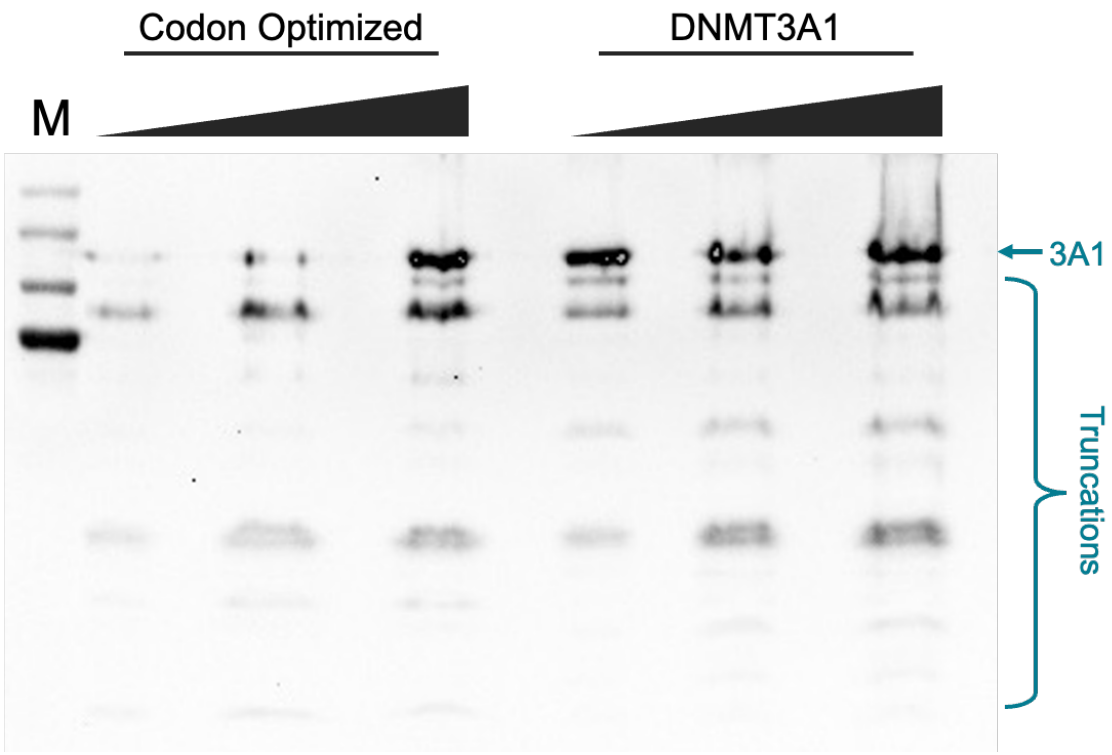



**Figure 7.** Western blot comparison of the DNMT3A1 expressed from either the native human coding sequence or a codon-optimized construct designed for expression in *E. coli*. Overall truncation pattern remained highly similar between constructs.

Future studies may benefit from combining low-temperature induction with additional approaches such as co-expression with molecular chaperones, alternative expression strains, or eukaryotic expression systems. Recombinant expression of DNMT3A1 using the Baculovirus Expression Vector System (BEVS) in *Spodoptera frugiperda* (Sf9) insect cells has previously been shown to yield intact DNMT3A1 with >95% purity[37]. Although baculovirus expression is generally ideal for recombinant expression of complex eukaryotic proteins, recombinant expression in *E. coli* is far more rapid and cost effective. The co-expression of GroEL/ES in DNMT3A1 could aid in proper domain folding during protein expression, as it has demonstrated greater efficiency of correct folding of both prokaryotic and eukaryotic recombinant proteins expressed in *E. coli*[38,39]. Alternative expression strains

such as Rosetta(DE3), which supplies tRNAs for rare codons in *E. coli*; C41(DE3), which aids in folding dynamic proteins; and Lemo21(DE3), which promotes slow protein production and proper folding; may improve DNMT3A1 purity by reducing truncation events[40–42]. However, co-expression with molecular chaperones, alternative expression strains, or eukaryotic expression systems are not explored in this work but may help optimize DNMT3A1 recombinant expression in *E. coli*.

**D. Methods**

*Protease Inhibitors*

AEBSF Protease Inhibitor (Thermo Scientific, Cat. No. 78431)

Pierce™ Protease Inhibitor Tablets, EDTA-free (Thermo Scientific, Cat. No. A32965)

*DNMT3A$^{MTase}$ Expression*

The DNMT3A methyltransferase domain (DNMT3A$^{MTase}$; residues 634-912) was transformed and expressed in NiCo21(DE3) *Escherichia coli* cells (New England Biolabs) with a codon-optimized pET28a-hDNMT3A$^{MTase}$ expression plasmid containing a N-terminal His-tag. Cell cultures were grown in LB medium at 37˚C to $OD_{600}$ of 0.8, cooled to 16˚C, and induced with 1 mM isopropyl β-D-1-thiogalactopyranoside (IPTG). Following 16 hours of expression, cells were harvested by centrifugation at 8,000 x g, flash frozen in liquid nitrogen, and stored at -80˚C.

*DNMT3A$^{MTase}$ Protein Purification*

Frozen cell pellets were resuspended in lysis buffer containing 50 mM Tris-HCl, 500 mM NaCl, 50 mM imidazole, 0.5 mM DTT, 1 mM PMSF, 10% glycerol (v/v), and 0.2% Triton-X100 (v/v) at pH 7.8. Cells were lysed by sonication and clarified by centrifugation at 18,000 x g for 2x 30 min. Following equilibration in 50 mM Tris-HCl, 500 mM NaCl, 50 mM

imidazole, and 10% glycerol (v/v) at pH 7.8; the resulting soluble extract was loaded onto an ÄKTA Start FPLC system (GE Healthcare) equipped with a 1 mL HisTrap Excel $Ni^{2+}$ IMAC column (Cytiva). The column was washed with 50-75 mM imidazole to remove nonspecifically bound proteins prior to elution with an imidazole gradient from 75-500 mM. Fractions corresponding to the primary $DNMT3A^{MTase}$ peak were pooled, concentrated with a 15 mL 10 kDa MWCO Amicon filter, and buffer-exchanged into storage buffer containing 50 mM Tris, 200 mM NaCl, 1 mM EDTA, 1 mM DTT, 20% glycerol (v/v) at pH 7.2, 7.5, 8.0 or 8.5. Purified protein was flash frozen in liquid nitrogen and stored at -80˚C. Protein concentrations were determined spectrophotometrically at 280 nm using a calculated extinction coefficient of 38,180 $M^{-1}$ $cm^{-1}$ for the monomeric subunit of $DNMT3A^{MTase}$.

*DNMT3A1 Expression*

DNMT3A1 (DNMT3A1; residues 1-912) was transformed and expressed in NiCo21(DE3) *Escherichia coli* cells (New England Biolabs) with a pET28a-hDNMT3A1 expression plasmid or a codon-optimized pET28a-hDNMT3A1 expression plasmid (Twist Bioscience) containing a N-terminal His-tag. Cell cultures were grown in LB medium at 37˚C to $OD_{600}$ of 0.7, cooled to 16˚C, and induced with 1 mM isopropyl β-D-1-thiogalactopyranoside (IPTG) for 16 h unless otherwise noted. Cells were harvested by centrifugation at 8,000 x g, flash frozen in liquid nitrogen, and stored at -80˚C.

*DNMT3A1 Protein Purification*

Frozen cell pellets were resuspended in lysis buffer containing 50 mM HEPES, 500 mM NaCl, 50 mM imidazole, 0.5 mM DTT, 1 mM PMSF, 25µg/mL DNAse 1, 1% glycerol (v/v), and 0.2% Triton-X100 (v/v) at pH 7.8. Cells were lysed by sonication and clarified by centrifugation at 18,000 x g for 2x 30 min. Following equilibration in 50 mM Tris-HCl, 500

mM NaCl, 50 mM imidazole, and 1% glycerol (v/v) at pH 7.8; the resulting soluble extract was loaded onto an ÄKTA Start FPLC system (GE Healthcare) equipped with a 5 mL HisTrap HP $Ni^{2+}$ IMAC column (Cytiva). The column was washed with 50-75 mM imidazole to remove nonspecifically bound proteins prior to elution with an imidazole gradient from 75-500 mM. Fractions corresponding to the primary DNMT3A1 peak were pooled, concentrated with a 15 mL 100 kDa MWCO Amicon filter, and buffer-exchanged into storage buffer containing 50 mM Tris, 200 mM NaCl, 1 mM EDTA, 1 mM DTT, 10% glycerol (v/v) at pH 7.8. Purified protein was flash frozen in liquid nitrogen and stored at -80˚C. Protein concentrations were determined spectrophotometrically at 280 nm using a calculated extinction coefficient of 142,010 $M^{-1}$ $cm^{-1}$ for the monomeric subunit DNMT3A1.

*Western immunoblot*

1 mL *Escherichia coli* culture aliquots were collected at the desired induction time points and pelleted by centrifugation at 6,000 x g. Cell pellets were directly resuspended in 100 µL of 2x Laemmli sample buffer and heated at 95˚C for 10 min. Samples were resolved by SDS-PAGE using 8% polyacrylamide gels at 120 V. Following electrophoresis, proteins were transferred to 0.45 µm polyvinylidene difluoride (PVDF) membranes (Thermo Fisher Scientific 88518). Prior to transfer, PVDF membranes were activated in methanol for 1 min and equilibrated in Towbin transfer buffer (25 mM Tris, 192 mM glycine, 20% methanol, pH 8.3) for 10-15 min. Wet transfer was performed at 100 V for 1 hour at 4˚C. Membranes were dried at 37˚C for 30 min, reactivated in methanol for 1 min, and equilibrated in Tris-buffered saline containing 0.1% Tween-20 (TBST; 20 mM Tris, 150 mM NaCl, 0.1% Tween-20, pH 7.6). Membranes were blocked for 1 hour at room temperature with 5% non-fat dry milk prepared in TBST (w/v). DNMT3A1 proteins were detected using a mouse monoclonal anti-

6xHis primary antibody (Invitrogen MA1-21315) diluted 1:2,500 in blocking buffer and incubated overnight at 4˚C with gentle agitation. Membranes were subsequently washed three times for 5-10 min in TBST and incubated for 1 hour at room temperature with a goat anti-mouse IgG horseradish peroxidase (HRP)-conjugated secondary antibody (Thermo Fisher Scientific 31430) diluted 1:2,500 in blocking buffer. Membranes were then washed three additional times with TBST. Protein bands were visualized using enhanced chemiluminescence (ECL) reagent as per manufacturer instructions (Thermo Fisher Scientific 32209) and imaged using an iBright 1500 imaging system.

*Methylation Assay*

Reactions were performed with 50mM Tris pH 7.8, 1mM EDTA, 15mM NaCl, 0.2 mg/mL BSA, 1 mM DTT, 5 µM SAM (1:50 [$^3$H]-SAM:SAM), and 50 nM DNMT3A$^{MTase}$ at pH 7.8. 12 µL reactions were initiated with 5 µM DNA substrate (Poly-dI-dC) and incubated at 37˚C for 30 min in triplicate, then quenched with 12 µL 0.3% SDS. 20 µL of quenched reactions were spotted on Hybond-N+ membranes (Cytiva RPN303B), then washed with gentle agitation 3x with 50 mM potassium phosphate buffer ($K_2HPO_4$/$KH_2PO_4$ at pH 7.8) for 5 min, 1x with 70% ethanol (v/v) for 5 min, and 1x with 100% ethanol for 5 min. Membranes were dried and counted with a Hidex 300 SL scintillation counter.

## E. Supplementary Information

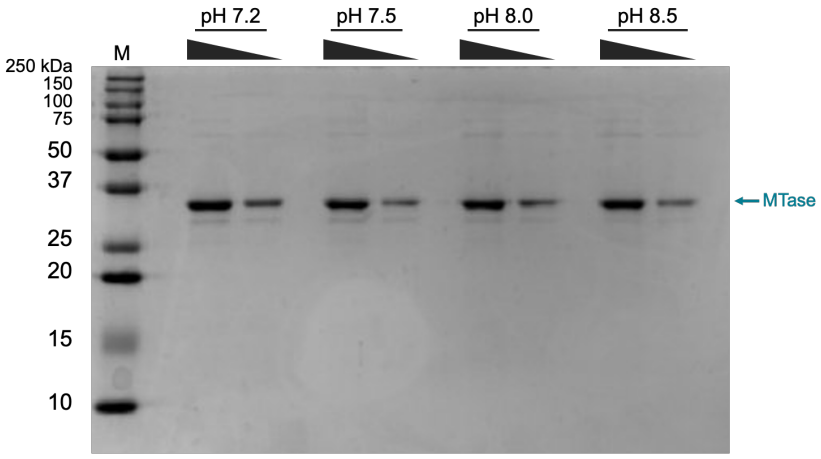



**Figure S1.** SDS-PAGE of DNMT3A$^{MTase}$ following $Ni^{2+}$ IMAC purification, ultrafiltration, and buffer-exchange into storage buffers at pH 7.2, 7.5, 8.0, or 8.5. Comparable purity was observed across all storage conditions.

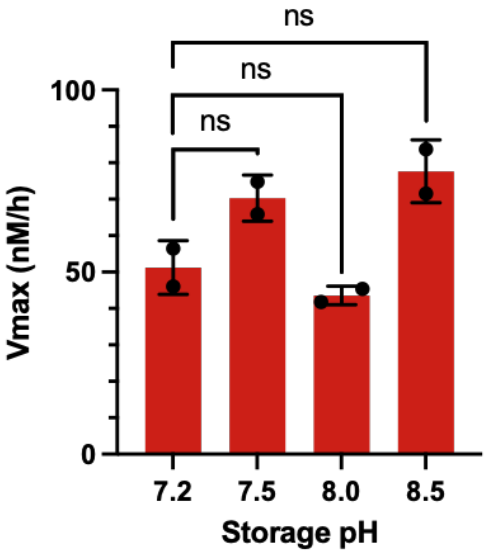



**Figure S2.** Methylation of DNMT3A$^{MTase}$ stored at pH 7.2, 7.5, 8.0, or 8.5. Reactions were performed using 50 nM DNMT3A$^{MTase}$ and 5 µM DNA substrate concentrations to compare maximal catalytic rates. No statistically significant differences were observed among storage conditions. Values are reported as mean ($n$ = 2 samples) ± SD. Data analyzed with unpaired t-test; comparisons between pH 7.2 and 7.5, 7.2 and 8.0, and 7.2 and 8.5. Analysis revealed non-significant variated between comparisons ($p>0.05$, $p>0.05$, and $p>0.05$, respectively). Data comparison performed with Prism v10.6.

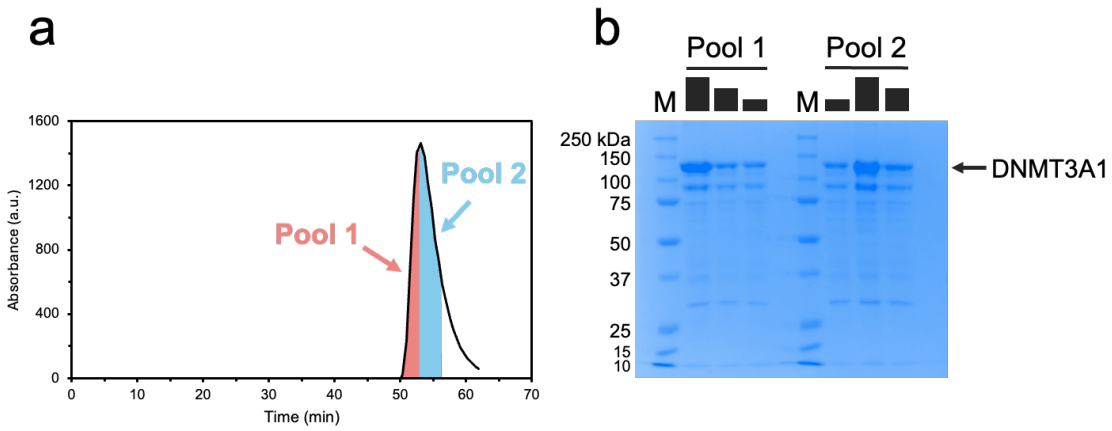



**Figure S3.** After HisTrap HP elutions, DNMT3A1 samples were concentrated with a 15 mL 100 kDa MWCO Amicon filter, and buffer-exchanged into storage buffer. a) Samples were then applied to a 16/60 HiLoad column (GE Pharmacia) packed with Superdex 200 pg (Cytivia) and eluted at 1 mL/min (detection λ at 230 nm). Fractions from 50-52 min (Pool 1) and 53-56 min (Pool 2) were collected and further concentrated before flash freezing and storing at -80˚C. b) Pool 1 and Pool 2 final purified DNMT3A1 samples resolved on an 8% SDS-PAGE gel showed 46% and 42% purity, respectively. Sample volume (5, 10, and 15 µL) indicated above each lane.

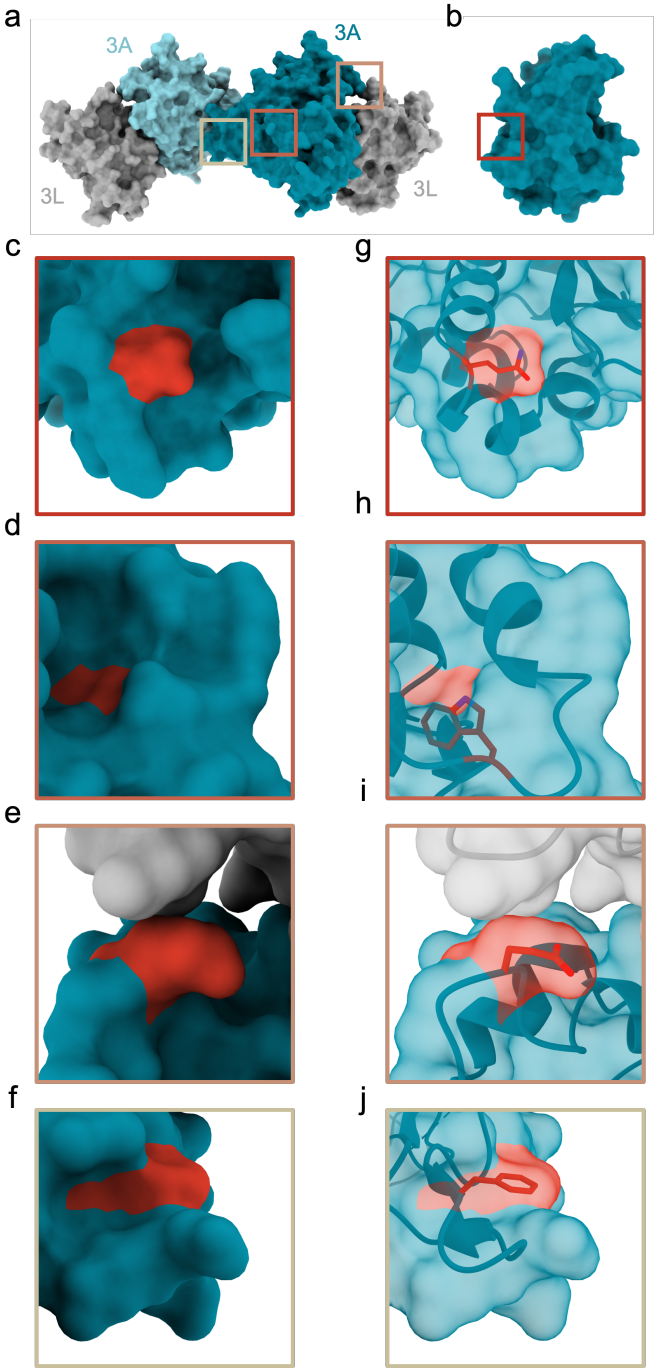



**Figure S4.** Surface representation of DNMT3A1 generated in ChimeraX showing residues corresponding to experimentally observed truncation positions. a) Surface representation of DNMT3A/3L heterotetramer (PBD: 4U7P). b) Surface representation of the PWWP domain (PDB: 3LLR). c-f) Surface representation and g-j) ribbon structure of truncation sites. c,g) Q362, d,h) W581, e,i), E745, and f,j) F851surface and ribbon representation. Solvent-accessible truncation-site residues are indicated in red. Truncation positions I221 and E469 do not have available resolved protein structures.

# III. Developing High-Throughput Screening Assays for Small-Molecule Inhibitors of DNMT3A Regulatory Interactions

## A. Abstract

DNMT3A is a critical epigenetic writer enzyme responsible for establishing *de novo* DNA methylation patterns during cellular differentiation and development. Recruitment and regulation of DNMT3A activity are mediated through extensive crosstalk with histone PTMs. Of note, histone H3 tail PTMs containing H3K4me0 and H3K36me3 interact with DNMT3A's ADD and PWWP domains, respectively. Dysregulation of these interactions contributes to aberrant DNA methylation patterns associated with hematological malignancies, including AML. While current FDA-approved DNMT inhibitors broadly inhibit catalytic activity via nucleoside incorporation, these compounds exhibit cytotoxicity with little selectivity for specific regulatory interactions. Fluorescence anisotropy and AlphaLISA assays were developed to establish screening platforms for identifying small-molecule inhibitors that selectively disrupt the PPIs of DNMT3A with histone-tail PTMs. Preliminary screening of twenty compounds from the NIH Diversity Set VII library using AlphaLISA did not yield reproducible selective inhibitors, yet these studies establish a workflow for future high-throughput screening of small molecules targeting DNMT3A regulatory PPIs.

## B. Introduction

Epigenetic regulation of gene expression relies on the dynamic crosstalk between DNA methylation, histone post-translational modifications (PTMs), chromatin-associated proteins, and non-coding RNAs[1–4]. DNA methyltransferase 3A (DNMT3A) is a *de novo* DNA methyltransferase that is responsible for establishing DNA methylation patterns crucial for

transcriptional silencing, genomic imprinting, X-chromosome inactivation, and cellular differentiation in a variety of organism including humans[5–7]. DNMT3A activity and genomic recruitment are tightly regulated through interactions with chromatin components, including interactions with histone H3 tail PTMs. These histone tail PTMs provide a mechanism through which DNMT3A can selectively target specific genomic loci despite having relatively low intrinsic sequence specificity in DNA[8,9].

Among the best-characterized regulatory interactions are the recognition of unmethylated histone H3 lysine 4 (H3K4me0) by the ATRX-DNMT3-DNMT3L (ADD) domain and the recognition of the dimethylated or trimethylated H3 lysine 36 (H3K36me2/3) by the Pro-Trp-Trp-Pro (PWWP) domain. Structural and biochemical investigations[10,11] have demonstrated that the ADD domain preferentially binds H3 tails lacking K4 methylation, whereas methylation of H3K4 (i.e. H3K4me3) disrupts this binding interaction and promotes an autoinhibitory conformation within DNMT3A (Figure 1a-b)[12]. Conversely, the PWWP domain recognizes H3K36me2/3 marks and contributes to DNMT3A recruitment towards actively transcribed gene bodies (Figure 1c-d) [13–15]. These histone-mediated recruitment mechanisms represent critical regulatory pathways controlling locus-specific DNA methylation patterns.

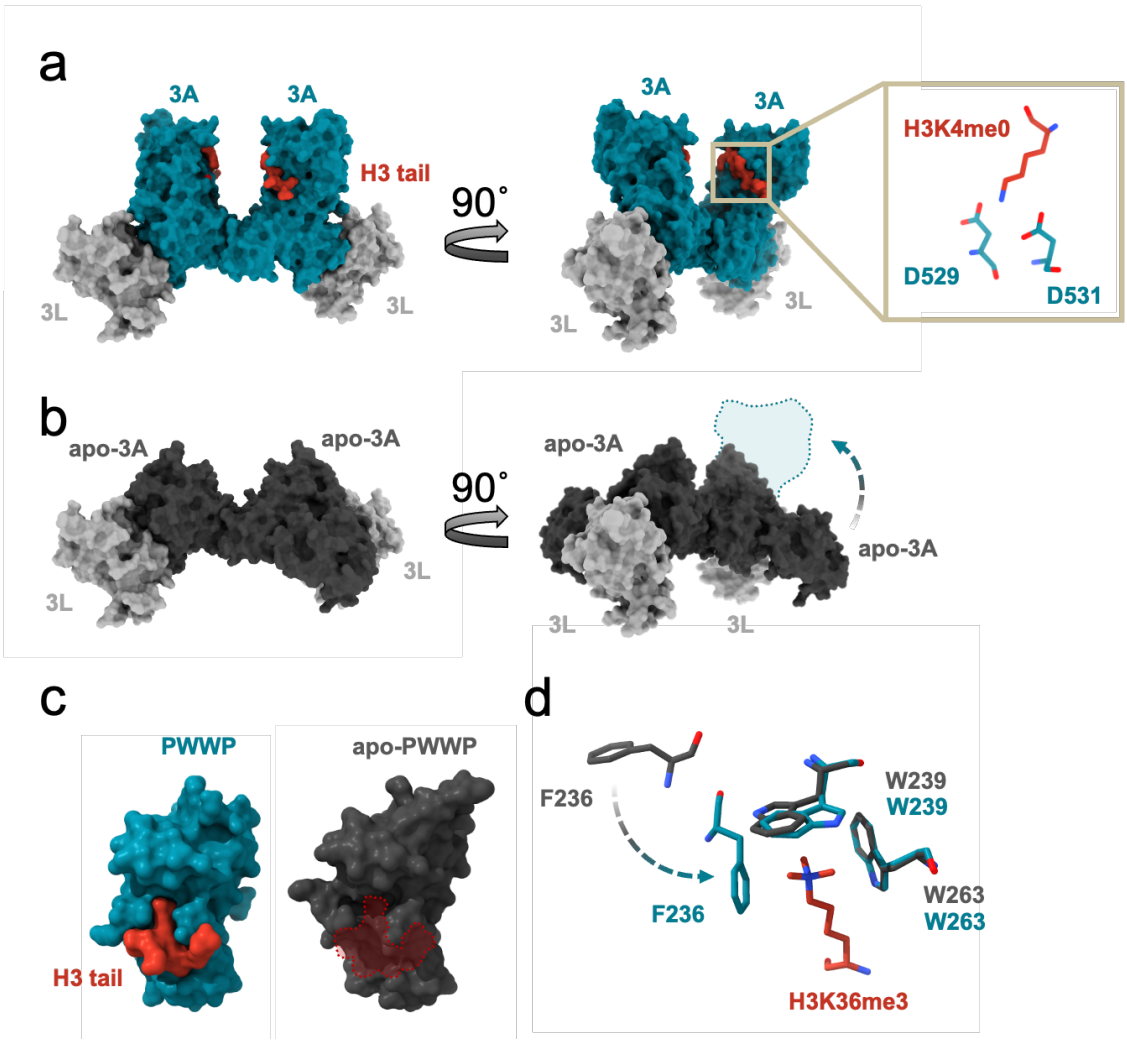



**Figure 1.** a) Protein crystal structure of the DNMT3A/3L bound with H3K4me0 peptide (aa 1-12). Inset displays key interactions between the unmethylated H3K4 and Asp529/Asp531 within the ADD domain binding pocket. (PDB: 4U7T; 3A residues 474-912, 3L residues 177-379) b) Protein crystal structure of the autoinhibited conformation of DNMT3A in the absence of H3K4me0 binding. Recognition of H3K4me0 relieves autoinhibition, undergoing a large conformational shift to promote DNMT3A activation. (PDB: 4U7P; 3A residues 474-912, 3L residues 179-378) c) Protein crystal structure of DNMT3B$^{PWWP}$ domain bound and unbound to an H3K36me3-containing histone tail (aa 32-39). (PDB: 5CIU; residues 216-351, PDB: 3FLG; residues 216-350) d) Aromatic cage responsible for recognition of H3K36me3.

Disruption of DNMT3A regulation can lead to aberrant methylation landscapes, ultimately contributing to dysregulated cellular differentiation and various forms of cancer development. For instance, DNMT3A mutations occur in approximately 20-30% of all acute

myeloid leukemia (AML) cases, making it the most mutated gene in AML patients[16–18]. Consequently, DNMT3A has emerged as an important therapeutic target in hematological malignancies[16]. The current FDA-approved drugs targeting DNMT activity are the nucleoside analogs azacitidine and decitabine[19,20]. These compounds are incorporated into DNA and irreversibly trap DNMT enzymes during DNA methylation, driving DNA demethylation during subsequent cycles of replication[21]. Although these nucleoside inhibitors demonstrate adequate clinical efficacy in certain leukemias and myelodysplastic syndromes, their therapeutic utility is limited by multiple shortcomings. Decitabine and azacitidine suffer from poor pharmacokinetic properties like rapid degradation by cytidine deaminase and a terminal half-life of less than one hour[22], which limits bioavailability and therapeutic efficacy. Furthermore, their mechanism-based inhibition broadly impedes DNA methylation machinery, resulting in a lack selectivity and ultimately substantial cytotoxicity[21]. These limitations expose an unmet clinical need for next-generation DNMT3A therapeutics that achieve greater target selectivity and minimize systemic cytotoxicity.

Inhibitors that target DNMT3A outside of the catalytic active site or S-adenosyl-L-methionine (SAM) binding pocket offer a promising alternative to currently approved DNMT-targeting therapies. Structure-activity relationship (SAR) studies from our laboratory identified phthalazinone-derived compounds that selectively inhibit DNMT3A through allosteric mechanisms instead of competition with DNA or SAM[23]. In addition, our group reported first-in-class small-molecule inhibitors capable of disrupting PPIs at the DNMT3A tetramer interface[24]. Because allosteric sites are generally less conserved than catalytic active sites, targeting these regions may provide enhanced selectivity and reduced cytotoxicity. DNMT3A relies on numerous partner proteins for enhanced methylation and locus-specific

methylation patterns; targeting offer a promising strategy for the development of next-generation epigenetic therapeutics.

This work explores the disruption of DNMT3A recruitment interactions with chromatin as a promising strategy for the development of selective and noncytotoxic anti-leukemia therapies. Epigenetic regulatory pathways have proven to be highly druggable therapeutic targets, as demonstrated by the clinical success of histone deacetylase (HDAC) inhibitors such as Vorinostat and Romidepsin[25,26], as well as the isocitrate dehydrogenase (IDH) targeting Enasidenib[27], all of which have received FDA approval for the treatment of hematological malignancies. Unlike nucleoside inhibitors' suicide inhibition of DNMTs, selectively modulating DNMT3A recruitment pathways may perturb aberrant methylation patterns while preserving basal methyltransferase activity required for normal cellular function. The interactions between DNMT3A and histone H3 tails containing H3K4me0 and H3K36me3 are compelling targets because both recruitment mechanisms are structurally characterized and mediated through distinct regulatory domains; the ADD domain recognizes H3K4me0, whereas the PWWP domain recognizes H3K36me2/3. High-resolution structural information is available for these complexes[8,12], providing a strong foundation for the rational design of biochemical assays and the identification of small molecules capable of selectively disrupting individual DNMT3A-histone tail interactions. Such inhibitors could offer a novel means of modulating disease-associated DNA methylation patterns while avoiding the broad cytotoxicity associated with current nucleoside-based therapies.

## C. Results & Discussion

*Development of AlphaLISA Assays for Monitoring DNMT3A-Histone Tail Interactions*

To identify inhibitors capable of selectively disrupting DNMT3A recruitment interactions with modified histone H3 tails, proximity-based AlphaLISA assays were developed using biotinylated H3K4me0 (aa 1-21) and H3K36me3 peptides (aa 23-44). AlphaLISA technology relies on donor and acceptor bead proximity to generate luminescent signal and is particularly well suited for detecting larger macromolecular interactions and protein complexes in solution. Compared to fluorescence resonance energy transfer (FRET)-based methods which measures molecular proximity at approximately 10 nm, AlphaLISA operates optimally at larger intermolecular distances (i.e. 200 nm)[28–30]. These characteristics make AlphaLISA attractive for monitoring DNMT3A-histone tail interactions and has been previously leveraged to investigate DNMT3A-histone tail PTMs on recombinant semi-synthetic nucleosomes[31,32].

To establish assay conditions suitable for inhibitor screening, $EC_{50}$ binding curves were generated by titrating increasing concentrations of DNMT3A1 (0.1-10 nM) against fixed concentrations of biotinylated H3K4me0 or biotinylated H3K36me3 peptides (12.5 nM). Streptavidin donor beads and nickel-chelate acceptor beads were used to detect proximity between the biotinylated peptide and His-tagged DNMT3A. Both H3K4me0 and H3K36me3 peptides produced concentration-dependent AlphaLISA signal upon addition of DNMT3A (Figure 2). Michaelis-Menten curve-fitting generated $EC_{50}$ values of approximately 0.58 nM for H3K4me0 and 0.75 nM for H3K36me3. Based on these binding curves, approximately 1 nM DNMT3A was selected for subsequent screening conditions. At this concentration, the assay produced a sufficient signal while remaining sensitive to decreases in proximity signal

caused by PPI disruption, which are necessary for detecting inhibitors capable of modulating DNMT3A-histone tail recruitment.

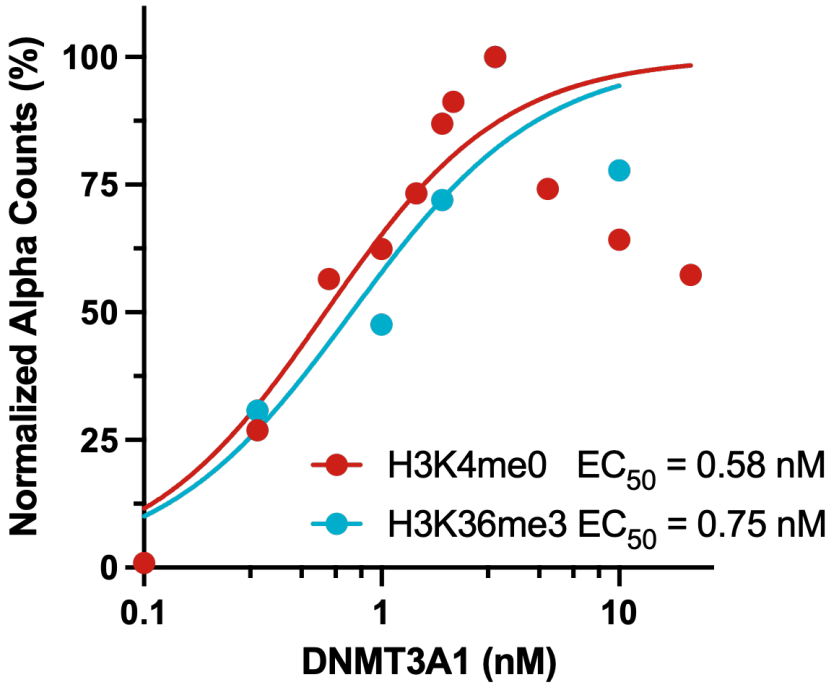



**Figure 2.** $EC_{50}$ AlphaLISA binding curve of DNMT3A1 with biotin-labeled H3K4me0 (aa 1-21) and H3K36me3 (aa 23-44) tails. Prism v10.6 [Agonist] vs. normalized response -- Variable slope fit generated $EC_{50}$ values of 0.58 nM for H3K4me0 ($R^2$ = 0.70) and 0.75 nM for H3K36me3 ($R^2$ = 0.89).

Although AlphaLISA provided a sufficiently robust platform for detecting DNMT3A recruitment interactions, signal variability and relatively modest signal-to-noise ratios were observed between experiments (Figure S1). One likely contributor to this limitation is the relatively small size of the biotinylated histone tail peptides used in these assays. The 21-amino-acid H3 tail peptides provide fewer opportunities for optimal bead proximity compared to larger nucleosome substrates, potentially reducing signal intensity. Previous results from our group[33] and others[31,32,34] have successfully employed AlphaLISA to monitor interactions between DNMT3A and nucleosomes, which provide substantially larger binding

platforms than isolated histone tail peptides. In principle, AlphaLISA assays with DNMT3A-nucleosome or DNMT3A-histone PTMs, as opposed to DNMT3A-histone tail PTMs, could improve assay performance by increasing alpha count detection and thereby increasing the signal-to-noise ratio. Advances in protein chemistry and semi-synthetic nucleosome assembly have enabled the generation of nucleosomes bearing site-specific histone PTMs, allowing precise interrogation of individual chromatin recruitment mechanisms[35,36]. However, despite their physiological relevance and larger complex, modified nucleosomes remain significantly more expensive to purchase and labor-intensive to produce than small synthetic biotinylated histone peptides. For the purposes of high-throughput screening at nanomolar concentration, biotinylated H3 peptides present a practical compromise between assay throughput, signal detection, scalability, and reagent cost. Nucleosome-substrate AlphaLISA assays may ultimately prove advantageous for secondary validation studies once initial compound screenings identify small molecules that disrupt DNMT3A recruitment interactions.

*Rational Design of Fluorescent Histone Tail Peptides for Fluorescence Anisotropy*

To further validate future hit and lead compounds identified from the AlphaLISA-based screening assay, fluorescence anisotropy assays were designed to detect the same modulation of DNMT3A-histone tail PPIs. Anisotropy assays require fluorescently labeled ligands whose rotational mobility changes upon protein-binding. To develop an anisotropy assay for DNMT3A histone tail interactions, fluorescently labeled histone H3 peptides were rationally designed based on available structural information for DNMT3A-histone tail complexes[12,15].

For the H3K4me0 peptide, a protein crystal structure of DNMT3A (amino acids 476-912) bound to histone H3 tails revealed that the H3K4me0 binds important interactions with

Asp529 and Asp531 of DNMT3A's ADD domain, critical for histone recognition (PDB: 4U7T)[12]. N-terminal residues of the H3 tail forms hydrophobic interactions with residues of the ADD domain that are positioned within a cup-like binding pocket formed by residues including Asp579, Trp581, and Ala575 (Figure 3). Because placement of a bulky fluorophore near this binding epitope would likely sterically interfere with histone tail binding, the fluorescent tag was positioned at the peptide C-terminus instead (Figure 3).

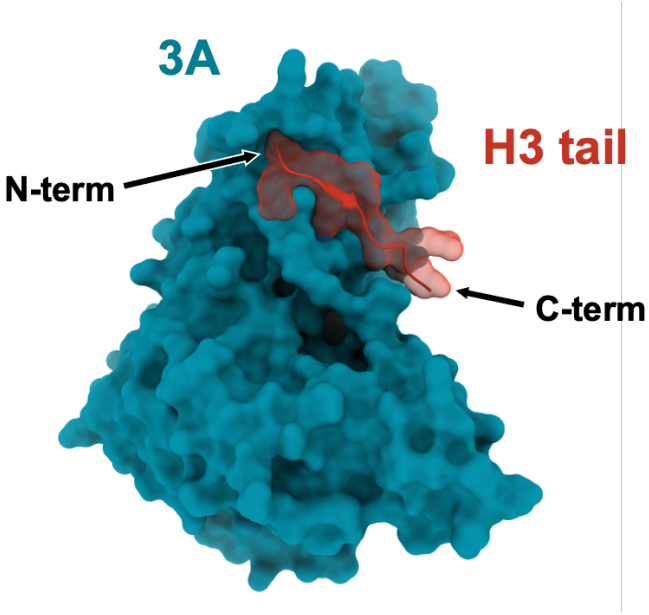



**Figure 3.** Structural analysis of the DNMT3A$^{ADD}$ domain-H3K4me0 complex (PDB: 4U7T) identified the N-terminal region of the histone H3 tail as the primary binding epitope. N-terminal region of the histone H3 tail binds a subtle DNMT3A$^{ADD}$ domain pocket. To minimize steric interference with DNMT3A recruitment, the fluorescein label was positioned at the peptide C-terminus with a flexible glycine linker.

A 14-residue H3K4me0 peptide containing a three-glycine linker followed by a fluorescein isothiocyanate (FITC)-labeled lysine residue was designed with the sequence $H_2N$-ARTKQTARKSGGGK(FITC)-OH. The glycine linker was incorporated to spatially separate the fluorophore from the histone binding epitope and minimize steric interference with DNMT3A recognition. The glycine linker was expected to provide sufficient distance

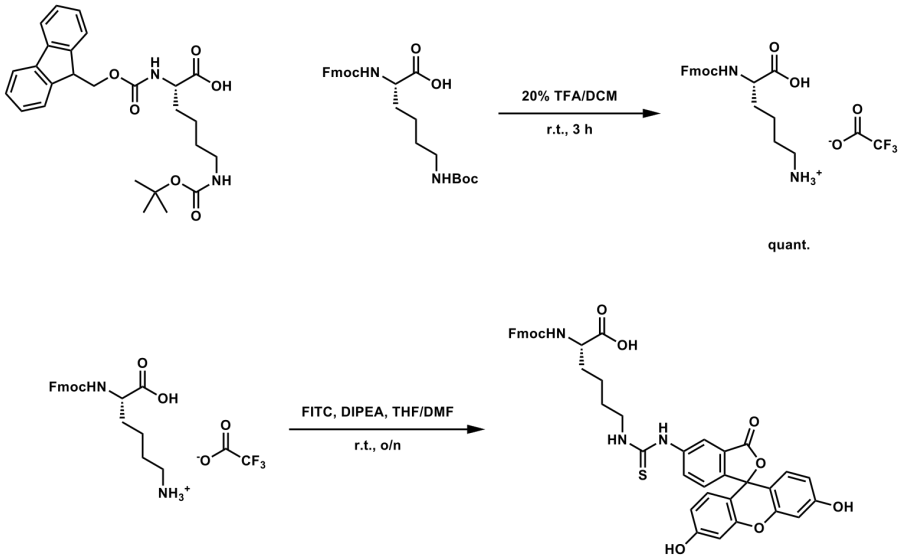
and flexibility to maintain the fluorophore in a solvent-exposed environment while preserving the native binding geometry of the histone peptide within the ADD domain. At the same time, the linker is short enough to avoid introducing excessive rotational freedom that would diminish anisotropy sensitivity upon protein binding.

In contrast, a crystal structure of the DNMT3B PWWP domain in complex with H3K36me3 (PDB: 5CIU)[15] demonstrate that recognition of the histone tail is mediated primarily by residues surrounding methylated Lys36, which inserts into an aromatic binding cage, and by Pro38, which forms an important hydrophobic contact with the PWWP domain (Figure S2). These interactions occur near the center and C-terminus of the peptide's binding epitope. Fluorophore placement at the peptide N-terminus was therefore predicted to minimize interference with H3K36me3 recognition by the PWWP domain. Similarly to the H3K4me0 peptide previously described, a 10-resiude H3K36me3 peptide containing a three-glycine linker with a N-term FITC-label was designed with the sequence (FITC)HN-GGGTGGVK(me3)KP-OH.

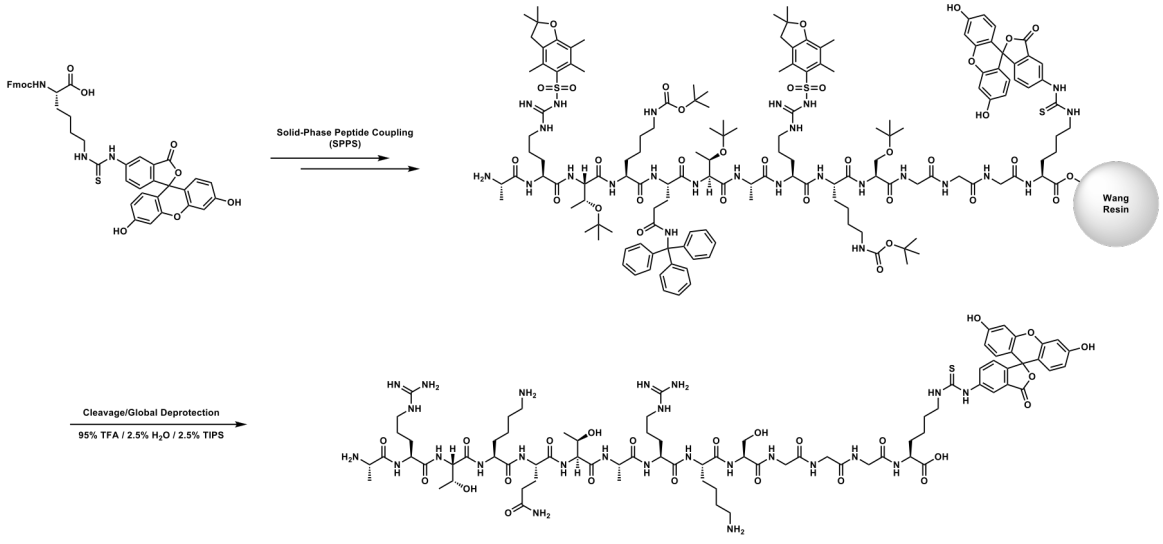
*Synthesis and Functional Validation of H3K4me0-FITC Peptide*

To generate fluorescent H3K4me0 peptides for anisotropy measurements, an Fmoc-Lys(FITC)-OH amino acid building block was synthesized for incorporation during solid-phase peptide synthesis (SPPS). The synthesis strategy involved initial deprotection of Fmoc-Lys(Boc)-OH to expose the lysine ε-amine followed by coupling of fluorescein isothiocyanate (FITC) to generate the fluorescent lysine derivative (Scheme 1). The resulting Fmoc-Lys(FITC)-OH building block was then incorporated at the peptide C-terminus during SPPS of the H3K4me0 peptide sequence (Scheme 2). Incorporation of the FITC-labeled peptide during peptide synthesis allowed for standard SPPS protocols; however, future

procedures could incorporate the FITC label during SPPS with a 4-methyltrityl (Mtt) orthogonal protecting group to allow for the first lysine amino acid to fully bind to the Wang resin, promoting higher conversion and yield. LC-MS analysis of the final H3K4me0-FITC peptide was deemed inconclusive, likely due to residual trifluoroacetic acid (TFA) interfering with electrospray ionization efficiency.




**Scheme 1.** Synthesis of Fmoc-Lys(FITC)-OH.




**Scheme 2.** Solid-phase synthesis of the H3K4me0-FITC peptide. The synthetic Fmoc-Lys(FITC)-OH was incorporated during solid-phase peptide synthesis to generate the H3K4me0-FITC probe.

Following synthesis, the H3K4me0-FITC peptide was evaluated to determine whether it produced fluorescence and anisotropy signals suitable for binding measurements. Increasing peptide concentrations were analyzed to identify conditions that generated robust fluorescence intensity while maintaining stable polarization measurements (Figure 4a-b). Fluorescence intensity measurements demonstrated that peptide concentrations of approximately ≥5 nM produced strong detectable signal above background (Figure 4). Likewise, anisotropy measurements became highly reproducible and stable at concentrations ≥5 nM, suggesting that this concentration range provided sufficient signal for following binding experiments.

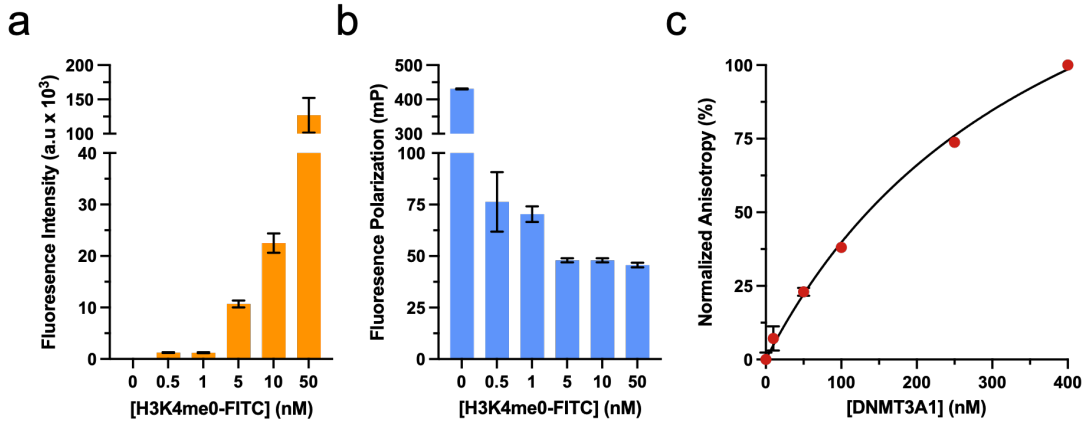



**Figure 4.** a) Fluorescence intensity of the H3K4me0-FITC peptide as a function of peptide concentration and b) corresponding fluorescence anisotropy measurements. Reproducible polarization values detected at concentrations ≥5 nM. Values represent mean ± SD ($n$ = 3 samples). c) Titration of DNMT3A1 against 10 nM H3K4me0-FITC peptide. Values represent mean ± SD ($n$ = 2 samples) except for [DNMT3A1] ≥ 100 nM due to large material consumption. Prism v10.6 Michaelis-Mentent fit generated $V_{max}$ = 195% and $K_m$ = 390 nM ($R^2$ = 0.99).

To determine whether the fluorescent peptide retained functional binding to DNMT3A, increasing concentrations of DNMT3A1 (0-400 nM) were titrated against fixed concentrations of H3K4me0-FITC peptide (10 nM). Increasing DNMT3A1 concentrations

produced a corresponding increase in fluorescence anisotropy, indicating the formation of the larger DNMT3A-H3 tail complex consistent with previous reports[37](Figure 4c). Importantly, labeled peptide remained competent for DNMT3A recognition despite incorporation of the fluorophore and glycine linker.

Additional control experiments were performed to assess assay specificity (Figure 5). Free Lys(FITC)-OH was incubated with DNMT3A1 to examine if the starting material had any non-specific binding interactions with the enzyme. In addition, the synthesized H3K4me0-FITC peptide was incubated with the DNMT3A1 and the DNMT3A methyltransferase domain ($DNMT3A_{MTase}$) which does not contain the N-terminal regulatory domains required for H3 tail peptide interactions (Figure 5b). Free Lys(FITC)-OH alone did not exhibit significant anisotropy changes in the presence of DNMT3A1, demonstrating that the FITC fluorophore itself does not interact with the protein. Furthermore, the H3K4me0-FITC peptide interacted with DNMT3A1 but showed minimal binding to the isolated $DNMT3A_{MTase}$. Since $DNMT3A_{MTase}$ does not contain the ADD domain responsible for H3K4me0 recognition, these findings strongly support the specificity of the fluorescently-labeled peptide and validated the H3K4me0-FITC peptide as a functional fluorescence anisotropy probe for monitoring DNMT3A recruitment interactions.

To further validate the specificity of the AlphaLISA assay as well as the functionality of the H3K4me0-FITC peptide, the H3K4me0-FITC peptide was evaluated as a pseudo-inhibitor capable of competing with biotinylated H3 peptides for DNMT3A binding. Addition of increasing concentrations of H3K4me0-FITC peptide selectively reduced AlphaLISA signal generated from DNMT3A interactions with biotinylated H3K4me0 peptides while producing substantially less effect on H3K36me3 interactions (Figure 5a).

The fluorescent peptide contains the same H3K4me0 recognition sequence, demonstrating that the AlphaLISA assay can adequately detect modulation of DNMT3A recruitment pathways. This further validates the funciton of the H3K4me0-FITC peptide and confirmed that the fluorescent modifications did not abolish biologically relevant DNMT3A-binding behavior. The ability of the peptide to selectively compete for H3K4me0 recognition provides strong evidence that both the AlphaLISA and anisotropy assays can monitor authentic DNMT3A recruitment interactions.

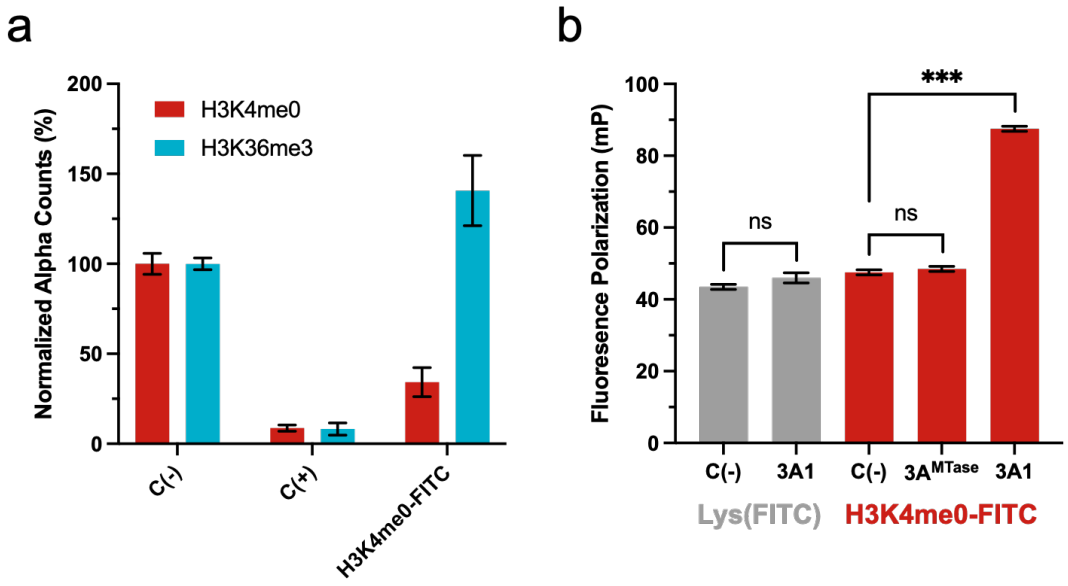



**Figure 5.** a) Addition of H3K4me0-FITC selectively reduced AlphaLISA signal generated by DNMT3A1/biotin-H3K4me0 binding. Values represent mean ± SD ($n$ = 3 samples). b) Fluorescence anisotropy controls evaluating H3K4me0-FITC probe specificity. Free Lys(FITC)-OH exhibited minimal interaction with DNMT3A, whereas the H3K4me0-FITC peptide displayed substantial binding to DNMT3A1 but not the isolated DNMT3AM$^{Tase}$ domain. Values represent mean ± SD ($n$ = 3 samples). Data analyzed with unpaired t-test; comparisons between Lys(FITC)-OH with Lys(FITC)-OH/DNMT3A1, H3K4me0-FITC with H3K4me0-FITC/DNMT3A$^{MTase}$, and H3K4me0-FITC with H3K4me0-FITC/DNMT3A1. Analysis revealed non-significant and significant variation between comparisons ($p>0.05$, $p>0.05$, and $p<0.001$, respectively). Data comparisons performed with Prism v10.6.

*Preliminary Screening of the NIH Diversity Set VII Compound Library*

To assess the feasibility of identifying selective inhibitors of DNMT3A-histone tail interactions with AlphaLISA for high-throughput screening, twenty compounds from the NIH Diversity Set VII library were screened. Compounds were evaluated for their ability to selectively disrupt interactions between DNMT3A and either H3K4me0 or H3K36me3 peptides (Figure 6). Because these histone marks are recognized by distinct DNMT3A reader domains – the ADD domain and the PWWP domain – a compound that selectively inhibits one interaction while leaving the other unaffected would suggest domain-specific inhibition rather than nonspecific interference of DNMT3A PPIs with histone tails. Consequently, this dual-screen strategy provides an internal selectivity control that can distinguish bona fide modulators of DNMT3A chromatin recognition from false-positive hits. Although several compounds initially appeared to modulate AlphaLISA signal, follow-up experiments revealed poor reproducibility. At present, no compounds have demonstrated robust and reproducible selective inhibition of DNMT3A interactions with either H3K4me0 or H3K36me3.

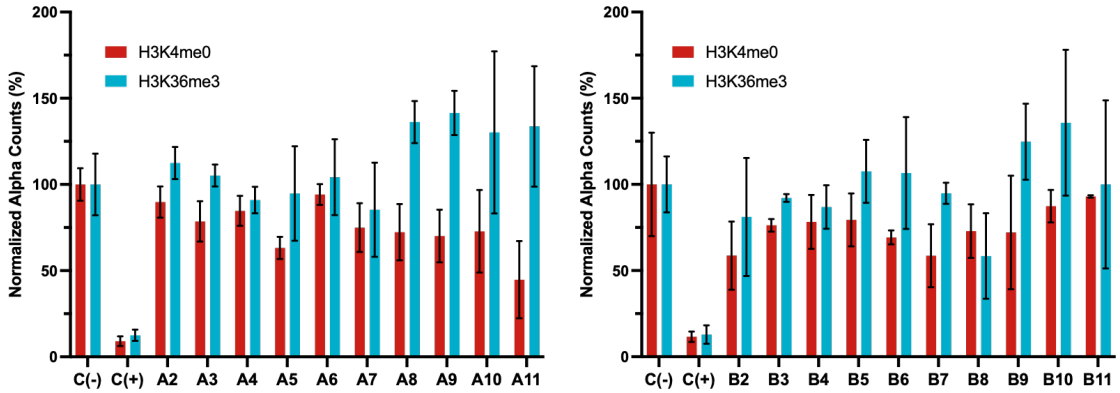



**Figure 6.** Preliminary screening of compounds from the NIH Diversity Set VII library against DNMT3A recruitment interactions. Twenty compounds were evaluated for their ability to disrupt DNMT3A interactions with H3K4me0 and H3K36me3 peptides using AlphaLISA. Although several compounds exhibit apparent modulation of AlphaLISA signal, repeat experiments failed to reproduce selective inhibition. Values are reported as mean ($n$ = 3 samples) ± SD.

These preliminary experiments establish proof-of-concept for the screening platform and provide a foundation for future expansion towards other larger compound libraries. Overall, both AlphaLISA and fluorescence anisotropy assays can robustly monitor DNMT3A recruitment interactions with modified histone tails and provide complementary platforms for identifying selective inhibitors targeting DNMT3A protein-protein interactions. AlphaLISA assays required relatively small quantities of protein to generate proximity-based signal suitable for potential high-throughput screening applications. Additionally, AlphaLISA tolerated the large size and multidomain architecture of DNMT3A1. However, AlphaLISA assays exhibited some limitations, such increased experimental variability and relatively modest signal-to-noise. In contrast, fluorescence anisotropy directly measures peptide binding in solution and produced highly reproducible binding measurements with clear concentration-dependent anisotropy increases. The orthogonal nature of anisotropy measurements provides an important validation platform for future screening hits identified by AlphaLISA as well as providing its own platform for small molecule compound

screening. A major drawback of fluorescence anisotropy, however, is the substantial quantity of purified protein required for titration experiments. Because recombinant purification of DNMT3A1 remains technically challenging, labor intensive, and relatively low yields; large-scale anisotropy screening may be difficult.

These preliminary experiments establish proof-of-concept for the screening platform and provide a foundation for future expansion towards other larger compound libraries. Overall, both AlphaLISA and fluorescence anisotropy assays can robustly monitor DNMT3A recruitment interactions with modified histone tails and provide complementary platforms for identifying selective inhibitors targeting DNMT3A protein-protein interactions. AlphaLISA assays required relatively small quantities of protein to generate proximity-based signal suitable for potential high-throughput screening applications. Additionally, AlphaLISA tolerated the large size and multidomain architecture of DNMT3A1. However, AlphaLISA assays exhibited some limitations, such increased experimental variability and relatively modest signal-to-noise. In contrast, fluorescence anisotropy directly measures peptide binding in solution and produced highly reproducible binding measurements with clear concentration-dependent anisotropy increases. The orthogonal nature of anisotropy measurements provides an important validation platform for future screening hits identified by AlphaLISA as well as providing its own platform for small molecule compound screening. A major drawback of fluorescence anisotropy, however, is the substantial quantity of purified protein required for titration experiments. Because recombinant purification of DNMT3A1 remains technically challenging, labor intensive, and relatively low yields; large-scale anisotropy screening may be difficult.

**D. Methods**

*DNMT3A1 Expression*

DNMT3A1 (DNMT3A1; residues 1-912) was transformed and expressed in NiCo21(DE3) *Escherichia coli* cells (New England Biolabs) with a pET28a-hDNMT3A1 expression plasmid or a codon-optimized pET28a-hDNMT3A1 expression plasmid (Twist Bioscience) containing a N-terminal His-tag. Cell cultures were grown in LB medium at 37˚C to $OD_{600}$ of 0.7, cooled to 16˚C, and induced with 1 mM isopropyl β-D-1-thiogalactopyranoside (IPTG) for 16 h unless otherwise noted. Cells were harvested by centrifugation at 8,000 x g, flash frozen in liquid nitrogen, and stored at -80˚C.

*DNMT3A1 Protein Purification*

Frozen cell pellets were resuspended in lysis buffer containing 50 mM HEPES, 500 mM NaCl, 50 mM imidazole, 0.5 mM DTT, 1 mM PMSF, 25µg/mL DNAse 1, 1% glycerol (v/v), and 0.2% Triton-X100 (v/v) at pH 7.8. Cells were lysed by sonication and clarified by centrifugation at 18,000 x g for 2x 30 min. Following equilibration in 50 mM Tris-HCl, 500 mM NaCl, 50 mM imidazole, and 1% glycerol (v/v) at pH 7.8; the resulting soluble extract was loaded onto an ÄKTA Start FPLC system (GE Healthcare) equipped with a 5 mL HisTrap HP $Ni^{2+}$ IMAC column (Cytiva). The column was washed with 50-75 mM imidazole to remove nonspecifically bound proteins prior to elution with an imidazole gradient from 75-500 mM. Fractions corresponding to the primary DNMT3A1 peak were pooled, concentrated with a 15 mL 100 kDa MWCO Amicon filter, and buffer-exchanged into storage buffer containing 50 mM Tris, 200 mM NaCl, 1 mM EDTA, 1 mM DTT, 10% glycerol (v/v) at pH 7.8. Samples were then applied to a 16/60 HiLoad column (GE Pharmacia) packed with Superdex 200 pg (Cytivia) and eluted at 1 mL/min. Fractions. Associated with DNMT3A1 were collected and

further concentrated before flash frozen in liquid nitrogen and stored at -80˚C. Protein concentrations were determined spectrophotometrically at 280 nm using a calculated extinction coefficient of 142,010 $M^{-1}$ $cm^{-1}$ for the monomeric subunit DNMT3A1.

*AlphaLISA Assay*

20 μL final-volume reactions in 384-well AlphaPlates containing of 1 nM DNMT3A1, 12.5 nM H3K4me0-biotin or H3K36me3-biotin peptide, and 10 μM test compound in binding buffer (20 mM Tris, pH 7.8, 100 mM NaCl, 0.01% BSA, 0.01% NP-40, 0.5 mM DTT, and 1% DMSO). Protein and peptide were preincubated for 15 min on ice prior to compound addition, followed by incubation at room temperature for 30 min. A bead mixture containing streptavidin donor beads (2.5 μg/mL final conc.) and nickel-chelate acceptor beads (1.25 μg/mL final conc.) in bead buffer (20 mM HEPES, pH 7.8, 100 mM NaCl, 0.01% BSA, and 0.01% NP-40) was added. Plates were then incubated for an additional 1 hour at room temperature before analysis. AlphaLISA signal was measured using a Tecan Spark microplate reader in Alpha Technology mode with a detection window of 610-635 nm. Vehicle (1% DMSO) and positive inhibition controls containing 1% SDS were included in each experiment, and all measurements were performed in triplicate.

*Fmoc-Lys(FITC)-OH Synthesis*

In a round-bottom flask, 6.42 mL of 20% (v/v) trifluoroacetic acid in dichloromethane was added to Fmoc-Lys(Boc)-OH (603.9 mg, 1.289 mmol, 1 equiv.). Reaction progressed for 3 hours at room temperature. Solution was diluted in 25 mL ethyl acetate and then wash 3x with 25 mL water, dried over $MgSO_4$, and solvent was removed under reduced pressure to afford white crude Fmoc-Lys-OH, which was used in the subsequent FITC-coupling reaction without need for further purification.

In a round-bottom flask under $N_2$ and subdued light, 50% (v/v) tetrahydrofuran in dimethylformamide was added to FITC (453.0 mg, 1.163 mmol, 1 equiv.), and Fmoc-Lys-OH/TFA (622.0 mg, 1.289 mmol, 1.1 equiv.). Reaction was initiated with *N*,*N*-diisopropylethylamine (202.6 µL, 1.745 mmol, 1.5 equiv.) and progressed for 14 hours at room temperature. Solution was then diluted in 100 mL ethyl acetate and 100 mL $H_2O$ and extracted 3x with ethyl acetate, dried over $MgSO_4$, and solvent was removed under reduced pressure. Crude product was purified via column chromatography ($SiO_2$; eluent: dichloromethane/methanol = 9:1) to afford yellow product (599.2 mg, 68%).

*Solid Phase Peptide Synthesis*

Wang resin (0.20 g) was swollen in dimethylformamide (DMF), and iterative cycles of Fmoc deprotection and amino acid coupling were performed according to the Symphony X peptide synthesizer (Gyros Protein Technologies) instrument protocol. Activated amino acid solutions were prepared using HCTU (11.417 g, 0.6 M) and *N*-methylmorpholine (NMM, 6.069 mL, 1.2 M) dissolved in DMF to a final volume of 40 mL. Coupling reactions were performed in a 10 mL reaction vessel. Coupling reaction progressed for 20 min per coupling cycle. Following each coupling step, excess reagents were removed by DMF washing, and Fmoc protecting groups were removed using 20% (v/v) piperidine in DMF.

Peptide elongation proceeded C-terminus to N-terminus to afford the desired H3K4me0-FITC peptide sequence; $H_2N$-ARTKQTARKSGGGK(FITC)-OH. The peptide was cleaved from the resin and globally deprotected using 4 mL of 2.5% $H_2O$, 2.5% Triisopropyl silane (TIPS), and 95% TFA. After 45 minutes of gentle agitation, deprotected peptide was syringe filtered into a vial, rinsed with dichloromethane, and dried under a gentle stream of compressed air. The crude peptide was precipitated with 40 mL cold diethyl ether and centrifuged 10 min

at 4,000 x g. Precipitation in cold diethyl ether and centrifuging was done 3x and then dried under reduced pressure to afford a yellow solid.

*Fluorescence Anisotropy Assay*

10 µL reactions were carried out in black 96-well microplates containing 50 mM Tris, 1 mM EDTA, 1 mM DTT, 0.2 mg/mL BSA, and 20 mM NaCl at pH 7.8. The H3K4me0-FITC peptide was used at a final concentration of 10 nM, while DNMT3A1 was titrated from 0-400 nM. Reactions were incubated for 15 min at room temperature prior to data acquisition. All measurements were performed in triplicate.

**E. Supplementary Information**

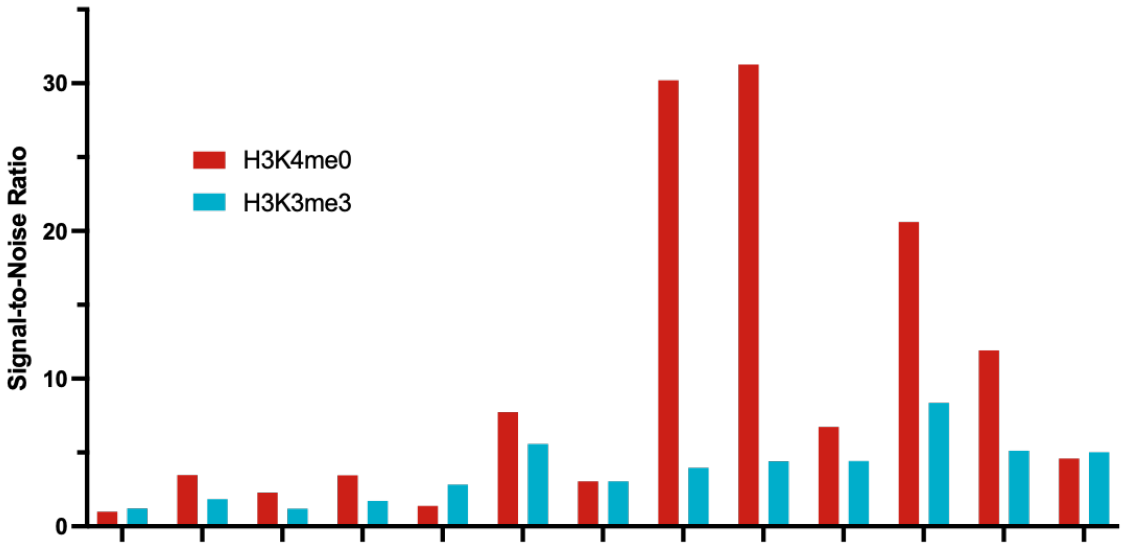



**Figure S1.** Signal-to-noise ratio of AlphaLISA assays for H3K4me0 and H3K36me3 biotin-tagged peptides.

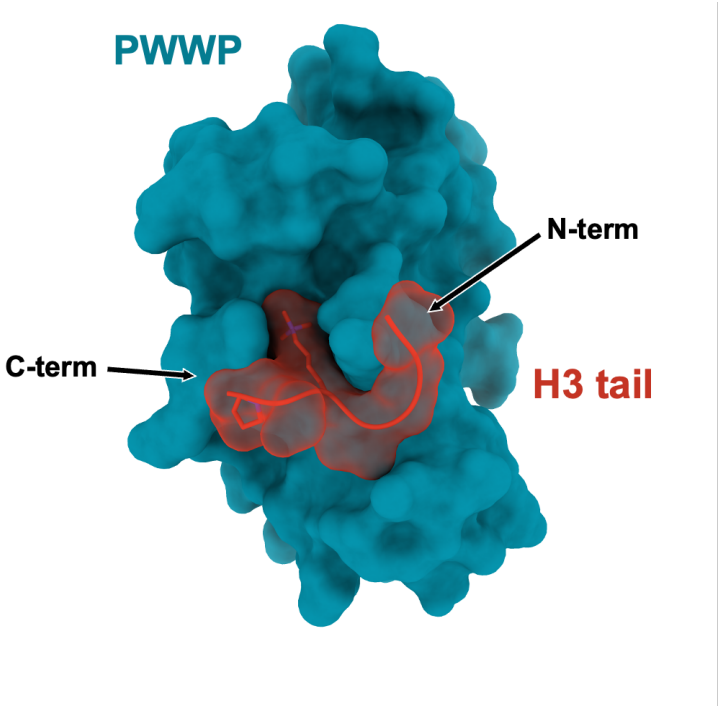



**Figure S2.** Protein crystal structure of H3K36me3 recognition by the PWWP domain. Lys36 and Pro38 contribute to histone-tail recognition.

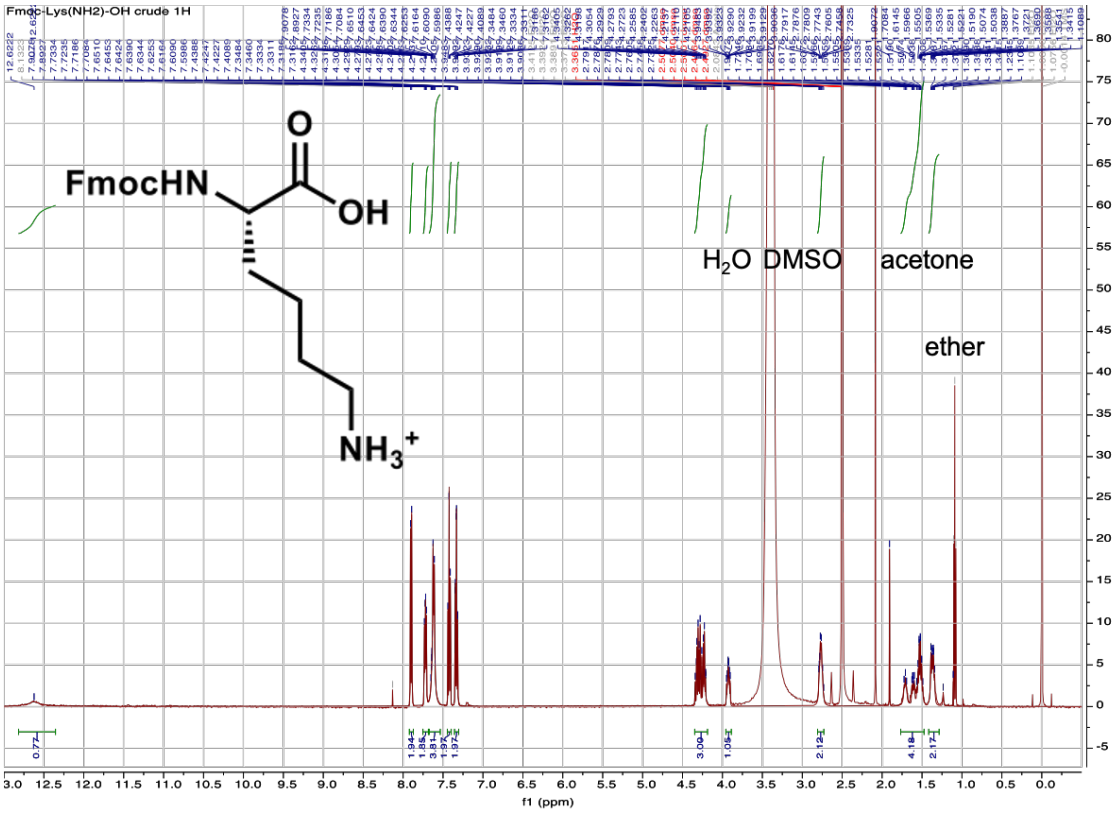



**Figure S3.** [1]HNMR spectra of Fmoc-Lys-OH.

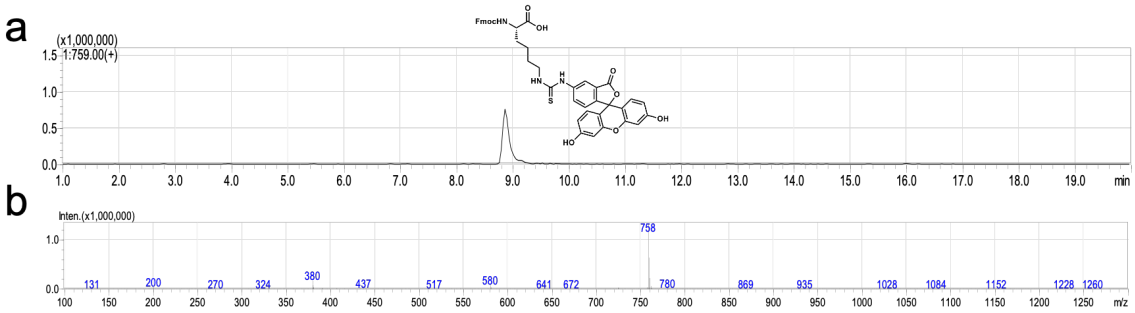



**Figure S4.** LC-MS data for Fmoc-Lys(FITC)-OH. Exact mass = 757.91 Da.

## IV. RNA-Mediated Regulation of DNMT3A by *Fos-1* ecRNA

### A. Abstract

DNA methyltransferase 3A (DNMT3A) is a *de novo* DNA methyltransferase responsible for establishing DNA methylation patterns during cellular differentiation, development, and epigenetic gene regulation. Recruitment and modulation of DNMT3A activity are governed by dynamic crosstalk with multiple components of the epigenetic machinery, including histone post-translational modifications, regulatory proteins, and non-coding RNAs. Recent studies have identified ecRNAs as important regulators of DNA methylation, where elevated ecRNA expression correlates with reduced DNA methylation at associated genomic loci. Specifically, the *Fos-1* ecRNA has previously been shown to selectively inhibit DNMT3A allosterically by binding near the DNMT3A tetramer interface. Previous kinetic studies suggested that RNA inhibition of DNMT3A differs depending on oligomeric state, with DNMT3A homotetramers and homodimers displaying distinct modes of inhibition. Despite these recent findings, the molecular mechanism by which the *Fos-1* ecRNA and other ecRNAs regulate DNMT3A is still not completely understood. Here, DNMT3A-DNMT3L heterotetramers exhibit inhibition behavior similar to DNMT3A homodimers, suggesting that ecRNA regulation may involve multiple simultaneous inhibitory mechanisms rather than the simple disruption of tetramer formation alone.

### B. Introduction

Epigenetic regulation of gene expression relies on coordinated crosstalk between DNA methylation, histone post-translational modifications (PTMs), partner proteins, and non-coding RNAs (ncRNAs)[1–4]. DNA methylation of cytosine to form 5-methylcytosine (5mC) is a central epigenetic modification involved in transcriptional silencing, genomic imprinting,

X-chromosome inactivation, stem cell differentiation, and maintenance of cellular identity[5–9]. In mammals, *de novo* DNA methylation is primarily established by DNA methyltransferase 3A (DNMT3A) and DNA methyltransferase 3B (DNMT3B), whose activities are tightly regulated through interactions with multiple epigenetic factors[5,10,11]. DNMT3A recruitment is influenced by histone PTMs including H3K4me0, H3K36me2/3, and H2AK119ub through interactions with the ADD, PWWP, and UDR domains, respectively[12–16]. In addition to histone-mediated recruitment, increasing evidence suggests that ncRNAs play important roles in regulating chromatin architecture and epigenetic signaling. ncRNAs comprise a diverse class of transcripts that regulate transcriptional processes through interactions with DNA, RNA-binding proteins, chromatin remodelers, and epigenetic enzymes[4,8,17]. One example are extra-coding RNAs (ecRNAs), which are a class of ncRNAs defined as sense-strand, non-polyadenylated transcripts that extend across and overlap the boundaries of their associated protein-coding genes[18,19].

Previous work from the Day lab[19] identified a strong relationship between ecRNA abundance and local epigenetic states. Gene clusters enriched with ecRNA displayed substantially lower DNA methylation signatures, suggesting that ecRNAs disrupt DNA methylation machinery. This work also identified the *Fos-1* ecRNA as a regulator of the *Fos* gene locus by mitigating DNMT3A hypermethylation. Previous work from our lab[20] further demonstrated that the *Fos-1* ecRNA selectively bind DNMT3A and inhibit its methyltransferase activity. Importantly, this inhibition displayed selectivity toward DNMT3A relative to other mammalian DNA methyltransferases, suggesting that ecRNAs may regulate DNMT3A through specific structural interactions rather than nonspecific nucleic acid competition. The proposed mechanism for ecRNA regulation stems from the

oligomeric architecture of DNMT3A. DNMT3A naturally forms homotetramers through interactions at both dimer and tetramer interfaces within the methyltransferase domain. Tetramer formation is essential for processive DNA methylation and contributes to allosteric regulation by partner proteins such as DNMT3L and p53. Mutations that disrupt the tetramer interface alter the oligomeric state and thereby the DNA binding affinity as well as processivity while maintaining varying degrees of catalytic activity[2,21–23].

In our lab's previous work[20], computational docking and mutation analyses investigated the regulatory mechanism of the *Fos-1* ecRNA. Because oligomerization is central to DNMT3A function, interactions between ecRNAs and oligomeric interfaces were investigated to provide a mechanism for regulating enzyme activity. HDOCK modeling predicted that *Fos-1* ecRNA binds preferentially near the DNMT3A tetramer interface. Furthermore, several tetramer interface mutants including R729A, R736A, and E733A remained susceptible to RNA-mediated inhibition, despite existing as homodimers rather than homotetramers. Comparison of inhibition models revealed that *Fos-1* ecRNA inhibited DNMT3A homotetramers through a noncompetitive mechanism, whereas inhibition of the R729A homodimer mutant follows an uncompetitive model. This evidence suggested that the oligomeric state of the enzyme is crucial in mediating ecRNA-dependent regulation. In contrast, the tetramer interface mutant R771A displayed resistance to ecRNA inhibition, but formation of DNMT3A-DNMT3L heterotetramers restored RNA-mediated inhibition of R771A. This observation suggests that the regulatory mechanisms governing DNMT3A activity are shaped by a complex interplay between RNA-mediated and protein-mediated regulation.

This work further investigates the relationship between ecRNA binding and DNMT3A oligomerization. Specifically, HDOCK modeling was extended to examine potential ecRNA interactions with the DNMT3A homodimer. In addition, kinetic inhibition models were performed using DNMT3A-DNMT3L heterotetramers to further evaluate how changes in oligomeric architecture influence ecRNA-mediated regulation. These studies aim to refine the understanding of the determinants underlying ecRNA recognition by DNMT3A and to elucidate the method of interplay between ecRNA and other epigenetic machinery.

**C. Results & Discussion**

*ecRNA Regulation Likely Involves Multiple Simultaneous Inhibitory Mechanisms*

Previous docking studies[20] using the HDOCK server[24,25] used the monomeric form of DNMT3A (PDB: 4U7T; residues 468-912)[12] and the *Fos-1* ecRNA sequence to predict DNMT3A-ecRNA interactions. Docking simulations with the monomeric form of DNMT3A revealed that the *Fos-1* ecRNA likely binds along the tetramer interface. This simulated observation is plausible given the importance of oligomerization for DNMT3A function. Although both dimeric and tetrameric forms of DNMT3A are catalytically active, homotetramers exhibit greater methyltransferase activity than homodimers, suggesting that the perturbation of tetramer assembly could represent an effective mechanism for regulating enzyme function. Consistent with this model, kinetic analyses of DNMT3A homotetramers demonstrated a noncompetitive mode of inhibition by *Fos-1* ecRNA, indicating that RNA binding can occur whether the enzyme is bound or unbound to its DNA substrate and affect catalysis without directly occluding the active site. However, this model cannot explain the inhibition observed in tetramer-interface mutants, which form a dimeric state and exhibit mechanistically distinct responses to ecRNA inhibition. The R729A dimer-mutant exhibited

uncompetitive inhibition by *Fos-1* ecRNA, indicating preferential binding to the enzyme-substrate complex rather than the free enzyme and that the homodimer mutant's susceptibility to ecRNA inhibition likely arises through a different regulatory mechanism.

To investigate this discrepancy, additional HDOCK simulations were performed using a dimeric DNMT3A model (PDB: 8TDR; residues 628-912)[26] (Figure 1, Table S1). Interestingly, despite the tetramer interface remaining solvent accessible as a dimer, *Fos-1* ecRNA was predicted to preferentially bind near the dimer interface rather than the putative tetramerization surface or DNA-binding region. Six of the top ten docking results places *Fos-1* ecRNA near the dimer interface, three near the DNA binding interface, and two along the tetramer interface (Table S1). The presence of ecRNA docking solutions near the DNA-binding region is not unexpected given the structural and electrostatic similarities between RNA and DNA. Likewise, docking along the tetramer interface is consistent with previous findings[20], which implicated oligomerization-dependent mechanisms in ecRNA-mediated regulation. However, the predominance of docking solutions at the dimer interface suggests that this surface may represent a previously unrecognized site of ecRNA interaction. Rather than a single discrete RNA binding site, the docking models suggested that ecRNAs may engage multiple dynamic surfaces of DNMT3A. Interactions with the tetramer interface may contribute to the noncompetitive inhibition observed for wild-type DNMT3A homotetramers, whereas preferential binding near the dimer interface may underlie the uncompetitive inhibition observed for dimeric mutants. Although these docking studies cannot definitively establish the molecular basis of inhibition, they suggest that ecRNA-mediated regulation may arise from dynamic interactions with multiple regulatory surfaces.

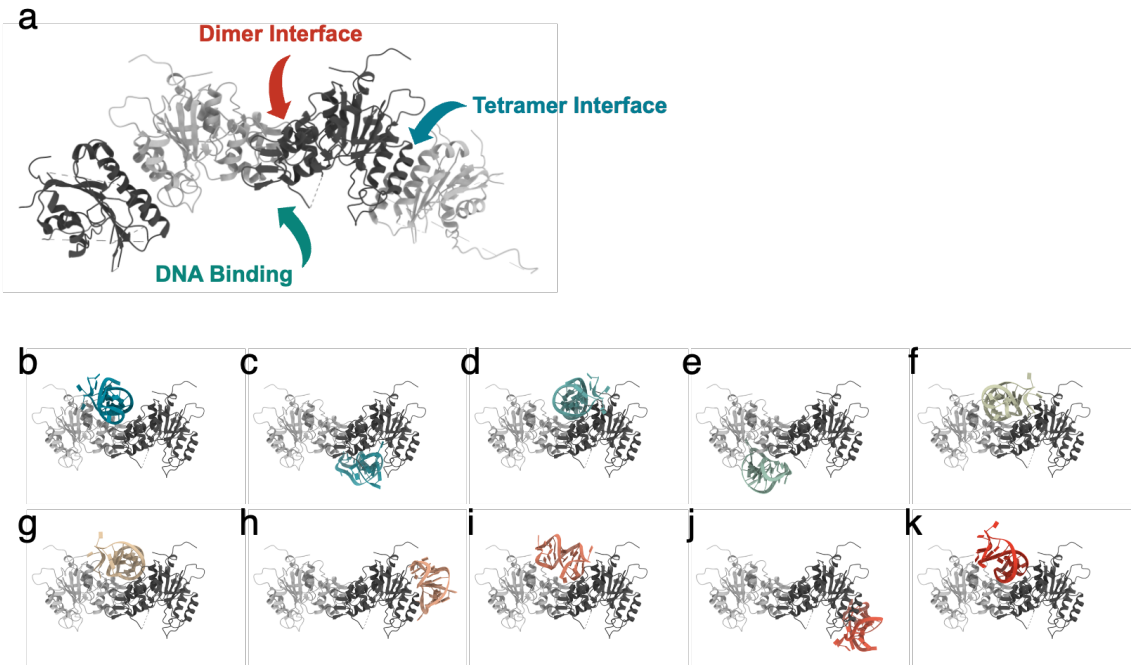



**Figure 1.** a) Protein crystal structure of DNMT3A homotetramer (PDB: 8TDR; residues 628-912). DNMT3A subunits colored in light grey and dark grey. b-k) Top ten prediction *Fos-1* ecRNA binding models with DNMT3A homodimer from b) highest confidence to k) lowest confidence. DNMT3A subunits colored in light grey and dark grey, *Fos-1* ecRNA colored in blue-to-red gradient signifying highest to lowest confidence prediction model.

To further investigate the dynamic regulatory relationship between ecRNA and DNMT3A, kinetic analyses were performed using DNMT3A$^{MTase}$/3L heterotetramers in the presence of *Fos-1* ecRNA (Figure 2). The methyltransferase domain of DNMT3A was selected because it exhibits kinetic properties comparable to those of the full-length enzyme while providing a simplified system for mechanistic analysis[5,27] and allowed for direct comparison with previous mechanistic studies[20]. DNMT3A$^{MTase}$/3L heterotetramers were chosen since DNMT3L was previously shown to restore ecRNA-mediated regulation to the tetramer-interface mutant R771A, which otherwise displays resistance to *Fos-1* ecRNA inhibition[20]. Consistent with the previous findings, varying DNA substrate concentration demonstrated that *Fos-1* ecRNA inhibits DNMT3A$^{MTase}$ homotetramers through a

noncompetitive mechanism, indicating that RNA binding can occur independently of substrate binding. Kinetic analysis of DNMT3A$^{MTase}$/3L heterotetramers exposed to the *Fos-1* ecRNA revealed an uncompetitive mode of inhibition, characterized by preferential inhibition of the enzyme-substrate complex. This inhibition pattern closely resembles that observed for the R729A homodimer mutant although DNMT3A$^{MTase}$/3L exists as a heterotetramer rather than a dimeric species. The ecRNA-mediated regulation likely cannot be explained solely by the oligomeric state of DNMT3A, indicating that more than one path for DNMT3A inhibition is available for *Fos-1* ecRNA. A single 25-nucleotide ecRNA that can induce multiple modes of inhibition is particularly noteworthy. Most characterized regulatory RNAs that modulate epigenetic enzymes are long noncoding RNAs (lncRNAs)[4,28], such as the 17 kb Xist RNA, which contains numerous structural domains capable of interacting with multiple protein partners and regulatory complexes[8,17]. In contrast, *Fos-1* ecRNA is relatively short, yet appears capable of engaging distinct regulatory mechanisms. The molecular basis for this behavior remains unclear. It is possible that a specific sequence, secondary structural elements, or a minimum RNA length are required to support alternative binding modes and regulatory outcomes. Further investigation will be required to determine how *Fos-1* ecRNA differentially interacts with distinct DNMT3A oligomeric assemblies and whether this behavior represents a broader mechanism of ecRNA-mediated regulation. While the underlying molecular mechanism remains unresolved, the possibility that short ecRNAs may regulate epigenetic enzymes through multiple mechanistically distinct modes of interaction suggests a level of regulatory complexity that has historically been attributed primarily to large lncRNAs.

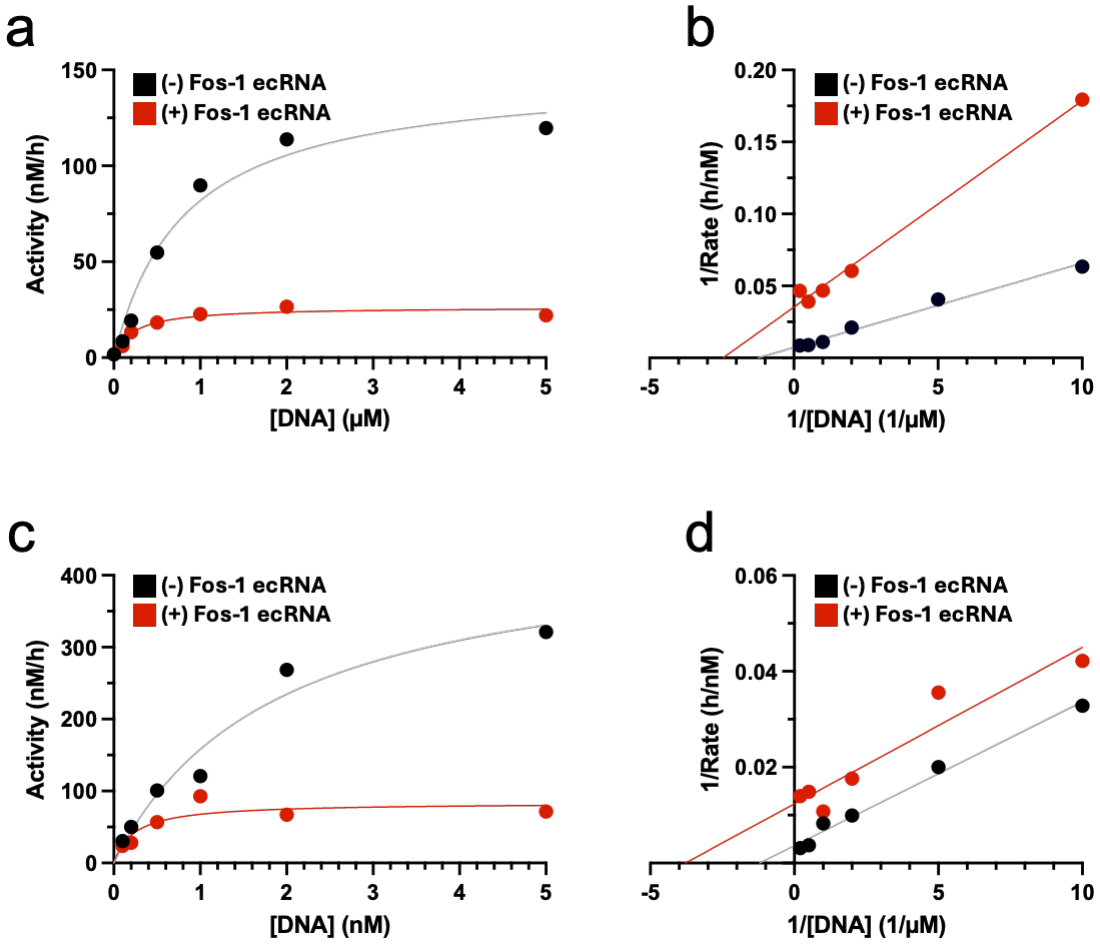



**Figure 2.** Michaelis-Menten curves of a) DNMT3A$^{MTase}$ homotetramers (-*Fos-1* $R^2$ = 0.91; +*Fos-1* $R^2$ = 0.69) and c) DNMT3A$^{MTase}$/3L heterotetramers in the absence and presence *Fos-1* ecRNA (-*Fos-1* $R^2$ = 0.90; +*Fos-1* $R^2$ = 0.97). Corresponding Lineweaver-Burk plots of b) DNMT3A$^{MTase}$ homotetramers (-*Fos-1* $R^2$ = 0.95; +*Fos-1* $R^2$ = 0.82) and d) DNMT3A$^{MTase}$/3L heterotetramers in the absence and presence *Fos-1* ecRNA (-*Fos-1* $R^2$ = 0.90; +*Fos-1* $R^2$ = 0.97). DNMT3A$^{MTase}$ homotetramers exhibit mixed-type inhibition with noncompetitive character ($V_{max}$: 148.5 to 26.4 nM/h; $K_m$ 0.814 μM to 0.221 μM). DNMT3A$^{MTase}$/3L heterotetramers exhibit uncompetetive inhibition ($V_{max}$: 454.7 to 83.9 nM/h; $K_m$ 1.878 μM to 0.238 μM). All curves generated with Prism v10.6.

**D. Methods**

*Fos-1 ecRNA sequence*

5'-GGGGACACGCCCUCUGUUCCCUUAU-3'

*DNMT3A$^{MTase}$ Expression*

The DNMT3A methyltransferase domain (DNMT3A$^{MTase}$; residues 634-912) was transformed and expressed in NiCo21(DE3) *Escherichia coli* cells (New England Biolabs) with a codon-optimized pET28a-hDNMT3A$^{MTase}$ expression plasmid containing a N-terminal His-tag. Cell cultures were grown in LB medium at 37˚C to $OD_{600}$ of 0.8, cooled to 16˚C, and induced with 1 mM isopropyl β-D-1-thiogalactopyranoside (IPTG). Following 16 hours of expression, cells were harvested by centrifugation at 8,000 x g, flash frozen in liquid nitrogen, and stored at -80˚C.

*DNMT3A$^{MTase}$ Protein Purification*

Frozen cell pellets were resuspended in lysis buffer containing 50 mM Tris-HCl, 500 mM NaCl, 50 mM imidazole, 0.5 mM DTT, 1 mM PMSF, 10% glycerol (v/v), and 0.2% Triton-X100 (v/v) at pH 7.8. Cells were lysed by sonication and clarified by centrifugation at 18,000 x g for 2x 30 min. Following equilibration in 50 mM Tris-HCl, 500 mM NaCl, 50 mM imidazole, and 10% glycerol (v/v) at pH 7.8; the resulting soluble extract was loaded onto an ÄKTA Start FPLC system (GE Healthcare) equipped with a HisTrap Excel $Ni^{2+}$ IMAC column (Cytiva). The column was washed with 50-75 mM imidazole to remove nonspecifically bound proteins prior to elution with an imidazole gradient from 75-500 mM. Fractions corresponding to the primary DNMT3A$^{MTase}$ peak were pooled, concentrated with a 15 mL 10 kDa MWCO Amicon filter, and buffer-exchanged into storage buffer containing 50 mM Tris, 200 mM NaCl, 1 mM EDTA, 1 mM DTT, 20% glycerol (v/v) at pH 7.8. Purified protein was flash

frozen in liquid nitrogen and stored at -80˚C. Protein concentrations were determined spectrophotometrically at 280 nm using a calculated extinction coefficient of 38,180 $M^{-1}$ $cm^{-1}$ for the monomeric subunit of $DNMT3A^{MTase}$.

*Computational docking*

The HDOCK docking server was used to predict protein-RNA docking simulations with DNMT3A homodimer and *Fos-1* ecRNA. Receptor molecule DNMT3A homodimer (PDB: 8TDR, chain A/B) and ligand molecule *Fos-1* ecRNA sequence were subjected to *ab initio* docking to determine the top ten predicted *Fos-1* ecRNA-binding surfaces on DNMT3A.

*Methylation assays*

Reactions were performed with 50mM Tris pH 7.8, 1mM EDTA, 15mM NaCl, 0.2 mg/mL BSA, 1 mM DTT, 5 µM SAM (1:50 [$^3$H]-SAM:SAM), and 50 nM $DNMT3A^{MTase}$ at pH 7.8 with or without 1 µM *Fos-1* ecRNA. 12 µL reactions were initiated with 0-5 µM DNA substrate (Poly-dI-dC) and incubated at 37˚C for 30 min in duplicate, then quenched with 12 µL 0.3% SDS. 20 µL of quenched reactions were spotted on Hybond-N+ membranes (Cytiva RPN303B), then washed with gentle agitation 3x with 50 mM potassium phosphate buffer ($K_2HPO_4$/$KH_2PO_4$ at pH 7.8) for 5 min, 1x with 70% ethanol (v/v) for 5 min, and 1x with 100% ethanol for 5 min. Membranes were dried and counted with a Hidex 300 SL scintillation counter.

## E. Supplementary Information

**Table S1.** Top ten predicted models for DNMT3A interaction with *Fos-1* ecRNA. *Fos-1* ecRNA docked to the DNMT3A homodimer (PDB: 8TDR). Docking models are ranked by HDOCK docking score and classified according to the DNMT3A interface proposed for ecRNA-binding. Associated confidence scores and ligand RMSD values are reported for each model.

| Model No. | Binding Region | Docking Score | Confidence Score | RMSD (Å) |
|---|---|---|---|---|
| i | Dimer Interface | -325.63 | 0.9710 | 92.06 |
| ii | DNA-Binding Site | -321.86 | 0.9688 | 71.41 |
| iii | Dimer Interface | -301.89 | 0.9543 | 93.99 |
| iv | DNA-Binding Site | -298.39 | 0.9511 | 66.84 |
| v | Dimer Interface | -283.06 | 0.9347 | 88.68 |
| vi | Dimer Interface | -276.37 | 0.9260 | 96.07 |
| vii | Tetramer Interface | -275.42 | 0.9247 | 87.00 |
| viii | Dimer Interface | -275.27 | 0.9245 | 94.90 |
| ix | Tetramer Interface | -267.68 | 0.9132 | 77.02 |
| x | Dimer Interface | -263.53 | 0.9064 | 93.45 |

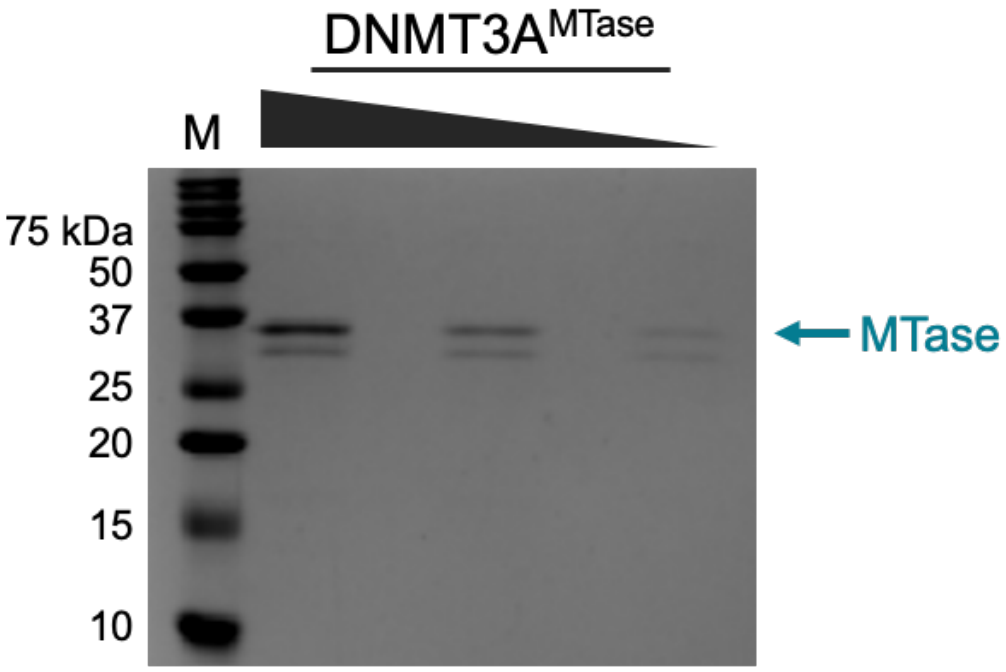



**Figure S2.** SDS-PAGE gel of purified DNMT3A$^{MTase}$. 5x-20x sample dilution indicated above each lane. Purified DNMT3A$^{MTase}$ is 80% pure.

# References

## Chapter I. Introduction


(1) Hellman, A.; Chess, A. Gene Body-Specific Methylation on the Active X Chromosome. *Science* **2007**, *315* (5815), 1141–1143. https://doi.org/10.1126/science.1136352.

(2) Holliday, R.; Pugh, J. E. DNA Modification Mechanisms and Gene Activity During Development. *Science* **1975**, *187* (4173), 226–232. https://doi.org/10.1126/science.187.4173.226.

(3) SanMiguel, J. M.; Bartolomei, M. S. DNA Methylation Dynamics of Genomic Imprinting in Mouse Development. *Biol. Reprod.* **2018**, *99* (1), 252–262. https://doi.org/10.1093/biolre/ioy036.

(4) Nan, B.; Gao, S. 5mC and 6mA DNA Methylation in Eukaryotic Genomes. *Trends Biochem. Sci.* **2026**, *51* (3), 261–274. https://doi.org/10.1016/j.tibs.2026.01.002.

(5) Yang, W.; Zhuang, J.; Li, C.; Cheng, G.-J. Unveiling the Methyl Transfer Mechanisms in the Epigenetic Machinery DNMT3A-3 L: A Comprehensive Study Integrating Assembly Dynamics with Catalytic Reactions. *Comput. Struct. Biotechnol. J.* **2023**, *21*, 2086–2099. https://doi.org/10.1016/j.csbj.2023.03.002.

(6) Christian, D. L.; Wu, D. Y.; Martin, J. R.; Moore, J. R.; Liu, Y. R.; Clemens, A. W.; Nettles, S. A.; Kirkland, N. M.; Papouin, T.; Hill, C. A.; Wozniak, D. F.; Dougherty, J. D.; Gabel, H. W. DNMT3A Haploinsufficiency Results in Behavioral Deficits and Global Epigenomic Dysregulation Shared across Neurodevelopmental Disorders. *Cell Rep.* **2020**, *33* (8), 108416. https://doi.org/10.1016/j.celrep.2020.108416.

(7) Yokoi, T.; Enomoto, Y.; Naruto, T.; Kurosawa, K.; Higurashi, N. Tatton-Brown-Rahman Syndrome with a Novel DNMT3A Mutation Presented Severe Intellectual Disability and Autism Spectrum Disorder. *Hum. Genome Var.* **2020**, *7* (1), 15. https://doi.org/10.1038/s41439-020-0102-6.

(8) Liu, P.; Yang, F.; Zhang, L.; Hu, Y.; Chen, B.; Wang, J.; Su, L.; Wu, M.; Chen, W. Emerging Role of Different DNA Methyltransferases in the Pathogenesis of Cancer. *Front. Pharmacol.* **2022**, *13*. https://doi.org/10.3389/fphar.2022.958146.

(9) Zhang, J.; Yang, C.; Wu, C.; Cui, W.; Wang, L. DNA Methyltransferases in Cancer: Biology, Paradox, Aberrations, and Targeted Therapy. *Cancers* **2020**, *12* (8), 2123. https://doi.org/10.3390/cancers12082123.

(10) Bestor, T.; Laudano, A.; Mattaliano, R.; Ingram, V. Cloning and Sequencing of a cDNA Encoding DNA Methyltransferase of Mouse Cells: The Carboxyl-Terminal Domain of the Mammalian Enzymes Is Related to Bacterial Restriction Methyltransferases. *J. Mol. Biol.* **1988**, *203* (4), 971–983. https://doi.org/10.1016/0022-2836(88)90122-2.

(11) Dahlet, T.; Argüeso Lleida, A.; Al Adhami, H.; Dumas, M.; Bender, A.; Ngondo, R. P.; Tanguy, M.; Vallet, J.; Auclair, G.; Bardet, A. F.; Weber, M. Genome-Wide Analysis in the Mouse Embryo Reveals the Importance of DNA Methylation for Transcription Integrity. *Nat. Commun.* **2020**, *11* (1), 3153. https://doi.org/10.1038/s41467-020-16919-w.

(12) Okano, M.; Bell, D. W.; Haber, D. A.; Li, E. DNA Methyltransferases Dnmt3a and Dnmt3b Are Essential for De Novo Methylation and Mammalian Development. *Cell* **1999**, *99* (3), 247–257. https://doi.org/10.1016/S0092-8674(00)81656-6.

(13) Challen, G. A.; Sun, D.; Mayle, A.; Jeong, M.; Luo, M.; Rodriguez, B.; Mallaney, C.; Celik, H.; Yang, L.; Xia, Z.; Cullen, S.; Berg, J.; Zheng, Y.; Darlington, G. J.; Li, W.; Goodell, M. A. Dnmt3a and Dnmt3b Have Overlapping and Distinct Functions in Hematopoietic Stem Cells. *Cell Stem Cell* **2014**, *15* (3), 350–364. https://doi.org/10.1016/j.stem.2014.06.018.
(14) Jia, D.; Jurkowska, R. Z.; Zhang, X.; Jeltsch, A.; Cheng, X. Structure of Dnmt3a Bound to Dnmt3L Suggests a Model for de Novo DNA Methylation. *Nature* **2007**, *449* (7159), 248–251. https://doi.org/10.1038/nature06146.
(15) Wapenaar, H.; Clifford, G.; Rolls, W.; Pasquier, M.; Burdett, H.; Zhang, Y.; Deák, G.; Zou, J.; Spanos, C.; Taylor, M. R. D.; Mills, J.; Watson, J. A.; Kumar, D.; Clark, R.; Das, A.; Valsakumar, D.; Bramham, J.; Voigt, P.; Sproul, D.; Wilson, M. D. The N-Terminal Region of DNMT3A Engages the Nucleosome Surface to Aid Chromatin Recruitment. *EMBO Rep.* **2024**, *25* (12), 5743–5779. https://doi.org/10.1038/s44319-024-00306-3.
(16) Lue, N. Z.; Garcia, E. M.; Ngan, K. C.; Lee, C.; Doench, J. G.; Liau, B. B. Base Editor Scanning Charts the DNMT3A Activity Landscape. *Nat. Chem. Biol.* **2023**, *19* (2), 176–186. https://doi.org/10.1038/s41589-022-01167-4.
(17) Gu, T.; Hao, D.; Woo, J.; Huang, T.-W.; Guo, L.; Lin, X.; Guzman, A. G.; Tovy, A.; Rosas, C.; Jeong, M.; Zhou, Y.; Deneen, B.; Huang, Y.; Li, W.; Goodell, M. A. The Disordered N-Terminal Domain of DNMT3A Recognizes H2AK119ub and Is Required for Postnatal Development. *Nat. Genet.* **2022**, *54* (5), 625–636. https://doi.org/10.1038/s41588-022-01063-6.
(18) Suetake, I.; Mishima, Y.; Kimura, H.; Lee, Y.-H.; Goto, Y.; Takeshima, H.; Ikegami, T.; Tajima, S. Characterization of DNA-Binding Activity in the N-Terminal Domain of the DNA Methyltransferase Dnmt3a. *Biochem. J.* **2011**, *437* (1), 141–148. https://doi.org/10.1042/BJ20110241.
(19) Yoo, J.; Kim, J. H.; Robertson, K. D.; Medina-Franco, J. L. Molecular Modeling of Inhibitors of Human DNA Methyltransferase with a Crystal Structure. *Adv. Protein Chem. Struct. Biol.* **2012**, *87*, 219–247. https://doi.org/10.1016/B978-0-12-398312-1.00008-1.
(20) Martin, J. L.; McMillan, F. M. SAM (Dependent) I AM: The S-Adenosylmethionine-Dependent Methyltransferase Fold. *Curr. Opin. Struct. Biol.* **2002**, *12* (6), 783–793. https://doi.org/10.1016/S0959-440X(02)00391-3.
(21) Yan, Y.; Zhou, X. E.; Thomas, S. L.; Liu, M.; Lai, G.-Q.; Worden, E. J.; Jones, P. A.; Xu, T.-H. Molecular Mechanisms of DNMT3A-3L-Mediated de Novo DNA Methylation on Chromatin. *Nat. Struct. Mol. Biol.* **2026**, *33* (1), 171–183. https://doi.org/10.1038/s41594-025-01704-4.
(22) Xu, T.-H.; Liu, M.; Zhou, X. E.; Liang, G.; Zhao, G.; Xu, H. E.; Melcher, K.; Jones, P. A. Structure of DNA Methyltransferases DNMT3A/DNMT3B Bound to a Nucleosome. *Nature* **2020**, *586* (7827), 151–155. https://doi.org/10.1038/s41586-020-2747-1.
(23) Holz-Schietinger, C.; Matje, D. M.; Harrison, M. F.; Reich, N. O. Oligomerization of DNMT3A Controls the Mechanism of de Novo DNA Methylation. *J. Biol. Chem.* **2011**, *286* (48), 41479–41488. https://doi.org/10.1074/jbc.M111.284687.
(24) Zeng, Y.; Ren, R.; Kaur, G.; Hardikar, S.; Ying, Z.; Babcock, L.; Gupta, E.; Zhang, X.; Chen, T.; Cheng, X. The Inactive Dnmt3b3 Isoform Preferentially Enhances Dnmt3b-

Mediated DNA Methylation. *Genes Dev.* **2020**, *34* (21–22), 1546–1558. https://doi.org/10.1101/gad.341925.120.
(25) Allis, C. D.; Jenuwein, T. The Molecular Hallmarks of Epigenetic Control. *Nat. Rev. Genet.* **2016**, *17* (8), 487–500. https://doi.org/10.1038/nrg.2016.59.
(26) Fischle, W. Talk Is Cheap—Cross-Talk in Establishment, Maintenance, and Readout of Chromatin Modifications. *Genes Dev.* **2008**, *22* (24), 3375–3382. https://doi.org/10.1101/gad.1759708.
(27) Yu, H.; Lesch, B. J. Functional Roles of H3K4 Methylation in Transcriptional Regulation. *Mol. Cell. Biol. 44* (11), 505–515. https://doi.org/10.1080/10985549.2024.2388254.
(28) Guo, X.; Wang, L.; Li, J.; Ding, Z.; Xiao, J.; Yin, X.; He, S.; Shi, P.; Dong, L.; Li, G.; Tian, C.; Wang, J.; Cong, Y.; Xu, Y. Structural Insight into Autoinhibition and Histone H3-Induced Activation of DNMT3A. *Nature* **2015**, *517* (7536), 640–644. https://doi.org/10.1038/nature13899.
(29) Kubo, N.; Uehara, R.; Uemura, S.; Ohishi, H.; Shirane, K.; Sasaki, H. Combined and Differential Roles of ADD Domains of DNMT3A and DNMT3L on DNA Methylation Landscapes in Mouse Germ Cells. *Nat. Commun.* **2024**, *15* (1), 3266. https://doi.org/10.1038/s41467-024-47699-2.
(30) Li, Z.; Zhang, X.; Xie, S.; Liu, X.; Fei, C.; Huang, X.; Tang, Y.; Zhou, L. H3K36me2 Methyltransferase NSD2 Orchestrates Epigenetic Reprogramming during Spermatogenesis. *Nucleic Acids Res.* **2022**, *50* (12), 6786–6800. https://doi.org/10.1093/nar/gkac533.
(31) Pfister, S. X.; Ahrabi, S.; Zalmas, L.-P.; Sarkar, S.; Aymard, F.; Bachrati, C. Z.; Helleday, T.; Legube, G.; La Thangue, N. B.; Porter, A. C. G.; Humphrey, T. C. SETD2-Dependent Histone H3K36 Trimethylation Is Required for Homologous Recombination Repair and Genome Stability. *Cell Rep.* **2014**, *7* (6), 2006–2018. https://doi.org/10.1016/j.celrep.2014.05.026.
(32) Li, F.; Mao, G.; Tong, D.; Huang, J.; Gu, L.; Yang, W.; Li, G.-M. The Histone Mark H3K36me3 Regulates Human DNA Mismatch Repair through Its Interaction with MutSα. *Cell* **2013**, *153* (3), 590–600. https://doi.org/10.1016/j.cell.2013.03.025.
(33) Rondelet, G.; Dal Maso, T.; Willems, L.; Wouters, J. Structural Basis for Recognition of Histone H3K36me3 Nucleosome by Human *de Novo* DNA Methyltransferases 3A and 3B. *J. Struct. Biol.* **2016**, *194* (3), 357–367. https://doi.org/10.1016/j.jsb.2016.03.013.
(34) Weinberg, D. N.; Papillon-Cavanagh, S.; Chen, H.; Yue, Y.; Chen, X.; Rajagopalan, K. N.; Horth, C.; McGuire, J. T.; Xu, X.; Nikbakht, H.; Lemiesz, A. E.; Marchione, D. M.; Marunde, M. R.; Meiners, M. J.; Cheek, M. A.; Keogh, M.-C.; Bareke, E.; Djedid, A.; Harutyunyan, A. S.; Jabado, N.; Garcia, B. A.; Li, H.; Allis, C. D.; Majewski, J.; Lu, C. The Histone Mark H3K36me2 Recruits DNMT3A and Shapes the Intergenic DNA Methylation Landscape. *Nature* **2019**, *573* (7773), 281–286. https://doi.org/10.1038/s41586-019-1534-3.
(35) Becker, J. S.; Nicetto, D.; Zaret, K. S. H3K9me3-Dependent Heterochromatin: Barrier to Cell Fate Changes. *Trends Genet.* **2016**, *32* (1), 29–41. https://doi.org/10.1016/j.tig.2015.11.001.

(36) Weirich, S.; Khella, M. S.; Jeltsch, A. Structure, Activity and Function of the Suv39h1 and Suv39h2 Protein Lysine Methyltransferases. *Life* **2021**, *11* (7), 703. https://doi.org/10.3390/life11070703.
(37) Dong, L.; Liao, H.; Zhao, L.; Wang, J.; Wang, C.; Wang, B.; Sun, Y.; Xu, L.; Xia, Y.; Ling, S.; Lou, X.; Qin, J. A Functional Crosstalk between the H3K9 Methylation Writers and Their Reader HP1 in Safeguarding Embryonic Stem Cell Identity. *Stem Cell Rep.* **2023**, *18* (9), 1775–1792. https://doi.org/10.1016/j.stemcr.2023.08.004.
(38) Lee, S. H.; Li, Y.; Kim, H.; Eum, S.; Lee, K. P. & C.-H. The Role of EZH1 and EZH2 in Development and Cancer. *BMB Rep.* **2022**, *55* (12), 595–601. https://doi.org/10.5483/BMBRep.2022.55.12.174.
(39) Laugesen, A.; Højfeldt, J. W.; Helin, K. Molecular Mechanisms Directing PRC2 Recruitment and H3K27 Methylation. *Mol. Cell* **2019**, *74* (1), 8–18. https://doi.org/10.1016/j.molcel.2019.03.011.
(40) Margueron, R.; Reinberg, D. The Polycomb Complex PRC2 and Its Mark in Life. *Nature* **2011**, *469* (7330), 343–349. https://doi.org/10.1038/nature09784.
(41) Viré, E.; Brenner, C.; Deplus, R.; Blanchon, L.; Fraga, M.; Didelot, C.; Morey, L.; Van Eynde, A.; Bernard, D.; Vanderwinden, J.-M.; Bollen, M.; Esteller, M.; Di Croce, L.; de Launoit, Y.; Fuks, F. The Polycomb Group Protein EZH2 Directly Controls DNA Methylation. *Nature* **2006**, *439* (7078), 871–874. https://doi.org/10.1038/nature04431.
(42) Tamburri, S.; Lavarone, E.; Fernández-Pérez, D.; Conway, E.; Zanotti, M.; Manganaro, D.; Pasini, D. Histone H2AK119 Mono-Ubiquitination Is Essential for Polycomb-Mediated Transcriptional Repression. *Mol. Cell* **2020**, *77* (4), 840-856.e5. https://doi.org/10.1016/j.molcel.2019.11.021.
(43) Cohen, I.; Bar, C.; Ezhkova, E. Activity of PRC1 and Histone H2AK119 Monoubiquitination: Revising Popular Misconceptions. *BioEssays* **2020**, *42* (5), 1900192. https://doi.org/10.1002/bies.201900192.
(44) Wapenaar, H.; Clifford, G.; Rolls, W.; Pasquier, M.; Burdett, H.; Zhang, Y.; Deák, G.; Zou, J.; Spanos, C.; Taylor, M. R. D.; Mills, J.; Watson, J. A.; Kumar, D.; Clark, R.; Das, A.; Valsakumar, D.; Bramham, J.; Voigt, P.; Sproul, D.; Wilson, M. D. The N-Terminal Region of DNMT3A Engages the Nucleosome Surface to Aid Chromatin Recruitment. *EMBO Rep.* **2024**, *25* (12), 5743–5779. https://doi.org/10.1038/s44319-024-00306-3.
(45) Ward, E.; McDonald, D.; Holl, T.; Reich, N. Mechanisms of DNA Methyltransferase 3A1-Mediated DNA Methylation of Nucleosomes. *J. Biol. Chem.* **2026**, *302* (4), 111303. https://doi.org/10.1016/j.jbc.2026.111303.
(46) Seto, E.; Yoshida, M. Erasers of Histone Acetylation: The Histone Deacetylase Enzymes. *Cold Spring Harb. Perspect. Biol.* **2014**, *6* (4), a018713. https://doi.org/10.1101/cshperspect.a018713.
(47) Holoch, D.; Moazed, D. RNA-Mediated Epigenetic Regulation of Gene Expression. *Nat. Rev. Genet.* **2015**, *16* (2), 71–84. https://doi.org/10.1038/nrg3863.
(48) Willbanks, A.; Wood, S.; Cheng, J. X. RNA Epigenetics: Fine-Tuning Chromatin Plasticity and Transcriptional Regulation, and the Implications in Human Diseases. *Genes* **2021**, *12* (5), 627. https://doi.org/10.3390/genes12050627.
(49) Holz-Schietinger, C.; Reich, N. O. RNA Modulation of the Human DNA Methyltransferase 3A. *Nucleic Acids Res.* **2012**, *40* (17), 8550–8557. https://doi.org/10.1093/nar/gks537.

(50) Zhang, G.; Estève, P.-O.; Chin, H. G.; Terragni, J.; Dai, N.; Corrêa, I. R., Jr; Pradhan, S. Small RNA-Mediated DNA (Cytosine-5) Methyltransferase 1 Inhibition Leads to Aberrant DNA Methylation. *Nucleic Acids Res.* **2015**, *43* (12), 6112–6124. https://doi.org/10.1093/nar/gkv518.
(51) Bhat, S. A.; Ahmad, S. M.; Mumtaz, P. T.; Malik, A. A.; Dar, M. A.; Urwat, U.; Shah, R. A.; Ganai, N. A. Long Non-Coding RNAs: Mechanism of Action and Functional Utility. *Non-Coding RNA Res.* **2016**, *1* (1), 43–50. https://doi.org/10.1016/j.ncrna.2016.11.002.
(52) Wei, J.-W.; Huang, K.; Yang, C.; Kang, C.-S. Non-Coding RNAs as Regulators in Epigenetics (Review). *Oncol. Rep.* **2017**, *37* (1), 3–9. https://doi.org/10.3892/or.2016.5236.
(53) Wang, K. C.; Chang, H. Y. Molecular Mechanisms of Long Noncoding RNAs. *Mol. Cell* **2011**, *43* (6), 904–914. https://doi.org/10.1016/j.molcel.2011.08.018.
(54) Meister, G.; Tuschl, T. Mechanisms of Gene Silencing by Double-Stranded RNA. *Nature* **2004**, *431* (7006), 343–349. https://doi.org/10.1038/nature02873.
(55) Hammond, S. M.; Bernstein, E.; Beach, D.; Hannon, G. J. An RNA-Directed Nuclease Mediates Post-Transcriptional Gene Silencing in Drosophila Cells. *Nature* **2000**, *404* (6775), 293–296. https://doi.org/10.1038/35005107.
(56) Elbashir, S. M.; Harborth, J.; Lendeckel, W.; Yalcin, A.; Weber, K.; Tuschl, T. Duplexes of 21-Nucleotide RNAs Mediate RNA Interference in Cultured Mammalian Cells. *Nature* **2001**, *411* (6836), 494–498. https://doi.org/10.1038/35078107.
(57) O'Brien, J.; Hayder, H.; Zayed, Y.; Peng, C. Overview of MicroRNA Biogenesis, Mechanisms of Actions, and Circulation. *Front. Endocrinol.* **2018**, *9*. https://doi.org/10.3389/fendo.2018.00402.
(58) Shu, J.; Silva, B. V. R. e; Gao, T.; Xu, Z.; Cui, J. Dynamic and Modularized MicroRNA Regulation and Its Implication in Human Cancers. *Sci. Rep.* **2017**, *7* (1), 13356. https://doi.org/10.1038/s41598-017-13470-5.
(59) Jia, D.-D.; Jiang, H.; Zhang, Y.-F.; Zhang, Y.; Qian, L.-L.; Zhang, Y.-F. The Regulatory Function of piRNA/PIWI Complex in Cancer and Other Human Diseases: The Role of DNA Methylation. *Int. J. Biol. Sci.* **2022**, *18* (8), 3358–3373. https://doi.org/10.7150/ijbs.68221.
(60) Siddiqi, S.; Matushansky, I. Piwis and Piwi-Interacting RNAs in the Epigenetics of Cancer. *J. Cell. Biochem.* **2012**, *113* (2), 373–380. https://doi.org/10.1002/jcb.23363.
(61) Thomas, A. L.; Rogers, A. K.; Webster, A.; Marinov, G. K.; Liao, S. E.; Perkins, E. M.; Hur, J. K.; Aravin, A. A.; Tóth, K. F. Piwi Induces piRNA-Guided Transcriptional Silencing and Establishment of a Repressive Chromatin State. *Genes Dev.* **2013**, *27* (4), 390–399. https://doi.org/10.1101/gad.209841.112.
(62) Murano, K.; Iwasaki, Y. W.; Ishizu, H.; Mashiko, A.; Shibuya, A.; Kondo, S.; Adachi, S.; Suzuki, S.; Saito, K.; Natsume, T.; Siomi, M. C.; Siomi, H. Nuclear RNA Export Factor Variant Initiates piRNA-guided Co-transcriptional Silencing. *EMBO J.* **2019**, *38* (17), EMBJ2019102870. https://doi.org/10.15252/embj.2019102870.
(63) Wang, K. C.; Chang, H. Y. Molecular Mechanisms of Long Noncoding RNAs. *Mol. Cell* **2011**, *43* (6), 904–914. https://doi.org/10.1016/j.molcel.2011.08.018.
(64) Chen, L.-L. Linking Long Noncoding RNA Localization and Function. *Trends Biochem. Sci.* **2016**, *41* (9), 761–772. https://doi.org/10.1016/j.tibs.2016.07.003.

(65) Pintacuda, G.; Young, A. N.; Cerase, A. Function by Structure: Spotlights on Xist Long Non-Coding RNA. *Front. Mol. Biosci.* **2017**, *4*. https://doi.org/10.3389/fmolb.2017.00090.
(66) Brockdorff, N.; Ashworth, A.; Kay, G. F.; Cooper, P.; Smith, S.; McCabe, V. M.; Norris, D. P.; Penny, G. D.; Patel, D.; Rastan, S. Conservation of Position and Exclusive Expression of Mouse Xist from the Inactive X Chromosome. *Nature* **1991**, *351* (6324), 329–331. https://doi.org/10.1038/351329a0.
(67) Bowness, J. S.; Nesterova, T. B.; Wei, G.; Rodermund, L.; Almeida, M.; Coker, H.; Carter, E. J.; Kadaster, A.; Brockdorff, N. Xist-Mediated Silencing Requires Additive Functions of SPEN and Polycomb Together with Differentiation-Dependent Recruitment of SmcHD1. *Cell Rep.* **2022**, *39* (7), 110830. https://doi.org/10.1016/j.celrep.2022.110830.
(68) Dixon-McDougall, T.; Brown, C. J. Independent Domains for Recruitment of PRC1 and PRC2 by Human XIST. *PLOS Genet.* **2021**, *17* (3), e1009123. https://doi.org/10.1371/journal.pgen.1009123.
(69) Di Ruscio, A.; Ebralidze, A. K.; Benoukraf, T.; Amabile, G.; Goff, L. A.; Terragni, J.; Figueroa, M. E.; De Figueiredo Pontes, L. L.; Alberich-Jorda, M.; Zhang, P.; Wu, M.; D'Alò, F.; Melnick, A.; Leone, G.; Ebralidze, K. K.; Pradhan, S.; Rinn, J. L.; Tenen, D. G. DNMT1-Interacting RNAs Block Gene-Specific DNA Methylation. *Nature* **2013**, *503* (7476), 371–376. https://doi.org/10.1038/nature12598.
(70) Savell, K. E.; Gallus, N. V. N.; Simon, R. C.; Brown, J. A.; Revanna, J. S.; Osborn, M. K.; Song, E. Y.; O'Malley, J. J.; Stackhouse, C. T.; Norvil, A.; Gowher, H.; Sweatt, J. D.; Day, J. J. Extra-Coding RNAs Regulate Neuronal DNA Methylation Dynamics. *Nat. Commun.* **2016**, *7* (1), 12091. https://doi.org/10.1038/ncomms12091.
(71) Sandoval, J. E.; Carullo, N. V. N.; Salisbury, A. J.; Day, J. J.; Reich, N. O. Mechanism of Non-Coding RNA Regulation of DNMT3A. *Epigenetics Chromatin* **2025**, *18* (1), 15. https://doi.org/10.1186/s13072-025-00574-w.
(72) Trowbridge, J. J.; Orkin, S. H. Dnmt3a Silences Hematopoietic Stem Cell Self-Renewal. *Nat. Genet.* **2012**, *44* (1), 13–14. https://doi.org/10.1038/ng.1043.
(73) Liu, M.; Urrutia, G.; Shereda, R.; Hostetter, G.; Thomas, S. L.; Liang, G.; Jones, P. A. Dnmt3a2 Expression during Embryonic Development Is Required for Phenotypic Stability. *Commun. Biol.* **2025**, *9* (1), 44. https://doi.org/10.1038/s42003-025-09311-1.
(74) Challen, G. A.; Sun, D.; Jeong, M.; Luo, M.; Jelinek, J.; Berg, J. S.; Bock, C.; Vasanthakumar, A.; Gu, H.; Xi, Y.; Liang, S.; Lu, Y.; Darlington, G. J.; Meissner, A.; Issa, J.-P. J.; Godley, L. A.; Li, W.; Goodell, M. A. Dnmt3a Is Essential for Hematopoietic Stem Cell Differentiation. *Nat. Genet.* **2012**, *44* (1), 23–31. https://doi.org/10.1038/ng.1009.
(75) Park, D. J.; Kwon, A.; Cho, B.-S.; Kim, H.-J.; Hwang, K.-A.; Kim, M.; Kim, Y. Characteristics of DNMT3A Mutations in Acute Myeloid Leukemia. *Blood Res.* **2020**, *55* (1), 17–26. https://doi.org/10.5045/br.2020.55.1.17.
(76) Huang, G.; Cai, X.; Li, D. Significance of Targeting DNMT3A Mutations in AML. *Ann. Hematol.* **2025**, *104* (3), 1399–1414. https://doi.org/10.1007/s00277-024-05885-8.
(77) Ley, T. J.; Ding, L.; Walter, M. J.; McLellan, M. D.; Lamprecht, T.; Larson, D. E.; Kandoth, C.; Payton, J. E.; Baty, J.; Welch, J.; Harris, C. C.; Lichti, C. F.; Townsend, R. R.; Fulton, R. S.; Dooling, D. J.; Koboldt, D. C.; Schmidt, H.; Zhang, Q.; Osborne, J. R.; Lin, L.; O'Laughlin, M.; McMichael, J. F.; Delehaunty, K. D.; McGrath, S. D.;

Fulton, L. A.; Magrini, V. J.; Vickery, T. L.; Hundal, J.; Cook, L. L.; Conyers, J. J.; Swift, G. W.; Reed, J. P.; Alldredge, P. A.; Wylie, T.; Walker, J.; Kalicki, J.; Watson, M. A.; Heath, S.; Shannon, W. D.; Varghese, N.; Nagarajan, R.; Westervelt, P.; Tomasson, M. H.; Link, D. C.; Graubert, T. A.; DiPersio, J. F.; Mardis, E. R.; Wilson, R. K. DNMT3A Mutations in Acute Myeloid Leukemia. *N. Engl. J. Med.* **2010**, *363* (25), 2424–2433. https://doi.org/10.1056/NEJMoa1005143.

(78) Yan, X.-J.; Xu, J.; Gu, Z.-H.; Pan, C.-M.; Lu, G.; Shen, Y.; Shi, J.-Y.; Zhu, Y.-M.; Tang, L.; Zhang, X.-W.; Liang, W.-X.; Mi, J.-Q.; Song, H.-D.; Li, K.-Q.; Chen, Z.; Chen, S.-J. Exome Sequencing Identifies Somatic Mutations of DNA Methyltransferase Gene DNMT3A in Acute Monocytic Leukemia. *Nat. Genet.* **2011**, *43* (4), 309–315. https://doi.org/10.1038/ng.788.

(79) Yuan, X.-Q.; Chen, P.; Du, Y.-X.; Zhu, K.-W.; Zhang, D.-Y.; Yan, H.; Liu, H.; Liu, Y.-L.; Cao, S.; Zhou, G.; Zeng, H.; Chen, S.-P.; Zhao, X.-L.; Yang, J.; Zeng, W.-J.; Chen, X.-P. Influence of DNMT3A R882 Mutations on AML Prognosis Determined by the Allele Ratio in Chinese Patients. *J. Transl. Med.* **2019**, *17*, 220. https://doi.org/10.1186/s12967-019-1959-3.

(80) Holz-Schietinger, C.; Matje, D. M.; Reich, N. O. Mutations in DNA Methyltransferase (DNMT3A) Observed in Acute Myeloid Leukemia Patients Disrupt Processive Methylation. *J. Biol. Chem.* **2012**, *287* (37), 30941–30951. https://doi.org/10.1074/jbc.M112.366625.

(81) Russler-Germain, D. A.; Spencer, D. H.; Young, M. A.; Lamprecht, T. L.; Miller, C. A.; Fulton, R.; Meyer, M. R.; Erdmann-Gilmore, P.; Townsend, R. R.; Wilson, R. K.; Ley, T. J. The R882H DNMT3A Mutation Associated with AML Dominantly Inhibits Wild-Type DNMT3A by Blocking Its Ability to Form Active Tetramers. *Cancer Cell* **2014**, *25* (4), 442–454. https://doi.org/10.1016/j.ccr.2014.02.010.

(82) Lu, R.; Wang, P.; Parton, T.; Zhou, Y.; Chrysovergis, K.; Rockowitz, S.; Chen, W.-Y.; Abdel-Wahab, O.; Wade, P. A.; Zheng, D.; Wang, G. G. Epigenetic Perturbations by Arg882-Mutated DNMT3A Potentiate Aberrant Stem Cell Gene-Expression Program and Acute Leukemia Development. *Cancer Cell* **2016**, *30* (1), 92–107. https://doi.org/10.1016/j.ccell.2016.05.008.

(83) Huang, G.; Cai, X.; Li, D. Significance of Targeting DNMT3A Mutations in AML. *Ann. Hematol.* **2025**, *104* (3), 1399–1414. https://doi.org/10.1007/s00277-024-05885-8.

(84) Wei, A. H.; Döhner, H.; Pocock, C.; Montesinos, P.; Afanasyev, B.; Dombret, H.; Ravandi, F.; Sayar, H.; Jang, J.-H.; Porkka, K.; Selleslag, D.; Sandhu, I.; Turgut, M.; Giai, V.; Ofran, Y.; Çakar, M. K.; Sousa, A. B. de; Rybka, J.; Frairia, C.; Borin, L.; Beltrami, G.; Čermák, J.; Ossenkoppele, G. J.; Torre, I. L.; Skikne, B.; Kumar, K.; Dong, Q.; Beach, C. L.; Roboz, G. J. Oral Azacitidine Maintenance Therapy for Acute Myeloid Leukemia in First Remission. *N. Engl. J. Med.* **2020**, *383* (26), 2526–2537. https://doi.org/10.1056/NEJMoa2004444.

(85) Geissler, K.; Koristek, Z.; del Castillo, T. B.; Novák, J.; Rodríguez-Macías, G.; Metzelder, S. K.; Illes, A.; Mayer, J.; Arnan, M.; Keating, M.-M.; Krauter, J.; Lunghi, M.; Fracchiolla, N. S.; Platzbecker, U.; Santini, V.; Sano, Y.; Oganesian, A.; Keer, H.; Lübbert, M. Oral Decitabine/Cedazuridine versus Intravenous Decitabine for Acute Myeloid Leukaemia: A Randomised, Crossover, Registration, Pharmacokinetics Study. *Br. J. Haematol.* **2024**, *205* (5), 1734–1745. https://doi.org/10.1111/bjh.19741.

(86) Derissen, E. J. B.; Beijnen, J. H.; Schellens, J. H. M. Concise Drug Review: Azacitidine and Decitabine. *The Oncologist* **2013**, *18* (5), 619–624. https://doi.org/10.1634/theoncologist.2012-0465.
(87) Khan, C.; Pathe, N.; Fazal, S.; Lister, J.; Rossetti, J. M. Azacitidine in the Management of Patients with Myelodysplastic Syndromes. *Ther. Adv. Hematol.* **2012**, *3* (6), 355–373. https://doi.org/10.1177/2040620712464882.
(88) Ye, F.; Huang, J.; Wang, H.; Luo, C.; Zhao, K. Targeting Epigenetic Machinery: Emerging Novel Allosteric Inhibitors. *Pharmacol. Ther.* **2019**, *204*, 107406. https://doi.org/10.1016/j.pharmthera.2019.107406.
(89) Marcucci, G.; Silverman, L.; Eller, M.; Lintz, L.; Beach, C. L. Bioavailability of Azacitidine Subcutaneous Versus Intravenous in Patients With the Myelodysplastic Syndromes. *J. Clin. Pharmacol.* **2005**, *45* (5), 597–602. https://doi.org/10.1177/0091270004271947.
(90) Sandoval, J. E.; Ramabadran, R.; Stillson, N.; Sarah, L.; Fujimori, D. G.; Goodell, M. A.; Reich, N. First-in-Class Allosteric Inhibitors of DNMT3A Disrupt Protein–Protein Interactions and Induce Acute Myeloid Leukemia Cell Differentiation. *J. Med. Chem.* **2022**, *65* (15), 10554–10566. https://doi.org/10.1021/acs.jmedchem.2c00725.
(91) Hernandez, I.; Ward, E.; Pettus, T. R. R.; Reich, N. O. Structural Investigations of Phthalazinone Derivatives as Allosteric Inhibitors of Human DNA Methyltransferase 3A. *ACS Med. Chem. Lett.* **2024**, *15* (5), 590–594. https://doi.org/10.1021/acsmedchemlett.3c00528.

## Chapter II. Optimizing Recombinant Expression and Purification of DNMT3A

(1) Holliday, R.; Pugh, J. E. DNA Modification Mechanisms and Gene Activity During Development. *Science* **1975**, *187* (4173), 226–232. https://doi.org/10.1126/science.187.4173.226.
(2) SanMiguel, J. M.; Bartolomei, M. S. DNA Methylation Dynamics of Genomic Imprinting in Mouse Development. *Biol. Reprod.* **2018**, *99* (1), 252–262. https://doi.org/10.1093/biolre/ioy036.
(3) Hellman, A.; Chess, A. Gene Body-Specific Methylation on the Active X Chromosome. *Science* **2007**, *315* (5815), 1141–1143. https://doi.org/10.1126/science.1136352.
(4) Okano, M.; Bell, D. W.; Haber, D. A.; Li, E. DNA Methyltransferases Dnmt3a and Dnmt3b Are Essential for De Novo Methylation and Mammalian Development. *Cell* **1999**, *99* (3), 247–257. https://doi.org/10.1016/S0092-8674(00)81656-6.
(5) Yang, W.; Zhuang, J.; Li, C.; Cheng, G.-J. Unveiling the Methyl Transfer Mechanisms in the Epigenetic Machinery DNMT3A-3 L: A Comprehensive Study Integrating Assembly Dynamics with Catalytic Reactions. *Comput. Struct. Biotechnol. J.* **2023**, *21*, 2086–2099. https://doi.org/10.1016/j.csbj.2023.03.002.
(6) Park, D. J.; Kwon, A.; Cho, B.-S.; Kim, H.-J.; Hwang, K.-A.; Kim, M.; Kim, Y. Characteristics of DNMT3A Mutations in Acute Myeloid Leukemia. *Blood Res.* **2020**, *55* (1), 17–26. https://doi.org/10.5045/br.2020.55.1.17.
(7) Huang, G.; Cai, X.; Li, D. Significance of Targeting DNMT3A Mutations in AML. *Ann. Hematol.* **2025**, *104* (3), 1399–1414. https://doi.org/10.1007/s00277-024-05885-8.

(8) Ley, T. J.; Ding, L.; Walter, M. J.; McLellan, M. D.; Lamprecht, T.; Larson, D. E.; Kandoth, C.; Payton, J. E.; Baty, J.; Welch, J.; Harris, C. C.; Lichti, C. F.; Townsend, R. R.; Fulton, R. S.; Dooling, D. J.; Koboldt, D. C.; Schmidt, H.; Zhang, Q.; Osborne, J. R.; Lin, L.; O'Laughlin, M.; McMichael, J. F.; Delehaunty, K. D.; McGrath, S. D.; Fulton, L. A.; Magrini, V. J.; Vickery, T. L.; Hundal, J.; Cook, L. L.; Conyers, J. J.; Swift, G. W.; Reed, J. P.; Alldredge, P. A.; Wylie, T.; Walker, J.; Kalicki, J.; Watson, M. A.; Heath, S.; Shannon, W. D.; Varghese, N.; Nagarajan, R.; Westervelt, P.; Tomasson, M. H.; Link, D. C.; Graubert, T. A.; DiPersio, J. F.; Mardis, E. R.; Wilson, R. K. DNMT3A Mutations in Acute Myeloid Leukemia. *N. Engl. J. Med.* **2010**, *363* (25), 2424–2433. https://doi.org/10.1056/NEJMoa1005143.

(9) Yan, X.-J.; Xu, J.; Gu, Z.-H.; Pan, C.-M.; Lu, G.; Shen, Y.; Shi, J.-Y.; Zhu, Y.-M.; Tang, L.; Zhang, X.-W.; Liang, W.-X.; Mi, J.-Q.; Song, H.-D.; Li, K.-Q.; Chen, Z.; Chen, S.-J. Exome Sequencing Identifies Somatic Mutations of DNA Methyltransferase Gene DNMT3A in Acute Monocytic Leukemia. *Nat. Genet.* **2011**, *43* (4), 309–315. https://doi.org/10.1038/ng.788.

(10) Dukatz, M.; Holzer, K.; Choudalakis, M.; Emperle, M.; Lungu, C.; Bashtrykov, P.; Jeltsch, A. H3K36me2/3 Binding and DNA Binding of the DNA Methyltransferase DNMT3A PWWP Domain Both Contribute to Its Chromatin Interaction. *J. Mol. Biol.* **2019**, *431* (24), 5063–5074. https://doi.org/10.1016/j.jmb.2019.09.006.

(11) Kubo, N.; Uehara, R.; Uemura, S.; Ohishi, H.; Shirane, K.; Sasaki, H. Combined and Differential Roles of ADD Domains of DNMT3A and DNMT3L on DNA Methylation Landscapes in Mouse Germ Cells. *Nat. Commun.* **2024**, *15* (1), 3266. https://doi.org/10.1038/s41467-024-47699-2.

(12) Ward, E.; McDonald, D.; Holl, T.; Reich, N. Mechanisms of DNA Methyltransferase 3A1-Mediated DNA Methylation of Nucleosomes. *J. Biol. Chem.* **2026**, *302* (4), 111303. https://doi.org/10.1016/j.jbc.2026.111303.

(13) Wapenaar, H.; Clifford, G.; Rolls, W.; Pasquier, M.; Burdett, H.; Zhang, Y.; Deák, G.; Zou, J.; Spanos, C.; Taylor, M. R. D.; Mills, J.; Watson, J. A.; Kumar, D.; Clark, R.; Das, A.; Valsakumar, D.; Bramham, J.; Voigt, P.; Sproul, D.; Wilson, M. D. The N-Terminal Region of DNMT3A Engages the Nucleosome Surface to Aid Chromatin Recruitment. *EMBO Rep.* **2024**, *25* (12), 5743–5779. https://doi.org/10.1038/s44319-024-00306-3.

(14) Yoo, J.; Kim, J. H.; Robertson, K. D.; Medina-Franco, J. L. Molecular Modeling of Inhibitors of Human DNA Methyltransferase with a Crystal Structure. *Adv. Protein Chem. Struct. Biol.* **2012**, *87*, 219–247. https://doi.org/10.1016/B978-0-12-398312-1.00008-1.

(15) Holz-Schietinger, C.; Matje, D. M.; Harrison, M. F.; Reich, N. O. Oligomerization of DNMT3A Controls the Mechanism of de Novo DNA Methylation. *J. Biol. Chem.* **2011**, *286* (48), 41479–41488. https://doi.org/10.1074/jbc.M111.284687.

(16) Jia, D.; Jurkowska, R. Z.; Zhang, X.; Jeltsch, A.; Cheng, X. Structure of Dnmt3a Bound to Dnmt3L Suggests a Model for de Novo DNA Methylation. *Nature* **2007**, *449* (7159), 248–251. https://doi.org/10.1038/nature06146.

(17) Wang, Y. A.; Kamarova, Y.; Shen, K. C.; Jiang, Z.; Hahn, M. J.; Wang, Y.; Brooks, S. C. DNA Methyltransferase-3a Interacts with P53 and Represses P53-Mediated Gene Expression. *Cancer Biol. Ther.* **2005**, *4* (10), 1138–1143. https://doi.org/10.4161/cbt.4.10.2073.

(18) Sandoval, J. E.; Reich, N. O. P53 and TDG Are Dominant in Regulating the Activity of the Human de Novo DNA Methyltransferase DNMT3A on Nucleosomes. *J. Biol. Chem.* **2021**, *296*. https://doi.org/10.1074/jbc.RA120.016125.
(19) Kunert, S.; Linhard, V.; Weirich, S.; Choudalakis, M.; Osswald, F.; Krämer, L.; Köhler, A. R.; Bröhm, A.; Wollenhaupt, J.; Schwalbe, H.; Jeltsch, A. The MECP2-TRD Domain Interacts with the DNMT3A-ADD Domain at the H3-Tail Binding Site. *Protein Sci.* **2023**, *32* (1), e4542. https://doi.org/10.1002/pro.4542.
(20) Hernandez, I.; Ward, E.; Pettus, T. R. R.; Reich, N. O. Structural Investigations of Phthalazinone Derivatives as Allosteric Inhibitors of Human DNA Methyltransferase 3A. *ACS Med. Chem. Lett.* **2024**, *15* (5), 590–594. https://doi.org/10.1021/acsmedchemlett.3c00528.
(21) Sandoval, J. E.; Carullo, N. V. N.; Salisbury, A. J.; Day, J. J.; Reich, N. O. Mechanism of Non-Coding RNA Regulation of DNMT3A. *Epigenetics Chromatin* **2025**, *18* (1), 15. https://doi.org/10.1186/s13072-025-00574-w.
(22) Sandoval, J. E.; Ramabadran, R.; Stillson, N.; Sarah, L.; Fujimori, D. G.; Goodell, M. A.; Reich, N. First-in-Class Allosteric Inhibitors of DNMT3A Disrupt Protein–Protein Interactions and Induce Acute Myeloid Leukemia Cell Differentiation. *J. Med. Chem.* **2022**, *65* (15), 10554–10566. https://doi.org/10.1021/acs.jmedchem.2c00725.
(23) Chen, T.; Ueda, Y.; Dodge, J. E.; Wang, Z.; Li, E. Establishment and Maintenance of Genomic Methylation Patterns in Mouse Embryonic Stem Cells by Dnmt3a and Dnmt3b. *Mol. Cell. Biol.* **2003**, *23* (16), 5594–5605. https://doi.org/10.1128/MCB.23.16.5594-5605.2003.
(24) Holz-Schietinger, C.; Matje, D. M.; Reich, N. O. Mutations in DNA Methyltransferase (DNMT3A) Observed in Acute Myeloid Leukemia Patients Disrupt Processive Methylation. *J. Biol. Chem.* **2012**, *287* (37), 30941–30951. https://doi.org/10.1074/jbc.M112.366625.
(25) Rong, Y.; Jensen, S. I.; Lindorff-Larsen, K.; Nielsen, A. T. Folding of Heterologous Proteins in Bacterial Cell Factories: Cellular Mechanisms and Engineering Strategies. *Biotechnol. Adv.* **2023**, *63*, 108079. https://doi.org/10.1016/j.biotechadv.2022.108079.
(26) *Strategies to Optimize Protein Expression in E. coli - Francis - 2010 - Current Protocols in Protein Science - Wiley Online Library*. https://currentprotocols.onlinelibrary.wiley.com/doi/10.1002/0471140864.ps0524s61 (accessed 2026-06-09).
(27) Andlinger, D. J.; Röscheisen, P.; Hengst, C.; Kulozik, U. Influence of pH, Temperature and Protease Inhibitors on Kinetics and Mechanism of Thermally Induced Aggregation of Potato Proteins. *Foods* **2021**, *10* (4), 796. https://doi.org/10.3390/foods10040796.
(28) Xiang, Y.; Zheng, Y.; Liu, S.; Liu, G.; Li, Z.; Dong, W. Comparison of the Sensitivity of Western Blotting between PVDF and NC Membranes. *Sci. Rep.* **2021**, *11* (1), 12022. https://doi.org/10.1038/s41598-021-91521-8.
(29) Chen, T.; Ueda, Y.; Xie, S.; Li, E. A Novel Dnmt3a Isoform Produced from an Alternative Promoter Localizes to Euchromatin and Its Expression Correlates with Active*de Novo* Methylation*. *J. Biol. Chem.* **2002**, *277* (41), 38746–38754. https://doi.org/10.1074/jbc.M205312200.
(30) Liu, D.; Wu, H.; Cui, S.; Zhao, Q. Comprehensive Optimization of Western Blotting. *Gels* **2023**, *9* (8), 652. https://doi.org/10.3390/gels9080652.

(31) Nguyen, T.-V.; Yao, S.; Wang, Y.; Rolfe, A.; Selvaraj, A.; Darman, R.; Ke, J.; Warmuth, M.; Smith, P. G.; Larsen, N. A.; Yu, L.; Zhu, P.; Fekkes, P.; Vaillancourt, F. H.; Bolduc, D. M. The R882H DNMT3A Hot Spot Mutation Stabilizes the Formation of Large DNMT3A Oligomers with Low DNA Methyltransferase Activity. *J. Biol. Chem.* **2019**, *294* (45), 16966–16977. https://doi.org/10.1074/jbc.RA119.010126.
(32) Matveev, E. V.; Safronov, V. V.; Ponomarev, G. V.; Kazanov, M. D. Predicting Structural Susceptibility of Proteins to Proteolytic Processing. *Int. J. Mol. Sci.* **2023**, *24* (13), 10761. https://doi.org/10.3390/ijms241310761.
(33) Weinberg, D. N.; Rosenbaum, P.; Chen, X.; Barrows, D.; Horth, C.; Marunde, M. R.; Popova, I. K.; Gillespie, Z. B.; Keogh, M.-C.; Lu, C.; Majewski, J.; Allis, C. D. Two Competing Mechanisms of DNMT3A Recruitment Regulate the Dynamics of de Novo DNA Methylation at PRC1-Targeted CpG Islands. *Nat. Genet.* **2021**, *53* (6), 794–800. https://doi.org/10.1038/s41588-021-00856-5.
(34) Guo, X.; Wang, L.; Li, J.; Ding, Z.; Xiao, J.; Yin, X.; He, S.; Shi, P.; Dong, L.; Li, G.; Tian, C.; Wang, J.; Cong, Y.; Xu, Y. Structural Insight into Autoinhibition and Histone H3-Induced Activation of DNMT3A. *Nature* **2015**, *517* (7536), 640–644. https://doi.org/10.1038/nature13899.
(35) Wu, H.; Zeng, H.; Lam, R.; Tempel, W.; Amaya, M. F.; Xu, C.; Dombrovski, L.; Qiu, W.; Wang, Y.; Min, J. Structural and Histone Binding Ability Characterizations of Human PWWP Domains. *PLOS ONE* **2011**, *6* (6), e18919. https://doi.org/10.1371/journal.pone.0018919.
(36) Liu, Y.; Yang, Q.; Zhao, F. Synonymous but Not Silent: The Codon Usage Code for Gene Expression and Protein Folding. *Annu. Rev. Biochem.* **2021**, *90* (Volume 90, 2021), 375–401. https://doi.org/10.1146/annurev-biochem-071320-112701.
(37) Grunseich, C.; Wang, I. X.; Watts, J. A.; Burdick, J. T.; Guber, R. D.; Zhu, Z.; Bruzel, A.; Lanman, T.; Chen, K.; Schindler, A. B.; Edwards, N.; Ray-Chaudhury, A.; Yao, J.; Lehky, T.; Piszczek, G.; Crain, B.; Fischbeck, K. H.; Cheung, V. G. Senataxin Mutation Reveals How R-Loops Promote Transcription by Blocking DNA Methylation at Gene Promoters. *Mol. Cell* **2018**, *69* (3), 426-437.e7. https://doi.org/10.1016/j.molcel.2017.12.030.
(38) Francis, D. M.; Page, R. Strategies to Optimize Protein Expression in E. Coli.
(39) Gupta, P.; Aggarwal, N.; Batra, P.; Mishra, S.; Chaudhuri, T. K. Co-Expression of Chaperonin GroEL/GroES Enhances in Vivo Folding of Yeast Mitochondrial Aconitase and Alters the Growth Characteristics of *Escherichia Coli*. *Int. J. Biochem. Cell Biol.* **2006**, *38* (11), 1975–1985. https://doi.org/10.1016/j.biocel.2006.05.013.
(40) Tegel, H.; Tourle, S.; Ottosson, J.; Persson, A. Increased Levels of Recombinant Human Proteins with the *Escherichia Coli* Strain Rosetta(DE3). *Protein Expr. Purif.* **2010**, *69* (2), 159–167. https://doi.org/10.1016/j.pep.2009.08.017.
(41) Dumon-Seignovert, L.; Cariot, G.; Vuillard, L. The Toxicity of Recombinant Proteins in *Escherichia Coli*: A Comparison of Overexpression in BL21(DE3), C41(DE3), and C43(DE3). *Protein Expr. Purif.* **2004**, *37* (1), 203–206. https://doi.org/10.1016/j.pep.2004.04.025.
(42) Schlegel, S.; Löfblom, J.; Lee, C.; Hjelm, A.; Klepsch, M.; Strous, M.; Drew, D.; Slotboom, D. J.; de Gier, J.-W. Optimizing Membrane Protein Overexpression in the *Escherichia Coli* Strain Lemo21(DE3). *J. Mol. Biol.* **2012**, *423* (4), 648–659. https://doi.org/10.1016/j.jmb.2012.07.019.

## Chapter III. Developing High-Throughput Screening Assays for Small-Molecule Inhibitors of DNMT3A Regulatory Interactions


(1) Allis, C. D.; Jenuwein, T. The Molecular Hallmarks of Epigenetic Control. *Nat. Rev. Genet.* **2016**, *17* (8), 487–500. https://doi.org/10.1038/nrg.2016.59.

(2) Fischle, W. Talk Is Cheap—Cross-Talk in Establishment, Maintenance, and Readout of Chromatin Modifications. *Genes Dev.* **2008**, *22* (24), 3375–3382. https://doi.org/10.1101/gad.1759708.

(3) Holoch, D.; Moazed, D. RNA-Mediated Epigenetic Regulation of Gene Expression. *Nat. Rev. Genet.* **2015**, *16* (2), 71–84. https://doi.org/10.1038/nrg3863.

(4) Willbanks, A.; Wood, S.; Cheng, J. X. RNA Epigenetics: Fine-Tuning Chromatin Plasticity and Transcriptional Regulation, and the Implications in Human Diseases. *Genes* **2021**, *12* (5), 627. https://doi.org/10.3390/genes12050627.

(5) SanMiguel, J. M.; Bartolomei, M. S. DNA Methylation Dynamics of Genomic Imprinting in Mouse Development. *Biol. Reprod.* **2018**, *99* (1), 252–262. https://doi.org/10.1093/biolre/ioy036.

(6) Hellman, A.; Chess, A. Gene Body-Specific Methylation on the Active X Chromosome. *Science* **2007**, *315* (5815), 1141–1143. https://doi.org/10.1126/science.1136352.

(7) Trowbridge, J. J.; Orkin, S. H. Dnmt3a Silences Hematopoietic Stem Cell Self-Renewal. *Nat. Genet.* **2011**, *44* (1), 13–14. https://doi.org/10.1038/ng.1043.

(8) Wu, H.; Zeng, H.; Lam, R.; Tempel, W.; Amaya, M. F.; Xu, C.; Dombrovski, L.; Qiu, W.; Wang, Y.; Min, J. Structural and Histone Binding Ability Characterizations of Human PWWP Domains. *PLOS ONE* **2011**, *6* (6), e18919. https://doi.org/10.1371/journal.pone.0018919.

(9) Kubo, N.; Uehara, R.; Uemura, S.; Ohishi, H.; Shirane, K.; Sasaki, H. Combined and Differential Roles of ADD Domains of DNMT3A and DNMT3L on DNA Methylation Landscapes in Mouse Germ Cells. *Nat. Commun.* **2024**, *15* (1), 3266. https://doi.org/10.1038/s41467-024-47699-2.

(10) Yu, H.; Lesch, B. J. Functional Roles of H3K4 Methylation in Transcriptional Regulation. *Mol. Cell. Biol. 44* (11), 505–515. https://doi.org/10.1080/10985549.2024.2388254.

(11) Kunert, S.; Linhard, V.; Weirich, S.; Choudalakis, M.; Osswald, F.; Krämer, L.; Köhler, A. R.; Bröhm, A.; Wollenhaupt, J.; Schwalbe, H.; Jeltsch, A. The MECP2-TRD Domain Interacts with the DNMT3A-ADD Domain at the H3-Tail Binding Site. *Protein Sci.* **2023**, *32* (1), e4542. https://doi.org/10.1002/pro.4542.

(12) Guo, X.; Wang, L.; Li, J.; Ding, Z.; Xiao, J.; Yin, X.; He, S.; Shi, P.; Dong, L.; Li, G.; Tian, C.; Wang, J.; Cong, Y.; Xu, Y. Structural Insight into Autoinhibition and Histone H3-Induced Activation of DNMT3A. *Nature* **2015**, *517* (7536), 640–644. https://doi.org/10.1038/nature13899.

(13) Dukatz, M.; Holzer, K.; Choudalakis, M.; Emperle, M.; Lungu, C.; Bashtrykov, P.; Jeltsch, A. H3K36me2/3 Binding and DNA Binding of the DNA Methyltransferase DNMT3A PWWP Domain Both Contribute to Its Chromatin Interaction. *J. Mol. Biol.* **2019**, *431* (24), 5063–5074. https://doi.org/10.1016/j.jmb.2019.09.006.

(14) Li, Z.; Zhang, X.; Xie, S.; Liu, X.; Fei, C.; Huang, X.; Tang, Y.; Zhou, L. H3K36me2 Methyltransferase NSD2 Orchestrates Epigenetic Reprogramming during Spermatogenesis. *Nucleic Acids Res.* **2022**, *50* (12), 6786–6800. https://doi.org/10.1093/nar/gkac533.
(15) Rondelet, G.; Dal Maso, T.; Willems, L.; Wouters, J. Structural Basis for Recognition of Histone H3K36me3 Nucleosome by Human *de Novo* DNA Methyltransferases 3A and 3B. *J. Struct. Biol.* **2016**, *194* (3), 357–367. https://doi.org/10.1016/j.jsb.2016.03.013.
(16) Huang, G.; Cai, X.; Li, D. Significance of Targeting DNMT3A Mutations in AML. *Ann. Hematol.* **2025**, *104* (3), 1399–1414. https://doi.org/10.1007/s00277-024-05885-8.
(17) Ley, T. J.; Ding, L.; Walter, M. J.; McLellan, M. D.; Lamprecht, T.; Larson, D. E.; Kandoth, C.; Payton, J. E.; Baty, J.; Welch, J.; Harris, C. C.; Lichti, C. F.; Townsend, R. R.; Fulton, R. S.; Dooling, D. J.; Koboldt, D. C.; Schmidt, H.; Zhang, Q.; Osborne, J. R.; Lin, L.; O'Laughlin, M.; McMichael, J. F.; Delehaunty, K. D.; McGrath, S. D.; Fulton, L. A.; Magrini, V. J.; Vickery, T. L.; Hundal, J.; Cook, L. L.; Conyers, J. J.; Swift, G. W.; Reed, J. P.; Alldredge, P. A.; Wylie, T.; Walker, J.; Kalicki, J.; Watson, M. A.; Heath, S.; Shannon, W. D.; Varghese, N.; Nagarajan, R.; Westervelt, P.; Tomasson, M. H.; Link, D. C.; Graubert, T. A.; DiPersio, J. F.; Mardis, E. R.; Wilson, R. K. DNMT3A Mutations in Acute Myeloid Leukemia. *N. Engl. J. Med.* **2010**, *363* (25), 2424–2433. https://doi.org/10.1056/NEJMoa1005143.
(18) Yan, X.-J.; Xu, J.; Gu, Z.-H.; Pan, C.-M.; Lu, G.; Shen, Y.; Shi, J.-Y.; Zhu, Y.-M.; Tang, L.; Zhang, X.-W.; Liang, W.-X.; Mi, J.-Q.; Song, H.-D.; Li, K.-Q.; Chen, Z.; Chen, S.-J. Exome Sequencing Identifies Somatic Mutations of DNA Methyltransferase Gene DNMT3A in Acute Monocytic Leukemia. *Nat. Genet.* **2011**, *43* (4), 309–315. https://doi.org/10.1038/ng.788.
(19) Wei, A. H.; Döhner, H.; Pocock, C.; Montesinos, P.; Afanasyev, B.; Dombret, H.; Ravandi, F.; Sayar, H.; Jang, J.-H.; Porkka, K.; Selleslag, D.; Sandhu, I.; Turgut, M.; Giai, V.; Ofran, Y.; Çakar, M. K.; Sousa, A. B. de; Rybka, J.; Frairia, C.; Borin, L.; Beltrami, G.; Čermák, J.; Ossenkoppele, G. J.; Torre, I. L.; Skikne, B.; Kumar, K.; Dong, Q.; Beach, C. L.; Roboz, G. J. Oral Azacitidine Maintenance Therapy for Acute Myeloid Leukemia in First Remission. *N. Engl. J. Med.* **2020**, *383* (26), 2526–2537. https://doi.org/10.1056/NEJMoa2004444.
(20) de Vos, D.; van Overveld, W. Decitabine: A Historical Review of the Development of an Epigenetic Drug. *Ann. Hematol.* **2005**, *84* (1), 3–8. https://doi.org/10.1007/s00277-005-0008-x.
(21) Ye, F.; Huang, J.; Wang, H.; Luo, C.; Zhao, K. Targeting Epigenetic Machinery: Emerging Novel Allosteric Inhibitors. *Pharmacol. Ther.* **2019**, *204*, 107406. https://doi.org/10.1016/j.pharmthera.2019.107406.
(22) Marcucci, G.; Silverman, L.; Eller, M.; Lintz, L.; Beach, C. L. Bioavailability of Azacitidine Subcutaneous Versus Intravenous in Patients With the Myelodysplastic Syndromes. *J. Clin. Pharmacol.* **2005**, *45* (5), 597–602. https://doi.org/10.1177/0091270004271947.
(23) Hernandez, I.; Ward, E.; Pettus, T. R. R.; Reich, N. O. Structural Investigations of Phthalazinone Derivatives as Allosteric Inhibitors of Human DNA Methyltransferase 3A. *ACS Med. Chem. Lett.* **2024**, *15* (5), 590–594. https://doi.org/10.1021/acsmedchemlett.3c00528.

(24) Sandoval, J. E.; Ramabadran, R.; Stillson, N.; Sarah, L.; Fujimori, D. G.; Goodell, M. A.; Reich, N. First-in-Class Allosteric Inhibitors of DNMT3A Disrupt Protein–Protein Interactions and Induce Acute Myeloid Leukemia Cell Differentiation. *J. Med. Chem.* **2022**, *65* (15), 10554–10566. https://doi.org/10.1021/acs.jmedchem.2c00725.
(25) Tiffon, C.; Adams, J.; van der Fits, L.; Wen, S.; Townsend, P.; Ganesan, A.; Hodges, E.; Vermeer, M.; Packham, G. The Histone Deacetylase Inhibitors Vorinostat and Romidepsin Downmodulate IL-10 Expression in Cutaneous T-Cell Lymphoma Cells. *Br. J. Pharmacol.* **2011**, *162* (7), 1590–1602. https://doi.org/10.1111/j.1476-5381.2010.01188.x.
(26) Lu, G.; Jin, S.; Lin, S.; Gong, Y.; Zhang, L.; Yang, J.; Mou, W.; Du, J. Update on Histone Deacetylase Inhibitors in Peripheral T-Cell Lymphoma (PTCL). *Clin. Epigenetics* **2023**, *15* (1), 124. https://doi.org/10.1186/s13148-023-01531-8.
(27) Myers, R. A.; Wirth, S.; Williams, S.; Kiel, P. J. Enasidenib: An Oral IDH2 Inhibitor for the Treatment of Acute Myeloid Leukemia. *J. Adv. Pract. Oncol.* **2018**, *9* (4), 435–440.
(28) Staerz, S. D.; Lisabeth, E. M.; Njomen, E.; Dexheimer, T. S.; Neubig, R. R.; Tepe, J. J. Development of a Cell-Based AlphaLISA Assay for High-Throughput Screening for Small Molecule Proteasome Modulators. *ACS Omega* **2023**, *8* (17), 15650–15659. https://doi.org/10.1021/acsomega.3c01158.
(29) Ishii, K. Functional Singlet Oxygen Generators Based on Phthalocyanines. *Coord. Chem. Rev.* **2012**, *256* (15), 1556–1568. https://doi.org/10.1016/j.ccr.2012.03.022.
(30) Ishikawa-Ankerhold, H. C.; Ankerhold, R.; Drummen, G. P. C. Advanced Fluorescence Microscopy Techniques—FRAP, FLIP, FLAP, FRET and FLIM. *Molecules* **2012**, *17* (4), 4047–4132. https://doi.org/10.3390/molecules17044047.
(31) Weinberg, D. N.; Papillon-Cavanagh, S.; Chen, H.; Yue, Y.; Chen, X.; Rajagopalan, K. N.; Horth, C.; McGuire, J. T.; Xu, X.; Nikbakht, H.; Lemiesz, A. E.; Marchione, D. M.; Marunde, M. R.; Meiners, M. J.; Cheek, M. A.; Keogh, M.-C.; Bareke, E.; Djedid, A.; Harutyunyan, A. S.; Jabado, N.; Garcia, B. A.; Li, H.; Allis, C. D.; Majewski, J.; Lu, C. The Histone Mark H3K36me2 Recruits DNMT3A and Shapes the Intergenic DNA Methylation Landscape. *Nature* **2019**, *573* (7773), 281–286. https://doi.org/10.1038/s41586-019-1534-3.
(32) Weinberg, D. N.; Rosenbaum, P.; Chen, X.; Barrows, D.; Horth, C.; Marunde, M. R.; Popova, I. K.; Gillespie, Z. B.; Keogh, M.-C.; Lu, C.; Majewski, J.; Allis, C. D. Two Competing Mechanisms of DNMT3A Recruitment Regulate the Dynamics of de Novo DNA Methylation at PRC1-Targeted CpG Islands. *Nat. Genet.* **2021**, *53* (6), 794–800. https://doi.org/10.1038/s41588-021-00856-5.
(33) Ward, E.; McDonald, D.; Holl, T.; Reich, N. Mechanisms of DNA Methyltransferase 3A1-Mediated DNA Methylation of Nucleosomes. *J. Biol. Chem.* **2026**, *302* (4), 111303. https://doi.org/10.1016/j.jbc.2026.111303.
(34) Yan, Y.; Zhou, X. E.; Thomas, S. L.; Liu, M.; Lai, G.-Q.; Worden, E. J.; Jones, P. A.; Xu, T.-H. Mechanisms of DNMT3A–3L-Mediated de Novo DNA Methylation on Chromatin. *Nat. Struct. Mol. Biol.* **2026**, *33* (1), 171–183. https://doi.org/10.1038/s41594-025-01704-4.
(35) Simon, M. D.; Shokat, K. M. Chapter Three - A Method to Site-Specifically Incorporate Methyl-Lysine Analogues into Recombinant Proteins. In *Nucleosomes, Histones &*

*Chromatin Part A*; Wu, C., Allis, C. D., Eds.; Methods in Enzymology; Academic Press, 2012; Vol. 512, pp 57–69. https://doi.org/10.1016/B978-0-12-391940-3.00003-2.
(36) Simon, M. D.; Chu, F.; Racki, L. R.; de la Cruz, C. C.; Burlingame, A. L.; Panning, B.; Narlikar, G. J.; Shokat, K. M. The Site-Specific Installation of Methyl-Lysine Analogs into Recombinant Histones. *Cell* **2007**, *128* (5), 1003–1012. https://doi.org/10.1016/j.cell.2006.12.041.
(37) Sandoval, J. E.; Carullo, N. V. N.; Salisbury, A. J.; Day, J. J.; Reich, N. O. Mechanism of Non-Coding RNA Regulation of DNMT3A. *Epigenetics Chromatin* **2025**, *18* (1), 15. https://doi.org/10.1186/s13072-025-00574-w.

## Chapter IV. RNA-Mediated Regulation of DNMT3A by *Fos-1* ecRNA

(1) Holz-Schietinger, C.; Matje, D. M.; Harrison, M. F.; Reich, N. O. Oligomerization of DNMT3A Controls the Mechanism of de Novo DNA Methylation. *J. Biol. Chem.* **2011**, *286* (48), 41479–41488. https://doi.org/10.1074/jbc.M111.284687.
(2) Jia, D.; Jurkowska, R. Z.; Zhang, X.; Jeltsch, A.; Cheng, X. Structure of Dnmt3a Bound to Dnmt3L Suggests a Model for de Novo DNA Methylation. *Nature* **2007**, *449* (7159), 248–251. https://doi.org/10.1038/nature06146.
(3) Wang, Y. A.; Kamarova, Y.; Shen, K. C.; Jiang, Z.; Hahn, M. J.; Wang, Y.; Brooks, S. C. DNA Methyltransferase-3a Interacts with P53 and Represses P53-Mediated Gene Expression. *Cancer Biol. Ther.* **2005**, *4* (10), 1138–1143. https://doi.org/10.4161/cbt.4.10.2073.
(4) Bhat, S. A.; Ahmad, S. M.; Mumtaz, P. T.; Malik, A. A.; Dar, M. A.; Urwat, U.; Shah, R. A.; Ganai, N. A. Long Non-Coding RNAs: Mechanism of Action and Functional Utility. *Non-Coding RNA Res.* **2016**, *1* (1), 43–50. https://doi.org/10.1016/j.ncrna.2016.11.002.
(5) Chen, T.; Ueda, Y.; Dodge, J. E.; Wang, Z.; Li, E. Establishment and Maintenance of Genomic Methylation Patterns in Mouse Embryonic Stem Cells by Dnmt3a and Dnmt3b. *Mol. Cell. Biol.* **2003**, *23* (16), 5594–5605. https://doi.org/10.1128/MCB.23.16.5594-5605.2003.
(6) Hellman, A.; Chess, A. Gene Body-Specific Methylation on the Active X Chromosome. *Science* **2007**, *315* (5815), 1141–1143. https://doi.org/10.1126/science.1136352.
(7) Fischle, W. Talk Is Cheap—Cross-Talk in Establishment, Maintenance, and Readout of Chromatin Modifications. *Genes Dev.* **2008**, *22* (24), 3375–3382. https://doi.org/10.1101/gad.1759708.
(8) Bowness, J. S.; Nesterova, T. B.; Wei, G.; Rodermund, L.; Almeida, M.; Coker, H.; Carter, E. J.; Kadaster, A.; Brockdorff, N. Xist-Mediated Silencing Requires Additive Functions of SPEN and Polycomb Together with Differentiation-Dependent Recruitment of SmcHD1. *Cell Rep.* **2022**, *39* (7), 110830. https://doi.org/10.1016/j.celrep.2022.110830.
(9) SanMiguel, J. M.; Bartolomei, M. S. DNA Methylation Dynamics of Genomic Imprinting in Mouse Development. *Biol. Reprod.* **2018**, *99* (1), 252–262. https://doi.org/10.1093/biolre/ioy036.
(10) Challen, G. A.; Sun, D.; Mayle, A.; Jeong, M.; Luo, M.; Rodriguez, B.; Mallaney, C.; Celik, H.; Yang, L.; Xia, Z.; Cullen, S.; Berg, J.; Zheng, Y.; Darlington, G. J.; Li, W.;

Goodell, M. A. Dnmt3a and Dnmt3b Have Overlapping and Distinct Functions in Hematopoietic Stem Cells. *Cell Stem Cell* **2014**, *15* (3), 350–364. https://doi.org/10.1016/j.stem.2014.06.018.
(11) Okano, M.; Bell, D. W.; Haber, D. A.; Li, E. DNA Methyltransferases Dnmt3a and Dnmt3b Are Essential for De Novo Methylation and Mammalian Development. *Cell* **1999**, *99* (3), 247–257. https://doi.org/10.1016/S0092-8674(00)81656-6.
(12) Guo, X.; Wang, L.; Li, J.; Ding, Z.; Xiao, J.; Yin, X.; He, S.; Shi, P.; Dong, L.; Li, G.; Tian, C.; Wang, J.; Cong, Y.; Xu, Y. Structural Insight into Autoinhibition and Histone H3-Induced Activation of DNMT3A. *Nature* **2015**, *517* (7536), 640–644. https://doi.org/10.1038/nature13899.
(13) Rondelet, G.; Dal Maso, T.; Willems, L.; Wouters, J. Structural Basis for Recognition of Histone H3K36me3 Nucleosome by Human *de Novo* DNA Methyltransferases 3A and 3B. *J. Struct. Biol.* **2016**, *194* (3), 357–367. https://doi.org/10.1016/j.jsb.2016.03.013.
(14) Tamburri, S.; Lavarone, E.; Fernández-Pérez, D.; Conway, E.; Zanotti, M.; Manganaro, D.; Pasini, D. Histone H2AK119 Mono-Ubiquitination Is Essential for Polycomb-Mediated Transcriptional Repression. *Mol. Cell* **2020**, *77* (4), 840-856.e5. https://doi.org/10.1016/j.molcel.2019.11.021.
(15) Cohen, I.; Bar, C.; Ezhkova, E. Activity of PRC1 and Histone H2AK119 Monoubiquitination: Revising Popular Misconceptions. *BioEssays* **2020**, *42* (5), 1900192. https://doi.org/10.1002/bies.201900192.
(16) Dukatz, M.; Holzer, K.; Choudalakis, M.; Emperle, M.; Lungu, C.; Bashtrykov, P.; Jeltsch, A. H3K36me2/3 Binding and DNA Binding of the DNA Methyltransferase DNMT3A PWWP Domain Both Contribute to Its Chromatin Interaction. *J. Mol. Biol.* **2019**, *431* (24), 5063–5074. https://doi.org/10.1016/j.jmb.2019.09.006.
(17) Dixon-McDougall, T.; Brown, C. J. Independent Domains for Recruitment of PRC1 and PRC2 by Human XIST. *PLOS Genet.* **2021**, *17* (3), e1009123. https://doi.org/10.1371/journal.pgen.1009123.
(18) Di Ruscio, A.; Ebralidze, A. K.; Benoukraf, T.; Amabile, G.; Goff, L. A.; Terragni, J.; Figueroa, M. E.; De Figueiredo Pontes, L. L.; Alberich-Jorda, M.; Zhang, P.; Wu, M.; D'Alò, F.; Melnick, A.; Leone, G.; Ebralidze, K. K.; Pradhan, S.; Rinn, J. L.; Tenen, D. G. DNMT1-Interacting RNAs Block Gene-Specific DNA Methylation. *Nature* **2013**, *503* (7476), 371–376. https://doi.org/10.1038/nature12598.
(19) Savell, K. E.; Gallus, N. V. N.; Simon, R. C.; Brown, J. A.; Revanna, J. S.; Osborn, M. K.; Song, E. Y.; O'Malley, J. J.; Stackhouse, C. T.; Norvil, A.; Gowher, H.; Sweatt, J. D.; Day, J. J. Extra-Coding RNAs Regulate Neuronal DNA Methylation Dynamics. *Nat. Commun.* **2016**, *7* (1), 12091. https://doi.org/10.1038/ncomms12091.
(20) Sandoval, J. E.; Carullo, N. V. N.; Salisbury, A. J.; Day, J. J.; Reich, N. O. Mechanism of Non-Coding RNA Regulation of DNMT3A. *Epigenetics Chromatin* **2025**, *18* (1), 15. https://doi.org/10.1186/s13072-025-00574-w.
(21) Yan, Y.; Zhou, X. E.; Thomas, S. L.; Liu, M.; Lai, G.-Q.; Worden, E. J.; Jones, P. A.; Xu, T.-H. Molecular Mechanisms of DNMT3A-3L-Mediated de Novo DNA Methylation on Chromatin. *Nat. Struct. Mol. Biol.* **2026**, *33* (1), 171–183. https://doi.org/10.1038/s41594-025-01704-4.
(22) Zeng, Y.; Ren, R.; Kaur, G.; Hardikar, S.; Ying, Z.; Babcock, L.; Gupta, E.; Zhang, X.; Chen, T.; Cheng, X. The Inactive Dnmt3b3 Isoform Preferentially Enhances Dnmt3b-

Mediated DNA Methylation. *Genes Dev.* **2020**, *34* (21–22), 1546–1558. https://doi.org/10.1101/gad.341925.120.
(23) Sandoval, J. E.; Reich, N. O. P53 and TDG Are Dominant in Regulating the Activity of the Human de Novo DNA Methyltransferase DNMT3A on Nucleosomes. *J. Biol. Chem.* **2021**, *296*. https://doi.org/10.1074/jbc.RA120.016125.
(24) Yan, Y.; Tao, H.; He, J.; Huang, S.-Y. The HDOCK Server for Integrated Protein–Protein Docking. *Nat. Protoc.* **2020**, *15* (5), 1829–1852. https://doi.org/10.1038/s41596-020-0312-x.
(25) Chong, N. H. H.; Tan, E. Z. T.; Tan, C. H. E.; Ilangovan, H.; Lim, Y. J.; Srivastava, A.; Tan, Y. S. Evaluation of Protein–RNA Docking Web Servers for Template-Free Docking and Comparison with the AlphaFold Server. *J. Chem. Theory Comput.* **2026**, *22* (7), 3746–3760. https://doi.org/10.1021/acs.jctc.5c01990.
(26) Lu, J.; Guo, Y.; Yin, J.; Chen, J.; Wang, Y.; Wang, G. G.; Song, J. Structure-Guided Functional Suppression of AML-Associated DNMT3A Hotspot Mutations. *Nat. Commun.* **2024**, *15* (1), 3111. https://doi.org/10.1038/s41467-024-47398-y.
(27) Holz-Schietinger, C.; Matje, D. M.; Reich, N. O. Mutations in DNA Methyltransferase (DNMT3A) Observed in Acute Myeloid Leukemia Patients Disrupt Processive Methylation. *J. Biol. Chem.* **2012**, *287* (37), 30941–30951. https://doi.org/10.1074/jbc.M112.366625.
(28) Chen, L.-L. Linking Long Noncoding RNA Localization and Function. *Trends Biochem. Sci.* **2016**, *41* (9), 761–772. https://doi.org/10.1016/j.tibs.2016.07.003.